U.S. DEPARTMENT OF COMMERCE
National Technical Information Service

PB-255 984

Rapping Reentrainment in a Nearly Full-Scale Pilot Electrostatic Precipitator

Southern Research Inst.

Prepared For
Industrial Environmental Research Lab.

May 1976

PB255984

TECHNICAL REPORT DATA

(Please read Instructions on the reverse before completing)

1. REPORT NO.
EPA-600/2-76-140

2.

3. RECIPIENT'S ACCESSION NO.

4. TITLE AND SUBTITLE
Rapping Reentrainment in a Nearly Full-Scale Pilot Electrostatic Precipitator

5. REPORT DATE
May 1976

6. PERFORMING ORGANIZATION CODE

7. AUTHOR(S)
Herbert W. Spencer, III

8. PERFORMING ORGANIZATION REPORT NO.
SORI-EAS-76-061
3489-V

9. PERFORMING ORGANIZATION NAME AND ADDRESS
Southern Research Institute
2000 Ninth Avenue South
Birmingham, Alabama 35205

10. PROGRAM ELEMENT NO.
1AB012; ROAP 21ADL-027

11. CONTRACT/GRANT NO.
68-02-1875

12. SPONSORING AGENCY NAME AND ADDRESS
EPA, Office of Research and Development
Industrial Environmental Research Laboratory
Research Triangle Park, NC 27711

13. TYPE OF REPORT AND PERIOD COVERED
Final; 3/75-1/76

14. SPONSORING AGENCY CODE
EPA-ORD

15. SUPPLEMENTARY NOTES IERL-RTP Project Officer for this report is Leslie E. Sparks, Mail Drop 61, Ext 2925.

16. ABSTRACT

The report gives results of an experimental investigation of rapping reentrainment in a nearly full-scale pilot electrostatic precipitator. The study included a fundamental examination of the mechanics of removal of dry dust by rapping and the quantification of rapping reentrainment in terms of the percentage and the particle size distribution of the reentrained dust. During the study, the contribution of rapping reentrainment to total emissions ranged from 53 to 18%, depending on rapping conditions. These percentages corresponded to 5.4 and 2.7% of the dust collected on the plates being emitted from the precipitator during plate rapping. A major portion of the reentrained material was observed to result from hopper 'boil-up.' A decrease in rapping emissions was obtained by increasing the time interval between raps. The mass median diameters of the size distributions of the particles emitted during the raps were observed to increase with increased time between raps.

17. KEY WORDS AND DOCUMENT ANALYSIS

a. DESCRIPTORS	b. IDENTIFIERS/OPEN ENDED TERMS	c. COSATI Field/Group
Air Pollution	Air Pollution Control	13B
Electrostatic Precipitators	Stationary Sources	
Dust	Rapping	11G
	Reentrainment	
	Particulate	

PRICES SUBJECT TO CHANGE

18. DISTRIBUTION STATEMENT Unlimited	19. SECURITY CLASS *(This Report)* Unclassified	21. NO. OF PAGES 179
	20. SECURITY CLASS *(This page)* Unclassified	22. PRICE 7.50 - 2.25

EPA Form 2220-1 (9-73)

229188

PB 255 984

EPA-600/2-76-140
May 1976

Environmental Protection Technology Series

[illegible]

UNITED STATES ENVIRONMENTAL PROTECTION AGENCY

REPRODUCED BY
NATIONAL TECHNICAL
INFORMATION SERVICE
U. S. DEPARTMENT OF COMMERCE
SPRINGFIELD, VA. 22161

RESEARCH REPORTING SERIES

Research reports of the Office of Research and Development, U.S. Environmental Protection Agency, have been grouped into five series. These five broad categories were established to facilitate further development and application of environmental technology. Elimination of traditional grouping was consciously planned to foster technology transfer and a maximum interface in related fields. The five series are:

1. Environmental Health Effects Research
2. Environmental Protection Technology
3. Ecological Research
4. Environmental Monitoring
5. Socioeconomic Environmental Studies

This report has been assigned to the ENVIRONMENTAL PROTECTION TECHNOLOGY series. This series describes research performed to develop and demonstrate instrumentation, equipment, and methodology to repair or prevent environmental degradation from point and non-point sources of pollution. This work provides the new or improved technology required for the control and treatment of pollution sources to meet environmental quality standards.

EPA REVIEW NOTICE

This report has been reviewed by the U.S. Environmental Protection Agency, and approved for publication. Approval does not signify that the contents necessarily reflect the views and policy of the Agency, nor does mention of trade names or commercial products constitute endorsement or recommendation for use.

This document is available to the public through the National Technical Information Service, Springfield, Virginia 22161.

EPA-600/2-76-140
May 1976

RAPPING REENTRAINMENT
IN A NEARLY FULL SCALE
PILOT ELECTROSTATIC PRECIPITATOR

by

Herbert W. Spencer, III

Southern Research Institute
2000 Ninth Avenue South
Birmingham, Alabama 35205

Contract No. 68-02-1875
ROAP No. 21ADL-027
Program Element No. 1AB012

EPA Project Officer: Leslie E. Sparks

Industrial Environmental Research Laboratory
Office of Energy, Minerals, and Industry
Research Triangle Park, NC 27711

Prepared for

U.S. ENVIRONMENTAL PROTECTION AGENCY
Office of Research and Development
Washington, DC 20460

ABSTRACT

The results of an experimental investigation of rapping reentrainment in a nearly full scale pilot electrostatic precipitator are reported. The objectives of the study included a fundamental study of the mechanics of removal of dry dust by rapping and the quantification of rapping reentrainment in terms of the percentage and the particle size distribution of the reentrained dust. During this study, the contribution of rapping reentrainment to total emissions ranged from 53% to 18% depending on rapping conditions. These percentages corresponded to 5.4% and 2.7% of the dust collected on the plates being emitted from the precipitator during plate rapping. A major portion of the reentrained material was observed to result from hopper "boil-up". A decrease in rapping emissions was obtained by increasing the time interval between raps. The mass median diameters of the size distributions of the particles emitted during the raps were observed to increase with increased time between raps.

TABLE OF CONTENTS

		Page
Abstract		ii
List of Figures		iv
List of Tables		ix
Acknowledgements		xi
Sections		
I	Summary	1
II	Introduction	5
III	Experimental Arrangement	19
IV	Test Conditions	46
V	Results and Discussion	76
VI	References	149
VII	Appendix	152

FIGURES

No.		Page
1	Theoretical efficiency of dust removal as a function of dust layer thickness	10
2	Rapping efficiency as a function of mass per unit area for a precipitated fly ash at 150°C, rapped with a maximum normal acceleration of 1.3 x 10^4 cm/sec^2 (13 G); measured by Sproull.[5]	11
3	Near full scale pilot precipitator at FluiDyne Engineering	20
4	Various views of FluiDyne pilot precipitator	21
5	Design details for pilot precipitator plates	24
6	Block diagram of experimental layout for rapping reentrainment study	29
7	Sampling locations during the rapping reentrainment study	30
8	Schematic of diluter for large particle sizing system	36
9	Block diagram of large particle sizing system	37
10	Load cell	39
11	Precipitator plate weight measurements system block diagram	41
12	Accelerometer system block diagram	42
13	Cumulative particle size distribution of the feed dust, Bahco analysis	48
14	Resistivities measured in Southern Research Institute laboratory for fly ash used during the test	50
15	Precipitator electrical characteristics	56
16	Precipitator outlet velocity profile	58

FIGURES

(continued)

No. Page

17 Precipitator inlet velocity profile 60

18 Precipitator outlet velocity profile 61

19 Correlation of measured feed rate and hopper feed rate 65

20 Plate 5-1 accelerations as a functional differential pressure on rapper, upstream rapper, dust on plate. 69

21 Plate 5-1 accelerations as a functional differential pressure on rapper, upstream rapper, no dust on plates. 70

22 Typical traces of plate accelerations for a dust covered plate [plate 5-2, 3m from top of plate, $\Delta P = 6.2 \times 10^5$ Pa (90 psi)]. 73

23 Typical traces of plate accelerations for a clean plate [plate 5-2; x_1, Y_1, Z_1, 0.9 m from top of plate; X_2, Y_2 3m from top of plate; $\Delta P = 6.2 \times 10^5$ Pa (90 psi)]. 75

24 Mass emission rates for lower 32% of the precipitator cross sectional area as a function of the time interval between raps 78

25 Mass emission rates for upper 68% of the precipitator cross sectional area as a function of the time interval between raps 79

26 Combined upper and lower mass emission rates as a function of the time interval between raps 80

27 Particulate loading - lower 32% of the precipitator as a function of time interval between raps 81

28 Particulate loading - upper 68% of the precipitator as a function of time interval between raps 82

FIGURES
(continued)

No.		Page
29	Combined particulate load as a function of time interval between raps	83
30	Percent of dust collected on precipitator plates that is emitted due to rapping	87
31	Inlet and weighted outlet particle size distributions, dm/d log D	90
32	Inlet cumulative percent particle size distribution	91
33	Inlet and outlet (lower 32% and upper 68% of the precipitator) particle size distribution, dm/d log D	92
34	Outlet emission rates between raps for various size intervals	94
35	Outlet emission rates measured with the impactors as a function of the time interval between raps	95
36	Average particulate load during a rap as a function of the time interval between raps	96
37	Particle size distribution for rapping puffs, dm/d log D's (average volume of gas sampled during the rapping puffs was determined from the sampling rate and the average persistence time of the rapping puffs) tests 5, 4 & 6, 7 & 8 had 12, 32, and 52 minutes, respectively, between-rap intervals	97
38	Cumulative percent distribution for rapping puffs, lower 32% of the precipitator cross sectional area, rapping intervals of 12, 32 and 52 minutes	98
39	Mass emission rates for rapping reentrainment, lower 32% of precipitator exit for various particle size intervals	100
40	Mass emission rates for rapping reentrainment, upper 68% of precipitator exit for various particle size intervals	101

FIGURES
(continued)

No.		Page
41	Percent emissions due to rapping reentrainment as a function of particle size	102
42	Spatial distribution of between rap emissions for various particle sizes	105
43	Spatial distribution of particles in upstream and downstream rapping puffs for 12 minute rap interval test	108
44	Spatial distribution of particles in combined upstream and downstream rapping puff	109
45	Rapping puffs lower portion of the precipitator, 32 minutes between raps. First set of puffs, upstream rap. Second set of puffs, downstream rap.	110
46	Rapping puffs upper portion of the precipitator, 32 minutes between raps. First set of puffs, upstream rap. Second set of puffs, downstream rap.	111
47	Rapping puffs, lower portion of the precipitator, 12 minutes between raps. First set of puffs, upstream rap. Second set of puffs, downstream rap.	112
48	Rapping puffs, upper portion of the precipitator, 12 minutes between raps. First set of puffs, upstream rap. Second set of puffs, downstream rap.	113
49	Percent contribution of a rapping puff to total emissions for several particle size bands as a function of the time interval between raps	116
50	Correlation of mass of dust removed from plate 4-1 and amplitude of Konitest meter current output for the upstream rapping puff for test 5 (12 minute rap interval)	120
51	Load cell data, mass collected on plate 4-1, 12 minute interval between raps	123
52	Load cell data, mass collected on plates 4-2 and 4-3, 12 minute intervals between raps	124

FIGURES
(continued)

No.		Page
53	Load cell data, mass collected on plate 4-1, 32 minute intervals between raps	125
54	Load cell data, mass collected on plates 4-2 and 4-3, 32 minute intervals between raps	126
55	Collection rate of particulate as a function of time interval between raps	127
56	Dust removal efficiency for dust on plate 4-1 versus the time interval between raps	130
57	Collection rate versus horizontal location in the precipitator	135
58	Fractional collection efficiency versus particle size, solid line theory, circles experimental between rap, diamonds experimental, include rapping reentrainment	136
59	Percentage of total emission due to rapping reentrainment	139

TABLES

No.		Page
1	Estimates and measurements, tensile strengths of precipitated fly ash layers	12
2	Design parameters, FluiDyne pilot precipitator	22
3	In situ resistivity data	49
4	Chemical analysis of Black Dog fly ash, percent by weight	52
5	Composition of gas entering the FluiDyne pilot precipitator	53
6	Average electrical conditions	55
7	Average velocities 76 cm downstream of the exit baffles	59
8	Volume flow rates during the test	62
9	Inlet particulate load and particulate feed rates	64
10	Composite average of plate accelerations during rapping for $\Delta P = 6.2 \times 10^5$ Pa, dust covered plate	66
11	Composite average of plate accelerations during rapping for $\Delta P = 4.8 \times 10^5$ Pa, dust covered plate	67
12	Composite average of plate accelerations during rapping for $\Delta P = 6.2 \times 10^5$ Pa, clean plates	71
13	Composite average of plate accelerations during rapping with modified rappers for $\Delta P = 6.2 \times 10^5$ Pa, light dust layer	72
14	Ratio of relative total emissions between raps in five particle size intervals for rapping intervals of 12, 32, and 52 minutes	106
15	Comparison of real-time system data and impaction data obtained between raps	118

TABLES

No.		Page
16	Mass per unit area on plates when rapped, mass per unit area collected between raps and mass per unit area removed by rap	129
17	Effect of rapping reentrainment on efficiency for rapping losses accounting for 20%, 30%, 40%, and 50% of emissions for various overall efficiencies (first approach)	141
18	Effect of rapping reentrainment on performance for various reentrainment percentages as a function of number of sections and a constant collection efficiency per section (second approach)	142
19	Fraction of collected material for a given particle size i that was emitted due to rapping reentrainment	147

ACKNOWLEDGEMENTS

The assistance of the staff of FluiDyne Engineering in conducting the experiments is gratefully acknowledged. The descriptions of the FluiDyne facility contained in this report were drafted by Dr. Henry Hanson of FluiDyne Engineering.

SECTION I

SUMMARY

An experimental investigation of rapping reentrainment was performed in a nearly full-scale pilot precipitator at FluiDyne Engineering Corporation's Rosemount Laboratory. The objectives of the experimental study included a fundamental study of the mechanics of removal of dry dust by rapping and the quantification of rapping reentrainment in terms of the percentage total emissions and particle size distribution of the reentrained dust.

During the experiment the percentage of dust removed from the plates was observed to depend on the mass per unit area of dust collected on the plates as predicted by theory. The build-up of a residual dust layer was also observed. A dust layer developed that could not be removed with the available rapping intensities (up to 20 G's).

During the study the contribution of rapping reentrainment to total emissions ranged from 53% to 18%, depending on rapping conditions. These percentages corresponded to 5.4% and 2.7%, respectively, of the dust collected on the plates being emitted from the precipitator during plate rapping. A significant decrease in rapping emissions was obtained by increasing the time interval between raps. This decrease was due to the resulting larger mass per unit area collected on the plates when they were rapped. Particle size distribution measurements showed that the mass median diameter of the particles emitted during the raps increased with increased time between raps. As would be expected, this produced lower overall emissions. The increase in the size of the particles emitted during rapping was ascribed to an increase in the agglomeration of the particulate removed from the precipitator plates with the respective increase in the mass per unit area collected on the plates (thicker dust layers) before the plates were rapped.

A major portion of the reentrained material was observed to result from hopper "boil-up". A small portion of the dust was observed to pass out the precipitator in a short burst at the velocity of the gas passing through the unit, while the remaining portion of the material was observed to fall into the hoppers, then to rebound, and finally to escape slowly over the baffles and out of the precipitator. This produced a significant vertical gradient in the concentration of the dust emitted from the precipitator due to rapping reentrainment.

The fractional collection efficiencies of the precipitator both excluding and including rapping reentrainment emissions were determined and compared with theoretical values. Rapping reentrainment increased the discrepancy between theory and measured fractional collection efficiencies for particles larger than 5 μm. However, rapping reentrainment did not account for all of the discrepancy. Reentrainment between raps and sneakage through the unelectrified regions of the precipitator appeared to contribute significantly to overall emissions.

The experiments pointed out some problems in detailed mathematical modelling of rapping reentrainment. It is difficult to predict the quantity of dust removed from a plate by an individual rap The calculation of the recollection of the reentrained material is difficult for several reasons. The particle size distribution of the reentrained particles can be changed significantly by moderate changes in rapping variables. Hopper boil-up also makes the calculation of the recollection of the reentrained dust difficult, since much of the reentrained material is in unelectrified regions of the precipitator. However, the experiments supplied some general values that could be used to estimate the effects of rapping reentrainment on the size of a precipitator for a given collection efficiency.

Two approaches using simplified assumptions were used to make estimates. The first assumed that a fixed percentage of rapping reentrainment emissions was emitted from a precipitator independent of the size of the unit, and the second assumed that the same percentage of collected unclean material was reentrained and emitted from each section due to rapping and that the recollection efficiency for the reentrained material for all sections having the same between rap collection efficiency. The estimates based on the above approaches showed that the increase in precipitator size needed to recover the rapping reentrainment emissions can account for 6% to greater than 80% of the size of the unit for the cases considered.

Rapping reentrainment emissions computed on the basis of the percentages obtained at FluiDyne account for a significant portion of precipitator emissions.

FUTURE RESEARCH

The parameters studied during the FluiDyne experiment were somewhat limited. A data bank for detailed modelling of rapping needs to include additional data on rapping emissions as a function of plate accelerations and gas velocity. The FluiDyne experiments also show the need for studies with multi-section precipitators.

The FluiDyne experiments also indicated a need for a study of the parameters affecting hopper "boil-up" and the development of methods for removing it. Conditioning with SO_3 and continuous removal of dust from the hoppers may be helpful, along with proper baffling. Additional studies on the effects of residual dust layers for high resistivity dust and studies of dust cohesive properties are also needed to aid in determining optimum rapping conditions.

SECTION II
INTRODUCTION

The efficiency of an electrostatic precipitator is governed by the quantity of dust that passes through the electrified region without being collected and the amount of collected material which is reentrained in the effluent. Reentrainment losses are the result of several factors. The primary one is that associated with rapping of the collection plates.

This report discusses the results of an experimental investigation of rapping reentrainment using a nearly full-scale pilot precipitator at FluiDyne Engineering Corporation's Rosemount Laboratory. The work had three main objectives: (1) a study of the basic mechanics of removal of dry dust by rapping and the variations in the removal mechanisms with changes in dust properties, (2) quantification of rapping reentrainment in terms of the percentage of the total losses, and of the particle size distribution of the reentrained dust, and (3) modification of the Southern Research Institute computer systems model to include losses due to rapping reentrainment.

BACKGROUND

The removal of particulate from a gas stream by a dry electrostatic precipitator involves four separate processes. The first is the precipitation of the particulate from the gas stream onto the collection plate. A recent Southern Research Institute report discusses the physical mechanisms involved and describes a computer model for the removal of the dust from the gas stream.[1] The second process is the removal of the particulate from the collection plate, and the third is the transfer of this particulate to a hopper. The fourth process is the removal of the collected particulate from the hopper to a disposal area.

In present-day precipitator applications, two philosophies are prevalent with regard to the removal and transfer of the particulate from the collecting plates. One approach is to rap often and to provide maximum rapping acceleration to the collection plates during each rap in an attempt to minimize the thickness of the residual dust layer. The other approach is to vary the intensity and frequency of rapping in an attempt to minimize the quantity of material reentrained.

The uncertainties with regard to rapping procedure are associated with the method by which dust is actually removed and transferred from the collection plates during a rapping sequence. Sproull[2] suggests that the rapping process occurs in a sequence whereby the collected dust is removed by what is termed a slip-stick process. The concept is that the dust layer builds up to a sufficient thickness so that the acceleration of the plate causes a shearing force between the dust layer and the plate. The dust then slides along the surface of the plate until it is recollected on the plate. The process is repeated with each successive rap until the dust finally falls into the hopper.

Another concept of rapping is that the collected dust is dislodged in large agglomerates or clumps and falls directly into the hopper without being recollected.

The mechanics of the dust removal process varies with the properties of the dust, precipitator operating conditions, and rapping parameters. The dust properties and precipitator operating conditions affect the adhesion and cohesion of the dust layer. The adhesion and cohesion of dust layers depend upon particle-to-particle forces. According to Tassicker[3], the forces comprise London-van der Waals, triboelectric, capillary, surface dipole, and electric-field corona forces. These component forces are influenced by the following: particle diameter, porosity and compaction of the layer, complex dielectric constant, humidity in the gas, adsorbed surface dipolar molecules, work-function interfaces on the material, and the electric field and current density in the dust layer.

The tensile strength of a dust layer is the longitudinal stress (force per unit area) that the layer can bear without tearing apart. Tassicker[3] has formulated the following equation for the tensile strength of a dust layer with a given degree of compaction by appropriately combining the above mentioned forces.

Tensile Strength of Dust for Given Degree of Compaction

$$P = (A_1/d)+(A_2/d) + 10^5(\varepsilon_0/2)[\varepsilon^1(J\rho k)^2 - E_g^2] \qquad (1)$$

where

A_1 = van der Waals and dipole constant
A_2 = the capillary constant
ε_0 = permittivity of free space
ε^1 = relative permittivity of dust
J = current density in dust layer
ρ = resistivity of dust layer
k = constant from 1 to 20 depending upon particle elasticity
E_g = electric field in gas space, (applied potential)/(electrode spacing)
d = particle diameter

According to this equation, the capillary, van der Waals, and dipole components are always adhesive and inversely proportional to particle diameter. The electrical components can be either adhesive or nonadhesive, depending on the resistivity of the particulate and the current density in the layer.

The development of this equation for the tensile strength of dust layers is discussed by Tassicker in his dissertation.[4] Tassicker estimates that the magnitude of the shear strength is probably twice that of the tensile strength. Data obtained by Sproull[5] also indicates that shear strengths are relatively larger than tensile strengths. Experiments by Ruckelhausen,[6] Brandt,[7] and Watson and Blecher[8] emphasized that it is peak acceleration normal to the precipitator plates which is effective in dislodging the collected particulate. Nevertheless, when shear accelerations are present, they must play some role in particle dislodgement, as indicated by the data obtained by Koschany,[9] who found that the peak normal acceleration required to attain a given percentage removal of particulate from a precipitator plate decreased as shear accelerations, applied simultaneously, increased.

Theory of the Mechanics of Dust Removal

An elementary theory of dust removal which considers only the tensile strength (P) of the dust layer and the acceleration (a) normal to the plate has been developed by Tassicker.[10] The theory shows that the dust layer is removed only when

$$a > \frac{P}{\delta \ell} = \frac{P}{M/A} \qquad (2)$$

where δ is the bulk density, ℓ is the dust layer thickness, and M/A the mass per unit area. Equation (2) shows that, for a given dust thickness, the rapping intensity must be of sufficient magnitude to produce an acceleration greater than the ratio of the tensile strength of the ash layer and the mass per unit area. Also, Tassicker shows that dust is removed for a given acceleration only when

$$M/A > P/a; \tag{3}$$

that is, when the mass per unit area is greater than the ratio of dust layer tensile strength to the normal plate acceleration. Since the mass per unit area depends on the dust layer thickness, which in turn is related to collection time between raps, the time interval between the raps is directly related to the efficiency of dust removal from the plates.

Tassicker also indicates that the maximum stress occurs at the boundary between the plate and the dust layer. However, in an operating precipitator, a thin layer is often left when a plate is rapped, indicating a stronger tensile strength between the plate and the dust than between particles in the dust layer.

When a thin skin of unremoved dust develops, 100% removal is not obtained. Dust is removed only for a dust layer thickness $\ell_1 + \ell_0$, where ℓ_0 is the thickness of the unremoved layer and ℓ_1 is the layer thickness needed to provide enough stress to break the dust layer for a given acceleration. Thus the efficiency of dust removal is a function of dust layer thickness, as shown in Figure 1. In practice the sharp step is not observed, as shown in the data obtained by Sproull[5] (Figure 2). The dependence of dust removal efficiency on mass/unit area (related to dust thickness) was also observed by Plato.[11]

Estimates of the tensile strength of fly ash were obtained from Equation (2) and tabulated in Table 1 from Sproull's data.[5]

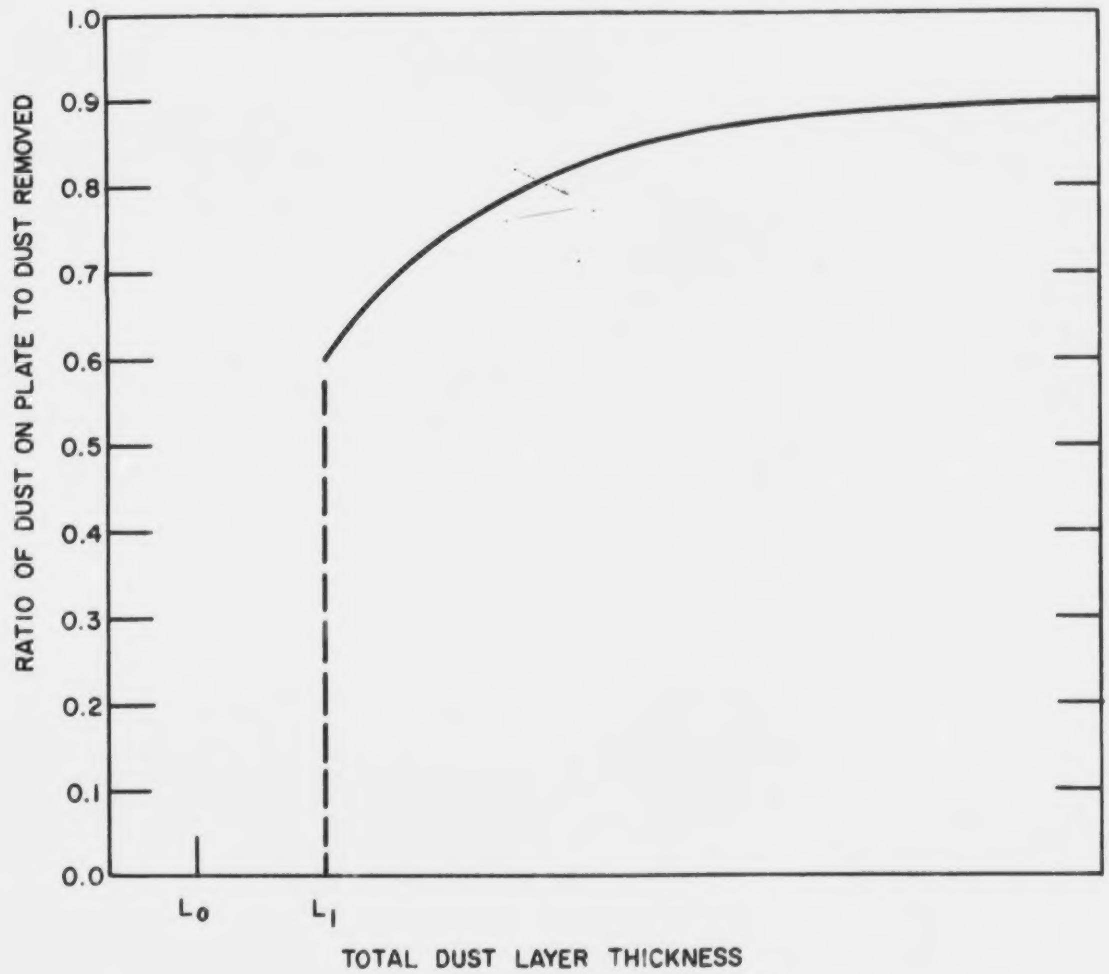

Figure 1. Theoretical efficiency of dust removal as a function of dust layer thickness.

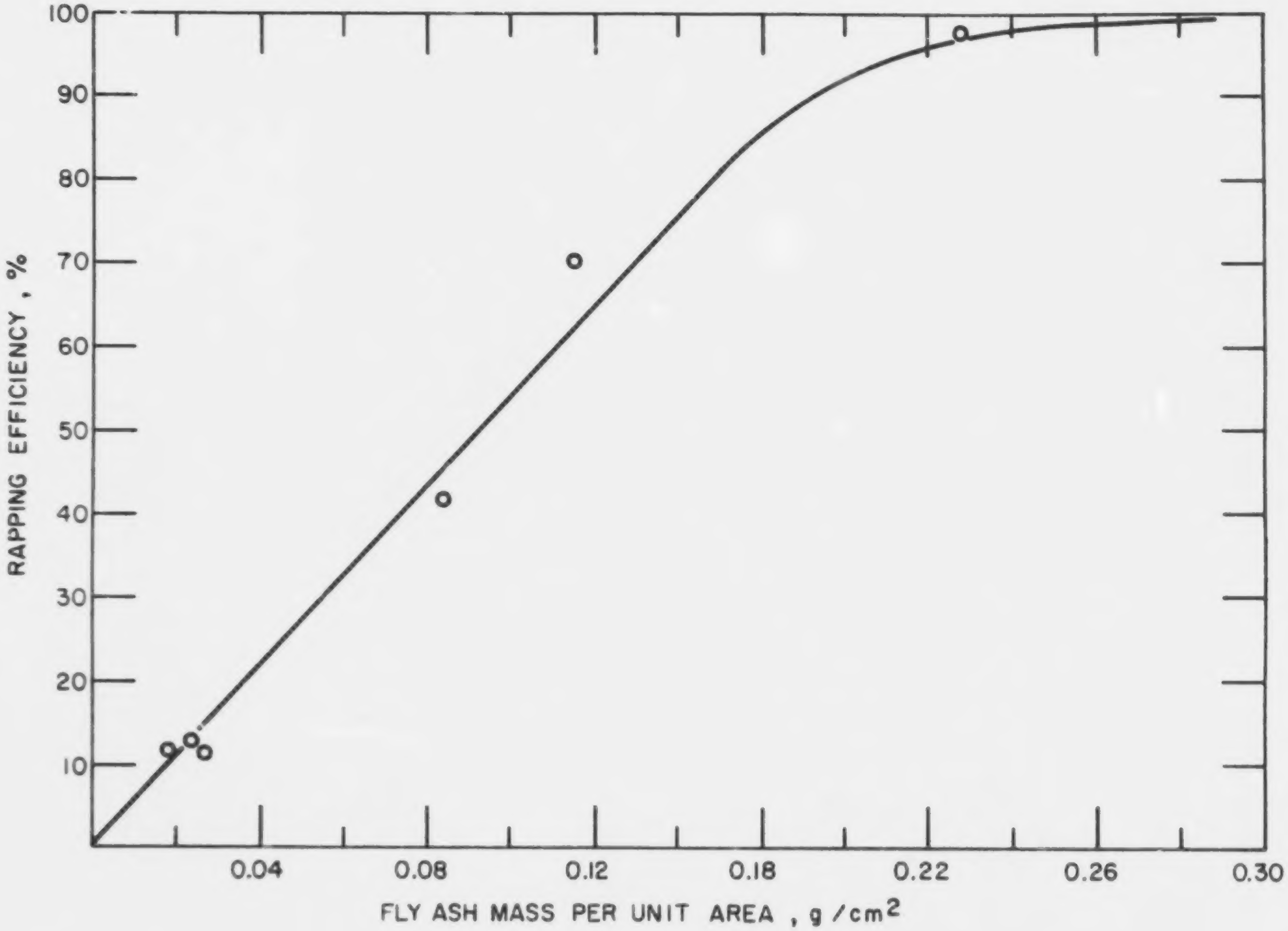

Figure 2. Rapping efficiency as a function of mass per unit area for a precipitated fly ash at 150°C, rapped with a maximum normal acceleration of 1.3 x 10^4 cm/sec^2 (13G); measured by Sproull.[5]

Table 1

ESTIMATES AND MEASUREMENTS
TENSILE STRENGTHS OF PRECIPITATED FLY ASH LAYERS

Percent Removal	Mass/Unit Area	Acceleration		Tensile Strength	Source
	g/cm^2	cm/sec^2	(G's)	$dynes/cm^2$	
90	0.17	1.3×10^4	(13)	2.2×10^3	Calculated using eq. 2, Sproull,[5] Fly ash 150°C, Power on
90	0.03	3.1×10^4	(32)	0.97×10^3	Calculated using eq. 2, Sproull,[5] Fly ash 150°C, Power on
89	0.04	6.3×10^4	(64)	2.5×10^3	Measured with precipifuge, Tassicker[4]
-	0.21	4.2×10^3	(4.3)	0.89×10^3	Measured with centrifuge, Penney and Klingler[13]
-	0.04	3.8×10^4	(39)	1.7×10^3	Measured with centrifuge, Penney and Klingler[13]
-	0.08	3.4×10^4	(35)	2.7×10^3	Measured with centrifuge, Penney and Klingler[13]
-	0.01	1.9×10^4	(19.5)	2.2×10^3	Measured with centrifuge, Penney and Klingler[13]
-	0.004	1.2×10^4	(12.0)	0.53×10^3	Measured with centrifuge, Penney and Klingler[13]
-	---	----		$1 \times 10^2 - 3 \times 10^3$*	Measured with power tensiometer, Dalmon and Tidy[14]

*Bulk density $0.2\ g/cm^3$ - $0.9\ g/cm^3$
no electric field, mechanically deposited.

Also included in the table are the results of laboratory measurements by Tassicker,[12] Penney and Klingler,[13] and Dalmon and Tidy.[14] These data indicate that the tensile strength of precipitated fly ash layers range from 0.5×10^3 dynes/cm^2 to 3×10^3 dynes/cm^2. As will be seen later, the tensile strength of the ash used during the FluiDyne experiments appears to also fall in this range of values.

Quantity of Material Reentrained

The intent of this research project was not only to study the mechanics of dust removal from the precipitator plates but also to determine quantitatively the amount of material reentrained under conditions representative of those found in full-scale precipitators. In an earlier study of reentrainment in a full-scale precipitator, Sproull[2] observed that emissions for a single rapping puff increased with time between raps and concluded that overall rapping emissions could be reduced by lessening the rap intervals, although he recognized that the interval should not be less than the minimum required for dust removal. It appears that he did not consider the cumulative effect of more frequent rapping. In addition, Sproull concluded that the rapping intensity should be kept to a minimum. Sproull observed a vertical stratification of the emissions during rapping with higher concentrations in the lower portion of the precipitator. Sproull's results on the frequency of rapping are somewhat contrary to the results obtained in the laboratory by Plato,[11] and by Sanayev and Reshidov,[15] who observed a reduction in the fraction of collected dust reentrained for larger accumulations on the plates. By increasing the time interval between raps, Plato,[11] Schwartz and Lieberstein,[16] and Nichols, Spencer, and McCain[17] have all observed improvements in performance of full-scale precipitators.

The time interval between raps and the intensity of the rap are the two major variables for the rapping study. The lack of quantitative measurements of all the parameters affecting rapping reentrainment probably accounts for the differences in the conclusions drawn from different investigations and for the large range of approaches to rapping used by various manufacturers.

Although the previous studies have added to our understanding of rapping reentrainment, they have not provided enough quantitative data to aid in calculations of the effect of rapping reentrainment losses on overall efficiency.

Penetration Including Rapping Reentrainment

Francis[18] has developed an expression for the penetration dust through a precipitator which includes losses due to rapping reentrainment.

$$P_T = [R + (1-R)(1-\eta)^{1/N}]^N \qquad (4)$$

where

P_T = penetration corrected for reentrainment

N = number of stages over which reentrainment is assumed to occur

R = fraction of collected material reentrained per section

η = fractional collection efficiency of a given particle size obtained with no reentrainment.

Francis assumed that a fixed fraction of the collected material of a given particle size is reentrained, and that the fraction does not vary with the length through the precipitator. A modification of Francis' development gives the fractional contribution of rapping reentrainment to emissions (f_R) for a given particle size to total emissions for a particle size as

$$f_R = \frac{R}{(1/\eta_i - 1) + R} \qquad (5)$$

in terms of the sectional efficiency (η_i) for each particle size or as

$$f_R = \frac{R[1-(1-\eta)^{1/N}]}{(R-1)\ [1-(1-\eta)^{1/N}]+1} \qquad (6)$$

in terms of the total collection efficiency of a given particle size with no reentrainment. These equations indicate that the percent contribution can be decreased by increasing the sectionalization of the precipitator and by decreasing the fraction of reentrained material (R). Quantitative measurements of f_R (fractional contribution rapping reentrainment to emissions for a given particle size) and η_i (sectional efficiency for a particle size) were obtained during the experiments discussed in this report for a limited set of parameters.

Other Methods of Dust Removal

There are two methods to dust removal from precipitator plates other than rapping. One method is to wash the plates, as in the so-called wet precipitator. This type of equipment is commercially available and is used in processes where rapping has not been a satisfactory method of removing the dust from the plates. Wet precipitators are sometimes also used for high resistivity dust. A second method is to use scrapers. However, the applications of scrapers are limited by expense and by the difficult mechanical problems involved in operating them in the harsh environments found inside industrial precipitators.

TEST PROGRAM

A test program was developed and carried out at FluiDyne to meet the objectives of this rapping reentrainment study. The following test program was completed during two weeks of testing.

The first week consisted of setting up equipment and preliminary tests and was followed by a second week of extensive testing that generated a substantial quantity of data.

Test Program During First Week at FluiDyne

June 16	Unloaded and set up equipment.
June 17	Set up equipment; turned burners on; measured clean plate rapping accelerations.
June 18	Began Testing. Conditioned impactor blanks, tested for weight gains, measured clean plate V-I characteristics, measured gas velocity at sampling locations, adjusted for desired flow, measured gas velocities at entrance and exit planes of the precipitator, tested dust feed system, tested real time sampling system.
June 19	Measured inlet particle size distribution, measured inlet grain loading, tested load cells, determined if rotating mass trains and impactors could detect rapping puffs, determined amount of dust picked up by rapping puff impactors and mass sampling train when pointed 110° downstream from the flow direction, measured dust resistivity, adjusted moisture and temperature for 10^{10} Ω-cm resistivity of fly ash.
June 20	Ran efficiency test with following conditions: Dust feed Current density - 23 nA/cm^2 Gas velocity between plates - $\sim$0.91 m/sec Rapper intensity - 80% of maximum Rapper interval - 30 minutes inlet (upstream rapper) - 60 minutes outlet (downstream rapper).

Test Program Second Week at FluiDyne

June 23	Start intensive test program. All variables except rapping intensity and time interval between raps were held constant. The quantity of dust reentrained and the variables affecting reentrainment were measured.	
	Test 1	150 minutes between raps, rapping intensity 100% of maximum, 1 rap
	Test 2	120 minutes between raps, rapping intensity 100% of maximum, 1 rap
June 24	Test 3	12 minutes between raps, rapping intensity 80% of maximum, 6 raps
	Test 4	32 minutes between raps, rapping intensity 80% of maximum, 3 raps
June 25	Test 5	12 minutes between raps, rapping intensity 100% of maximum, 6 raps
	Test 6	32 minutes between raps, rapping intensity 100% of maximum, 3 raps
June 26	Test 7	52 minutes between raps, rapping intensity 80% of maximum, 3 raps
	Test 8	52 minutes between raps, rapping intensity 100% of maximum, 2 raps (rain and wind knocked out electrical power and burners, test was terminated 15 minutes after second rap)
June 27	Test 9	Deleted due to internal electrical short in the precipitator.

The following test procedure was utilized for each of the tests during the second week of testing.

Before the start of each test, sampling probes and the pilot precipitator were warmed up to the desired operating temperature. The gas velocity at the outlet sampling ports was then measured. The precipitator hoppers were emptied and the dust feed hoppers were filled. The dust feed was then turn on, checked with continuous monitors and allowed to stabilize. The plates were then rapped. Once the rapping puff was over as indicated by the real time sampling systems, a test was started. At the end of the between-rap time interval, mass trains and impactor probes were shut down and rotated out of the gas flow. The dust feed was then turned off. When the outlet real time system could no longer detect particulate, a separate set of mass sampling probes and impactors were rotated into the gas stream to measure emissions from rapping. The plates were then rapped, first with an upstream rapper and then with a downstream rapper. After the rapping puffs had passed the rapping puff mass sampling trains, probes and impactor probes were rotated out of the gas stream. The dust feed was then turned on again and sampling with the between-rap systems was resumed. A semi-traverse of one outlet lane with the mass train system was obtained for the rapping puffs by sampling at three separate vertical locations with two probes. The rapping tests were set up so that for each test condition, rapping puffs were sampled in multiples of three, except for the long interval tests.

The experimental arrangement, test conditions, results of the experiments and analysis of the data are discussed in the following sections.

SECTION III
EXPERIMENTAL ARRANGEMENT

This study of rapping reentrainment was conducted in a nearly full-scale pilot precipitator owned and operated by FluiDyne Engineering. The precipitator is equipped with extensive instrumentation. The FluiDyne Engineering facility, the test apparatus, and the operating procedures used during this investigation are discussed in this section.

FLUIDYNE ENGINEERING TEST FACILITY

The test facility at FluiDyne is illustrated in Figures 3 and 4. The test facility was selected for this study because it closely represented operation of a full-scale unit while at the same time providing a facility for studying a variety of rapping variables. The ability to turn the dust feed on and off during the tests simplified the measurements of emissions due to rapping reentrainment. A detailed description of the facility follows.

Precipitator Design

The design parameters for the precipitator are tabulated in Table 2.

This pilot-scale precipitator effectively represents one electrical section in a full-scale precipitator. The six meter plate height is high enough that the reentrainment loss should be approximately representative of those in a full-scale unit. The precipitator was originally constructed to study operation of a full-scale unit.

In the original design, the plates in the precipitator were constructed from expanded metal. For this rapping reentrainment

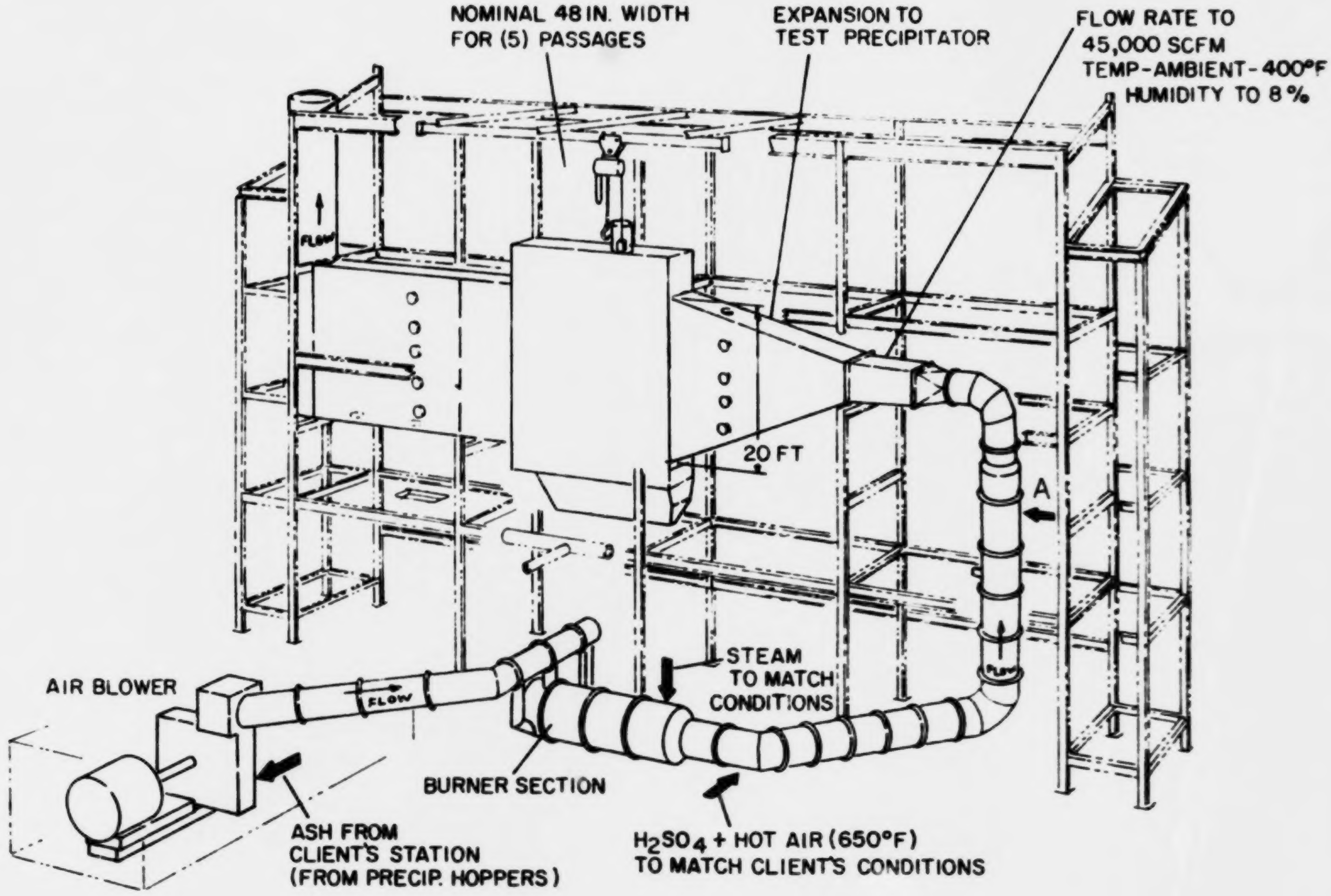

Figure 3. Near full scale pilot precipitator at FluiDyne Engineering.

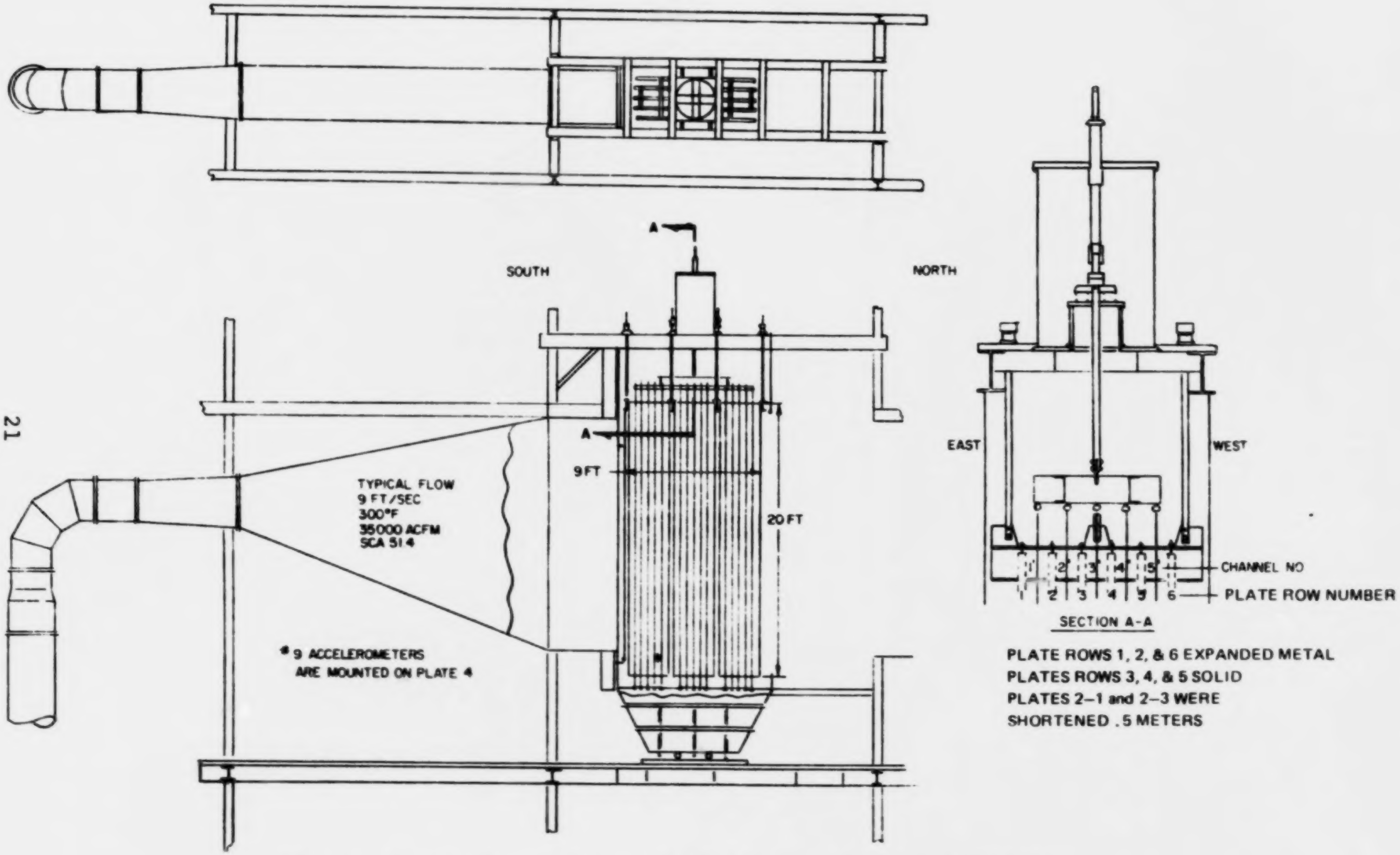

Figure 4. Various views of FluiDyne pilot precipitator.

Table 2

DESIGN PARAMETERS, FLUIDYNE PILOT PRECIPITATOR

Design Parameters	Units
Number of electrical sections in direction of gas flow	1
Length of electrical sections	2.7 m
Plate area of each electrical section	167 m^2
Total length of corona wire per electrical section	457 m
Corona wire	0.48 cm (square wire)
Wire-to-plate spacing	11 cm
Number of wires per linear section	75
One-half wire-to-wire spacing	7.6 cm

study three of these plates were replaced to provide two lanes with solid plates on each side of the lane. Outlet sampling was confined to the lanes with solid plates.

Plate Construction -
There are 18 (0.9 m x 6 m) plates in the precipitator. The six rows of plates are numbered from one to six as viewed from the outlet looking towards the inlet and numbering from left to right. Rows 1, 2, and 6 have expanded metal plates, and rows 3, 4, and 5 have solid plates. Plates in each row are numbered from 1 to 3 from the inlet to the outlet. Lanes are number 1', 2', 3', 4', and 5' from left to right as viewed looking from the outlet towards the inlet.

The solid plates are constructed from 18 ga. (1.2 mm) hot rolled steel with 4.4 cm x 3.2 cm x 0.32 cm angle iron on the sides. Design details are shown in Figure 5. No additional internal baffling or supports were provided. Plates 2-1 and 2-3 were shortened 0.5 meters to permit viewing of dust on the adjacent solid plates.

The plates are suspended from four I-beams by 1.3 cm threaded rods welded to the plates as shown in the Section A-A view in Figure 4. The four I-beams are supported by eight rods (4.4 cm diameter) which are floated from eight springs (McMaster Carr 9622K25).

Plate Rappers -
There are two plate rappers; one raps the upstream section of the plates (I-beam support between first and second section of plates) and the other the downstream section (I-beam support

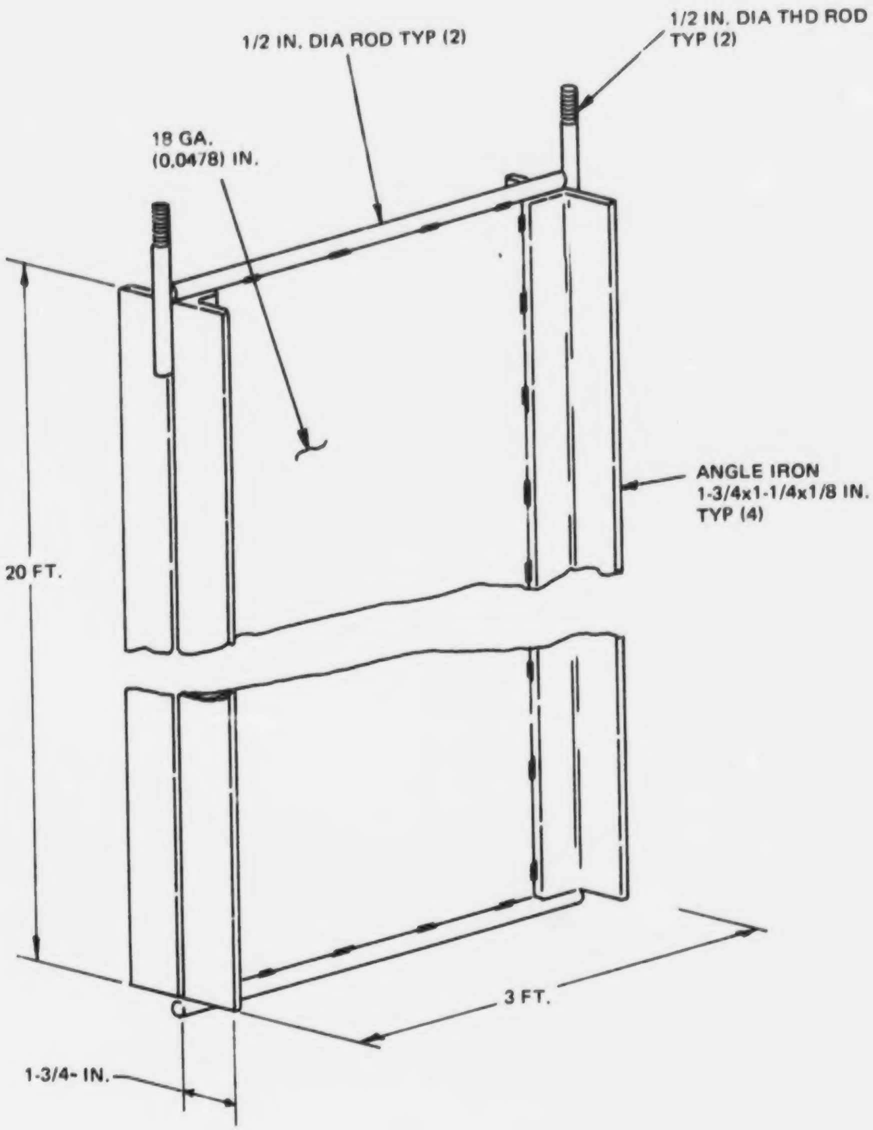
1/2 IN. DIA ROD TYP (2)
1/2 IN. DIA THD ROD TYP (2)
18 GA. (0.0478) IN.
ANGLE IRON 1-3/4x1-1/4x1/8 IN. TYP (4)
20 FT.
3 FT.
1-3/4- IN.

Figure 5. Design details for pilot precipitator plates.

between the second and third section of plates—see Figure 4). A third rapper is used to rap the high voltage section; this rapper is insulated electrically by a glass rod.

The plate rappers are the single-shot type of pneumatic rapper. The rapper weight, a cold rolled steel rod, 12.7 cm long and 7.46 cm in diameter, is housed in an air cylinder. Between raps, the rapper weight is supported in the cylinder by low-pressure [L = 1.0×10^5 Pa ($\sim$15 psi gauge)] compressed air. When a rap is desired, a signal to a solenoid valve pressurizes the other side of the cylinder and forces the weight down on top of a rod that transmits the force to a plate support beam. The compressed air used was under pressure up to 7.6×10^5 Pa (110 psi gauge) and the cylinder stroke was approximately 12.7 cm in length.

Hopper and Baffle Design -

The hopper and the baffles of the FluiDyne pilot precipitator are shown in Figure 4. The baffles that extend down from between the sections of plates come to within about 0.4 meters of the bottom surface of the hopper. There are two such baffles, one between the first and second section of plates, and one between the second and third section of plates. There is also a central baffle that extends up 0.8 meters from the floor of the hopper directly underneath the second set of plates.

Downstream of the third section of plates a baffle extends down from the top of the precipitator box to about 0.76 meters below the top of the plates. Similarly, a baffle extends up from the bottom to the level of the inlet ducting floor. At this same streamwise location lateral baffles block the space between the precipitator box walls and the outside plates.

Precipitator Power Supply -

The FluiDyne test precipitator is powered by a General Electric transformer rectifier and control. The transformer is a 480 volt primary, 93 kVA transformer with a secondary voltage of 77,200 volts. The rectifier is mounted outside the building in the transformer yard and the high voltage is transmitted to the top of the precipitator through a Belden 8871 coaxial cable. This cable runs approximately 200 feet in a 3.8 cm conduit up to the top of the precipitator. The precipitator is currently energized with full wave rectification, although the transformer rectifier is set up to provide double half wave operation if desired. The precipitator power supply control panel is mounted inside the building near the transformer rectifier. The instrumentation on the front panel of this control includes primary current and voltage and secondary high voltage and secondary direct current for both halves of the double half wave.

Other Components of the FluiDyne Facility

In addition to a nearly full-scale precipitator, the FluiDyne facility includes the systems necessary for producing simulated flue gas conditions at the inlet of the pilot precipitator.

Feed Hopper Design and Dust Dispersion System -

The dust dispersion system consists of a feed hopper and a primary blower which provides a forced draft to the precipitator. The feed hopper is a bin made out of sheet metal in the form of a cone with a cylindrical extension on top of it. The 1.8 meter high feed hopper is filled by pneumatically transferring fly ash through a 5 cm pipe from fly ash storage tanks which are located outside of the building wall. The hopper holds about 680 kg of fly ash and has a 8.9 cm outlet at the bottom of the cone. A dry chemical screw feeder has been adapted to the bottom outlet of the large feed hopper. This screw feeder consists of a flexible vinyl trough having a 10 cm diameter feed helix at the bottom which is rotated by a variable speed motor which can be set from 0 to 80 rpm. Dust flow rates up to 362 kg (800 pounds) per hour can be maintained. The dust is kept flowing through the 8.9 cm outlet into the small hopper of the dry chemical screw feeder by vibrating the large feed hopper with a pneumatically powered vibrator. The dust that is fed out of the screw feeder falls into a funnel which is connected to a 7.6 cm line running over to the inlet plenum of the primary blower that supplies the gas for the entire precipitator test system. The blower acts to mix the dust well into the air flow. The weight of the entire dust system is measured by a FluiDyne Flex-Cell. The load cell is powered by a low voltage direct current power supply and the signal is amplified and displayed on a pair of pen recorders. One of these recorders is calibrated to display the total capacity in pounds of the feed hopper system. The other recorder has a much higher sensitivity and also an adjustable bias so that only a small portion of the hopper load is displayed on the range of the chart. The slope of the load trace on this second recorder is used in setting the dust flow rate out of the hopper system.

Oil Burner System -

Three oil burners, each of which is rated at approximately 2.9 mw are used to heat the test gas stream to the desired temperature level. These burners are mounted in a large tank in the gas flow path downstream of the primary blower and fired horizontally (see Figure 3). Any or all of these oil burners can be fired simultaneously. Temperature control is achieved by adjusting individual burner outputs and/or changing the number of energized burners. During most of the test runs only two burners were used.

Number 2 fuel oil is used in these burners.

Water Injection System -

The gas flow through the precipitator test system is conditioned by injecting and vaporizing a known amount of water into the gas flow. This is accomplished utilizing three atomization nozzles, each of which has a capacity of about eleven liters of water per minute. The water is atomized using compressed air and is vaporized by the same burners that heat the system gas flow up to the design temperature. The amount of water injected in this manner is measured by a pair of flow meters in the water line, and the amount of water is determined by taking into consideration the over-all volumetric content of water desired, the atmospheric humidity, and the amount of water in the gas flow due to the combustion of oil. Typically, the amount of moisture due to atmospheric humidity runs about 1% or as much as 2% during very humid days. The amount of water from the combustion of oil can amount to about 0.5 to 1% and the rest of the water up to the amount desired is then added through the water vaporization nozzles.

TEST APPARATUS AND OPERATING PROCEDURES

The instrumentation for this study of rapping reentrainment characteristics in the FluiDyne Engineering pilot precipitator provided quantitative data about the parameters that affect rapping reentrainment and the effect of rapping reentrainment on overall precipitator operation.

A block diagram (Figure 6) of the experimental layout for the rapping reentrainment study shows the instrumentation that was put together for this study. In Figure 7, the sampling locations for the real-time particle measurement system, inlet and outlet impactors, outlet mass trains, and transmissometer and resistivity probe are indicated.

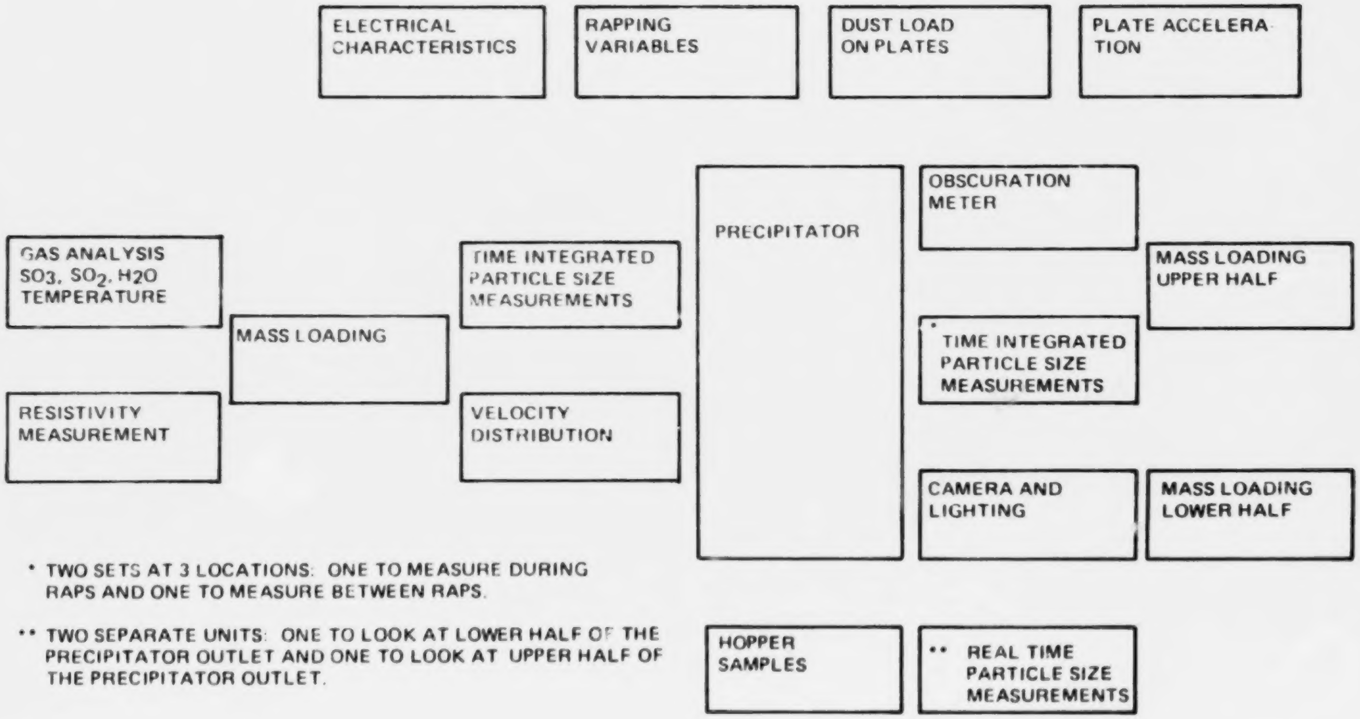

* TWO SETS AT 3 LOCATIONS: ONE TO MEASURE DURING RAPS AND ONE TO MEASURE BETWEEN RAPS.

** TWO SEPARATE UNITS: ONE TO LOOK AT LOWER HALF OF THE PRECIPITATOR OUTLET AND ONE TO LOOK AT UPPER HALF OF THE PRECIPITATOR OUTLET.

Figure 6. Block diagram of experimental layout for rapping reentrainment study.

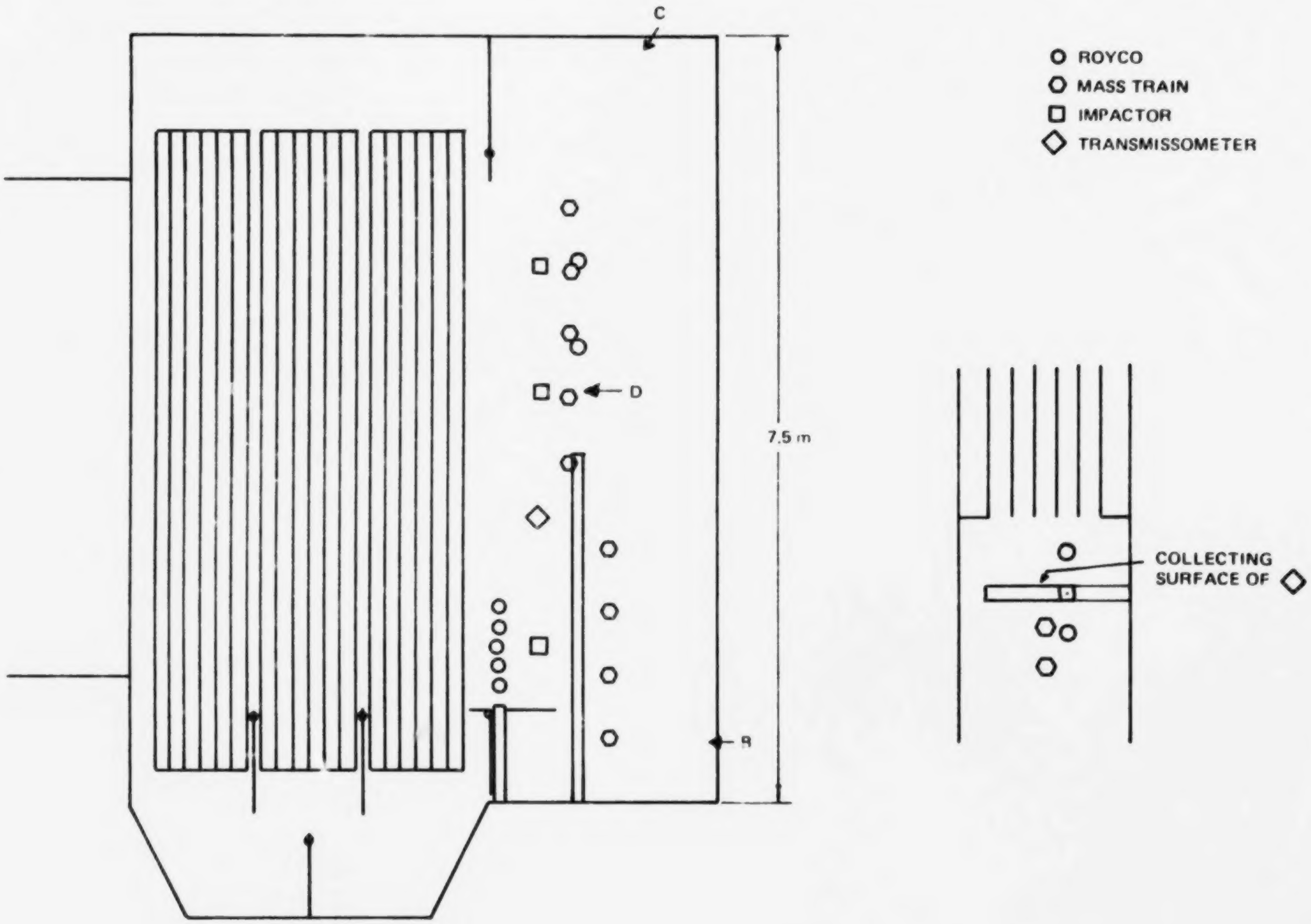

Figure 7. Sampling locations during the rapping reentrainment study.

The gas analysis apparatus, IKOR mass monitor, and inlet mass sampling trains were located in the inlet ducting at point A in Figure 3. The Konitest mass monitor was located 6 feet downstream of the precipitator in the rectangular outlet duct. Motion pictures of the rapping puffs leaving the precipitator were taken from points B, C, and D in Figure 7.

Apparatus and Operating Procedures

Mass Trains -

Three separate mass trains were used to measure inlet and outlet particulate concentrations during the rapping reentrainment test at FluiDyne Engineering. The inlet mass train consisted of an SF-Carborundum filter with a 0.95-cm nozzle on a 12-meter probe, a stainless steel condenser, a calcium sulfate drying tube, and a Research Appliance Corporation metering box. The gas velocity at the sampling point averaged approximately 8.35 m/sec in a 1.1 m diameter duct. A 16-point sampling traverse was made along two paths 90° to each other.

Two outlet sampling trains were used: (1) the upper sampling train for the upper 68% of the precipitator outlet, and (2) the lower sampling train for the lower 32% of the precipitator. As shown in Figure 7, the outlet sampling locations were approximately 1 meter from the plane of the outlet baffles. Only one lane of the precipitator was sampled. The outlet mass trains were modified so that each train consisted of two systems. One system was used to measure emissions between raps and the other system was used to measure emissions during the raps. Each outlet sampling probe consisted of a 2.5 cm pipe, to the end of which two 47 mm Gelman filters with 1.25 cm nozzles pointed 110° apart were attached. Separate 0.95 cm copper tubes were run to each filter from a three-way valve. The valve was used to connect the appropriate filter to the condenser and modified metering box. The metering boxes at the outlet were modified to accommodate the low sampling rates at the outlet. The velocities at the sampling locations were only on the order of 1 m/sec to 0.15 m/sec. The standard metering orifices were changed to a 2.1 mm orifice to give reasonable pressure drops.

The operating procedure for the outlet mass trains was as described below. Before the start of each test a velocity traverse of the five upper sampling points and the four lower sampling points was made. The velocities obtained at these points were used for setting the sampling rates. The velocity at the inlet was periodically monitored during the day to insure that the same volume flow rate was maintained throughout the test.

One of the two filters on each of the two outlet probes was designated the between-rap sampler and the other the rapping-puff sampler. The between-rap systems were started after stable conditions were obtained, as indicated by the real-time particle size system, the transmissometer, and the Konitest meter. Before rapping the plates, sampling was discontinued and the probes were rotated so that both nozzles on each probe pointed downstream. The dust feed was then turned off. After a clear flue was obtained, the second filter was rotated into the gas stream. Sampling was resumed and the plates were rapped. When a clean stack was again obtained, sampling with this second set of filters was discontinued and the nozzles to the filters were again pointed downstream. The dust feed was then turned on and sampling was resumed again with the between-rap system.

A test was made during the early stage of the test program to insure that the filter with the nozzle pointing downstream did not pick up dust. One mass train was pointed downstream during an entire day of testing without sampling any gas. The weight gain of the filter and nozzle washing was insignificant compared to the weight gains of approximately 0.1 g by the filters that sampled dust.

The data obtained between raps were handled in the usual manner. These data gave the particulate mass loading between raps and, combined with the volume flow rate, gave the mass emission rates on an emission per hour basis. The data from the second set of filters, or rap filters, was used to calculate hourly mass emission rates from the rapping puffs, independent of the between-rap emissions. These emission rates were calculated using the following equation:

$$E_p = \frac{M_p A_s N_H}{A_N N_S} \qquad (7)$$

where

E_p = emission rate from rapping puffs

M_p = mass collected by the filter while sampling the flue gas during rapping

A_s = cross-sectional area of the precipitator sampled by the probe

A_N = cross-sectional area of the probe nozzle

N_H = number of raps per hour

N_s = number of raps sampled

The emission rates between raps and from raps were combined to obtain the overall hourly emission rate. The effective particulate grain loading, including the rapping loss, was calculated from the overall emission rate and the average volume flow rate through the precipitator.

Impactors -

The impactors used for particle-size distribution measurements were modified Brink Cascade Impactors for the inlet and Andersen Stack Samplers for the outlet.

At the inlet, the runs consisted of traverses and single-point samples. The run times were 30 minutes each at a flow rate of about 1.9x10 ^{5}m^{3}/sec (0.04 acfm). The modified Brink impactor consisted of seven stages with a precollector cyclone and a back-up filter. Its sizing range was approximately 0.5 μm to about 10 μm particle diameter.

At the outlet, four Andersen impactors sampled from two ports; each port contained two impactors. One impactor per port sampled between raps while the other sampled the rapping puffs. Before the discontinuance of the dust feed and the start of rapping, the two between-rap impactors were shut off and rotated downstream; the two rapping puff impactors were rotated upstream and sampled during the rapping sequence. After the rapping puffs ceased, these impactors were shut off and turned downstream; when the dust feed was resumed, the first two impactors were turned upstream, and sampling was continued. This procedure was repeated throughout each test. The Andersen impactors consisted of eight stages and a back-up filter and sampled at about 1.4x10 ^{4}m^{3}/sec (0.3 acfm). They also had a sizing range of approximately 0.5 μm to about 10 μm particle diameter.

Real-Time Particle Size System -

The contribution of reentrained particulate to the flue gas, in the form of rapping puffs, was measured in real time by two modified Royco Model 225 Particle Counters. The particle counters utilize five-channel analog ratemeter modules, which provide parallel monitoring of the instantaneous concentration of particles in five pre-selected diameter intervals. The diameter interval thresholds in this case were 1.5 μm, 3 μm, 6 μm, 12 μm, and 24 μm optical diameters.

The analog ratemeters, designed by Southern Research Institute for this application, have approximately a half-second response time. This resolution is good enough to show concentration changes throughout a rapping puff. The information from the analog ratemeters' five channels of output was recorded on a six-channel chart recorder. The sixth channel was shared alternately by a PILLS instrument and a transmissometer. Two eventmarkers on the recorders were used to individually indicate when the upstream and downstream rappers were energized.

The temperature and aerosol concentration limits of the particle counters require that the flue gas be diluted before measurement. Because of the very steep gradient in the number size distribution, the diluter was constructed as a size segregating device to dilute the smaller particles more extensively than the larger particles. The diluter is shown schematically in Figure 8.

The sampling probes were configured and installed in such a manner as to permit a vertical traverse to be made along the center line of one lane at the exit plane of the precipitator. Probe losses were minimized by installing the particle sampling train (probe, diluter, particle counter) underneath the outlet duct and extracting the aerosol sample through a vertical probe with a single 90° bend between the sampling point and the particle sensor. The probe and nozzle were constructed from a continuous length of 4 mm I.D. stainless steel tubing. As used in these tests, the probe flow was laminar with a Reynolds number of 100. A block diagram of the sampling train is illustrated in Figure 9.

Although the large particle sampling train had been calibrated, the data on the particulate transfer efficiency of the nozzle were badly scattered. Also, at FluiDyne a problem arose with water condensation in the sample probe tubing inside the

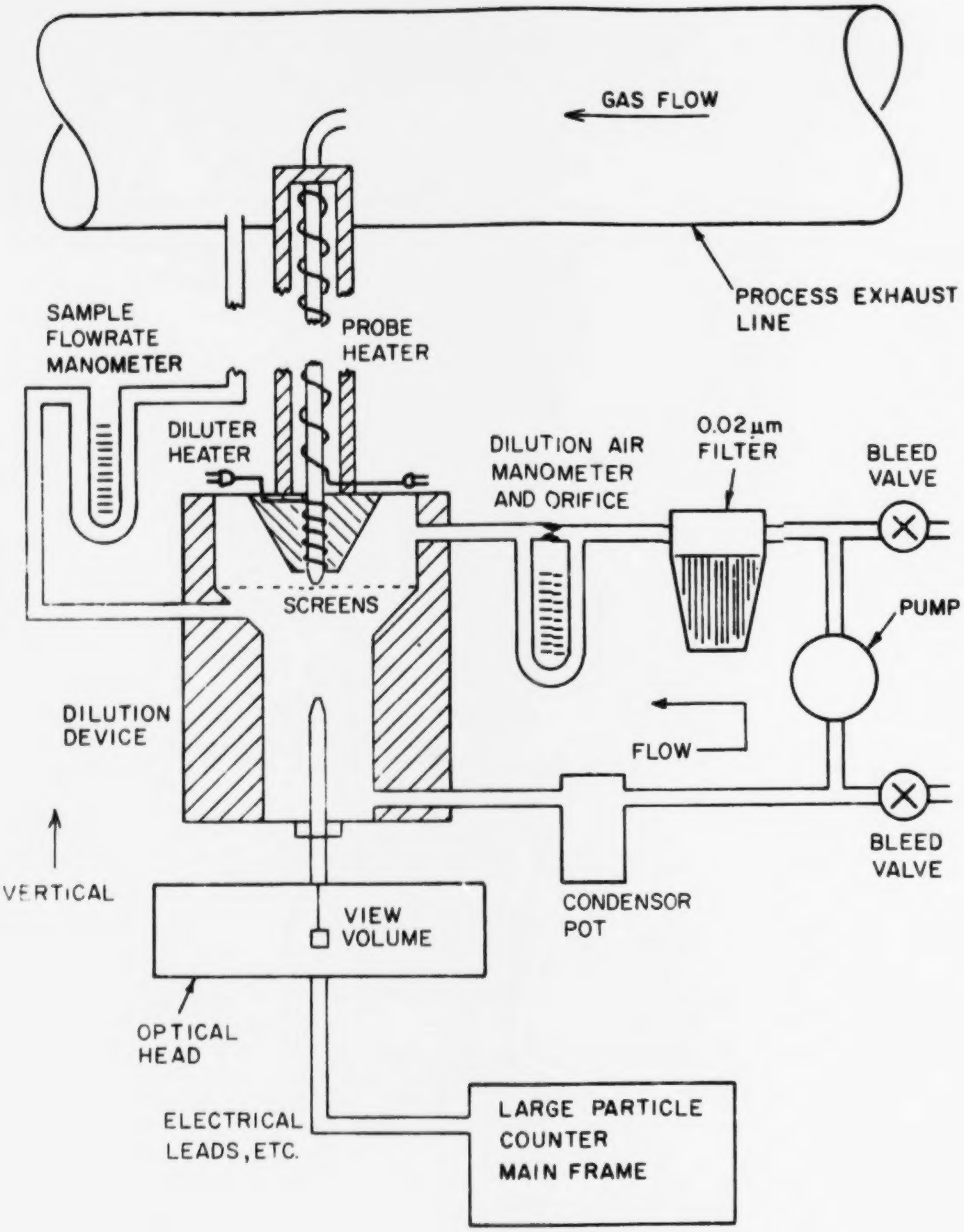

Figure 8. Schematic of diluter for large particle sizing system.

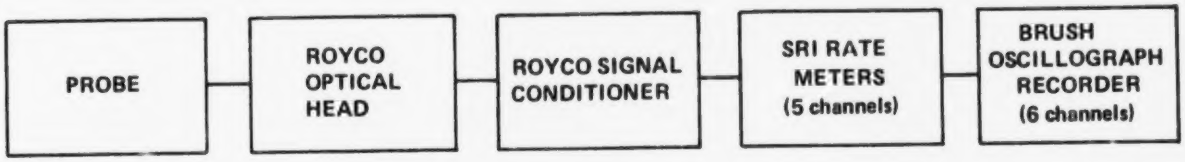
PROBE
ROYCO OPTICAL HEAD
ROYCO SIGNAL CONDITIONER
SRI RATE METERS (5 channels)
BRUSH OSCILLOGRAPH RECORDER (6 channels)

Figure 9. Block diagram of large particle sizing system.

diluter (which was unheated and in the path of the dilution air). Increasing the flow rate and adding insulation in appropriate places eliminated the condensation, but because of the required high flow rate to eliminate the condensation, isokinetic sampling was not possible. The nonisokinetic sampling and uncertain particle losses in the nozzles made it impossible to reliably determine the particulate concentrations on an absolute basis. The nozzles and sampling rates in both setups were identical, however, allowing meaningful relative comparisons of the data obtained with the two trains.

The two large-particle sampling trains had different probe lengths (2.1 meters and 5.2 meters), because the sampling location allowed only a 76 cm traverse. The 2.1 m train sampled the lower 0.76 m of the precipitator and the 5.2 m train sampled a region in the upper third of the precipitator exit. These sampling locations are shown in Figure 7. Vertical traverses were made with each large particle train while the dust feed was on. Traverses of the puffs were approximated for each rapping interval by positioning the sampling probes at different points after the dust feed was turned off and before the inlet-outlet rapping combination was started.

Load Cells -

Beam type load cells were used to monitor collection plate weights of plates 4-1, 4-2, and 4-3. The cells (Figure 10) are mounted on the plate support beam and the plate support bolt is attached to the cell beam instead of directly to the support beam. Two cells support each plate (one on each support bolt). Stops are provided to prevent excessive deflection during rapping.

The load cells were read out on a FluiDyne-Vidar System. The system has six channels of signal conditioning and the Vidar

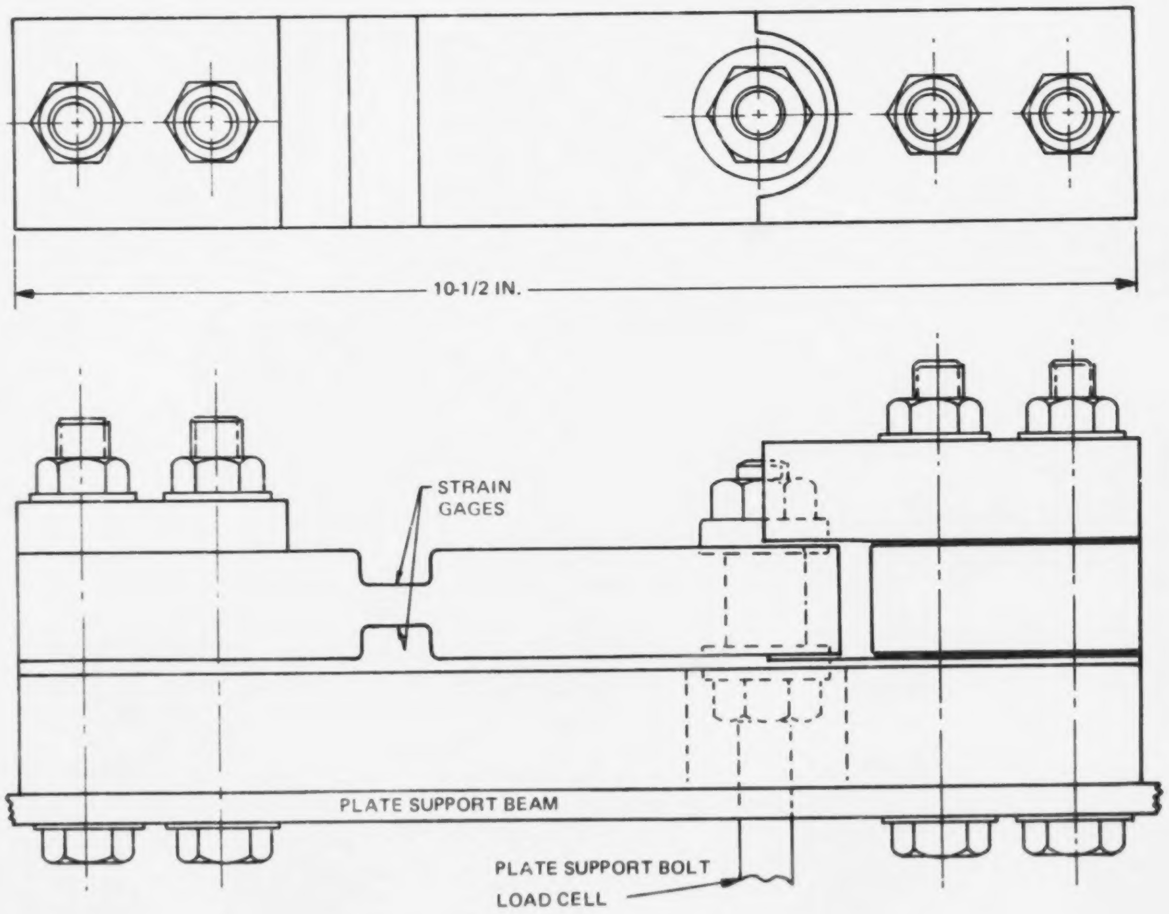

Figure 10. Load cell.

and its associated printer were capable of reading and printing at a rate of approximately 4 channels per second. A block diagram of the complete measurement system is shown in Figure 11.

Accelerometers -
Plate accelerations were measured during the test with piezoelectric accelerometers mounted on plates 5-1, 5-2, and 5-3. Three accelerometers were mounted along the centerline of each plate at locations 0.91 m, 3.05 m, and 5.17 m from the top of the plates. The accelerometers were Gulton Industries Model AHT-40TM, which have a frequency range from 3 Hz to 9 kHz and a dynamic range from 0.1 g to 250 g. The weight of each unit, exclusive of cable, is 52 grams.

The nine accelerometers were mounted to the plates with four screws and the cables were run up the plates in 1.3 cm conduit which was strapped all the way up the centerline of the plates. The accelerometers were mounted so that the Z-channel connector was perpendicular to the plate surface and the X and Y-connectors were on the two side surfaces of the block. Figure 12 shows the accelerometer system block diagram.

It should be noted that the recording oscillograph limited the system frequency range to 2 kHz and below.

Camera and Lighting -
Motion pictures were taken of the emissions during rapping; the camera used was a Bell & Howell Model 70-DL. This is a 16mm camera with a spring drive. The film used for black and white pictures was Kodak Tri-X reversal film #7278, and the film used for color motion pictures was Kodak Ectrachrome type #7242. The lighting was furnished by movie lights of

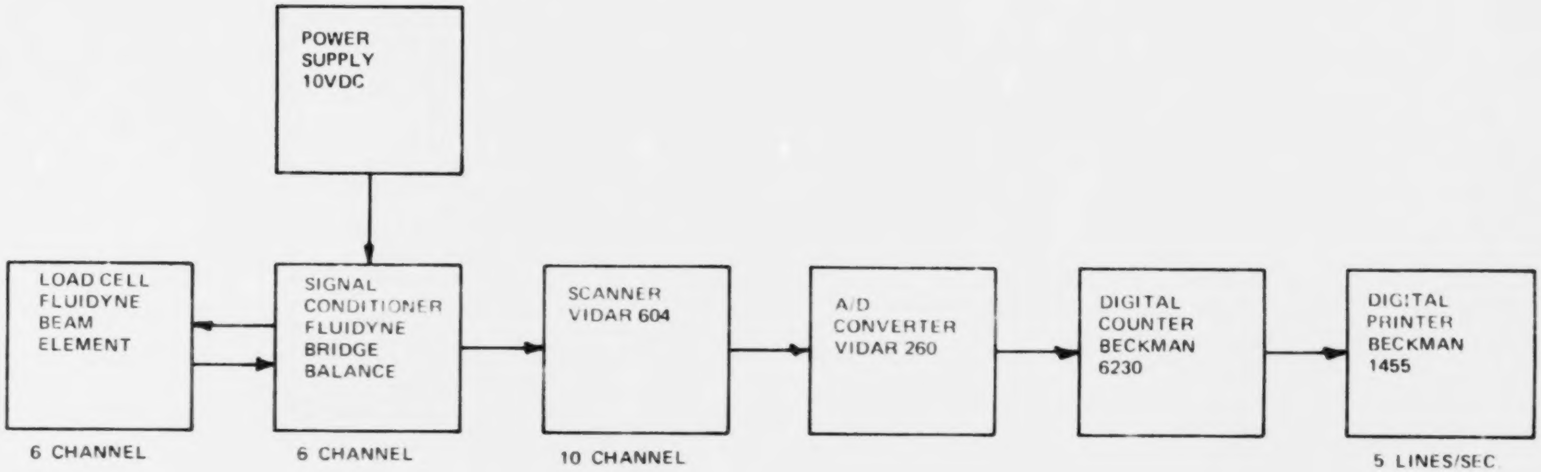

Figure 11. Precipitator plate weight measurements system block diagram.

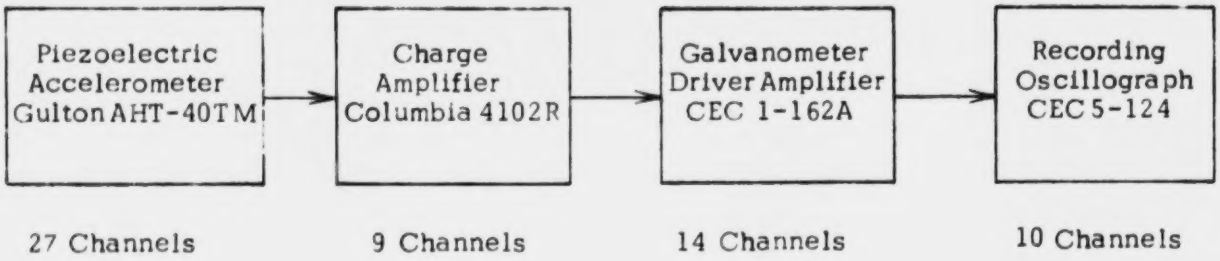
Piezoelectric Accelerometer Gulton AHT-40TM
Charge Amplifier Columbia 4102R
Galvanometer Driver Amplifier CEC 1-162A
Recording Oscillograph CEC 5-124
27 Channels
9 Channels
14 Channels
10 Channels

Figure 12. Accelerometer system block diagram.

250 watt and 650 watt intensities. These lights were aimed at the area of interest from portholes adjacent to that through which the pictures were made.

Transmissometer -
A Lear-Siegler RM41p portable optical transmissometer was used to monitor the particulate emissions at one point at the outlet of the FluiDyne pilot precipitator. A similar on-stack transmissometer has been described by Beutner.[19] The portable unit that was used at FluiDyne has an optical path length of two meters and compensation circuitry for determining opacity in terms of the stack exit diameter. For simplicity, all of the opacity and optical density measurements in this report are given in terms of a two-meter optical path length.

Konitest -
A vortex type Konitest with a Keithley Multi-Range Model 610-CK electrometer was used to continuously monitor particulate loading in the rectangular exit duct 3 m downstream of the precipitator box. The sample probe nozzle was located near the duct vertical centerline, about 2 m up from the duct floor. The Konitest uses electrical charge generation by the particle-surface contact as a measure of particulate concentration. The current-versus-particulate mass concentration is usually linear[20] for constant test conditions.

IKOR -
An IKOR Model 206 portable particulate monitor was used to monitor inlet grain loadings. In this system, sampled particles are continuously drawn through an electronic sensing head, generating an electric current by charge transfer. According to the manufacturer, the current output is precisely related to mass flow. Some problems were encountered with dust buildup in the sampling line.

Resistivity Probe -

A point-plane in situ resistivity probe was used to measure the electrical resistivity of dust entering the FluiDyne pilot precipitator. The operation and description of this probe are given by Nichols and Spencer.[21]

Anemometer -

A Thermo-Systems model 1610 velocity transducer with a special high temperature ceramic probe was used to make velocity measurements in the pilot precipitator. The two-needle hot film sensor .015 mm (6 mil) with special epoxy resin was designed for temperatures up to 162°C (325°F). A special 7.6 meter, high temperature cable connecting the sensor to the system electronics allows vertical scanning of the entire precipitator test section. This temperature compensated anemometer was factory calibrated for the velocity range 0 to 4.6 m/sec (0.3-3.0 volts output). The manufacturers estimated accuracy is 2%.

Gas Analysis -

The gas entering the pilot precipitator was analyzed to determine the concentrations of O_2, H_2O, SO_2, and SO_3. The concentrations of SO_2 and SO_3 were expected to be low.

The apparatus for determination of SO_2 and SO_3 consisted of the following items in sequence: a heated pyrex probe, a heated (60-90°C) glass spiral condenser having a fritted glass plate at the outlet, a 250-ml gas washing bottle (coarse fritted glass bubbler) containing dilute hydrogen peroxide, a drying tube containing Drierite, a dry gas meter, and a vacuum pump.

A measured volume of gas was drawn through the system; SO_3 was captured in the condenser and SO_2 was oxidized to SO_3 in the washing bottle. The resulting sulfate solutions were titrated with 0.005 N barium perchlorate, with thorin indicator.

The CO_2 and O_2 concentrations were determined with Fyrite gas absorbing solutions. The moisture contents were determined by passing a known volume of gas through a column of Drierite and measuring its weight gain.

SECTION IV

TEST CONDITIONS

During this study of rapping reentrainment the following variables were controlled:

1. Dust properties
    - resistivity
    - adhesion and cohesion
    - particle size distribution
    - chemical composition
    - bulk density of collected ash layer
2. Gas composition
    - H_2O concentration
    - SO_3 concentration
    - SO_2 concentration
3. Corona current density
4. Gas temperature
5. Gas velocity
6. Dust loading
7. Plate construction and suspension system
8. Rapping variables
    - Type
        - impulse
        - vibration
    - Location and orientation
    - Intensity
    - Time interval between raps (amount of dust collected on a plate prior to rapping)

On the basis of previous rapping studies discussed in the introduction, these variables were considered to be the ones that would affect the removal of the dust from the plates and the amount of emissions due to plate rapping.

In this section, the results of the measurements of most of these variables are reported. The dust loading on the precipitator plates is discussed in a later section. The plate construction and suspension system were discussed in the previous section.

DUST PROPERTIES

Fly ash was obtained from the Black Dog Power Plant in Minneapolis, Minnesota for this study. The ash was selected to give a representative particle size distribution of dust entering a precipitator and to have typical properties. Studies with a dust with a size distribution representing dust entering an outlet section were also contemplated. The difficulties in obtaining such an ash at the test location and the time limits for the investigation of rapping reentrainment at the test location prevented such a study.

The results of a Bahco analysis of the fly ash used in the study are shown in Figure 13. The mass median diameter of the sample was 16μm with a geometric standard deviation of 5 and a mode of 4μm. This distribution is typical of fly ash from pulverized coal-fired boilers.

The resistivity of the fly ash measured with the in situ probe is tabulated in Table 3. Dust resistivity varied over a larger range than desired during the test, due to changes in gas temperature and moisture content. However, by operating the precipitators at a reduced spark rate, less than one per minute, the effects of these changes on precipitator operation were minimized. Laboratory measurements of the fly ash resistivity are shown in Figure 14.

The true density of the fly ash was determined with a helium pycnometer to be 2.65 g/cm^3. The porosity of a dust layer

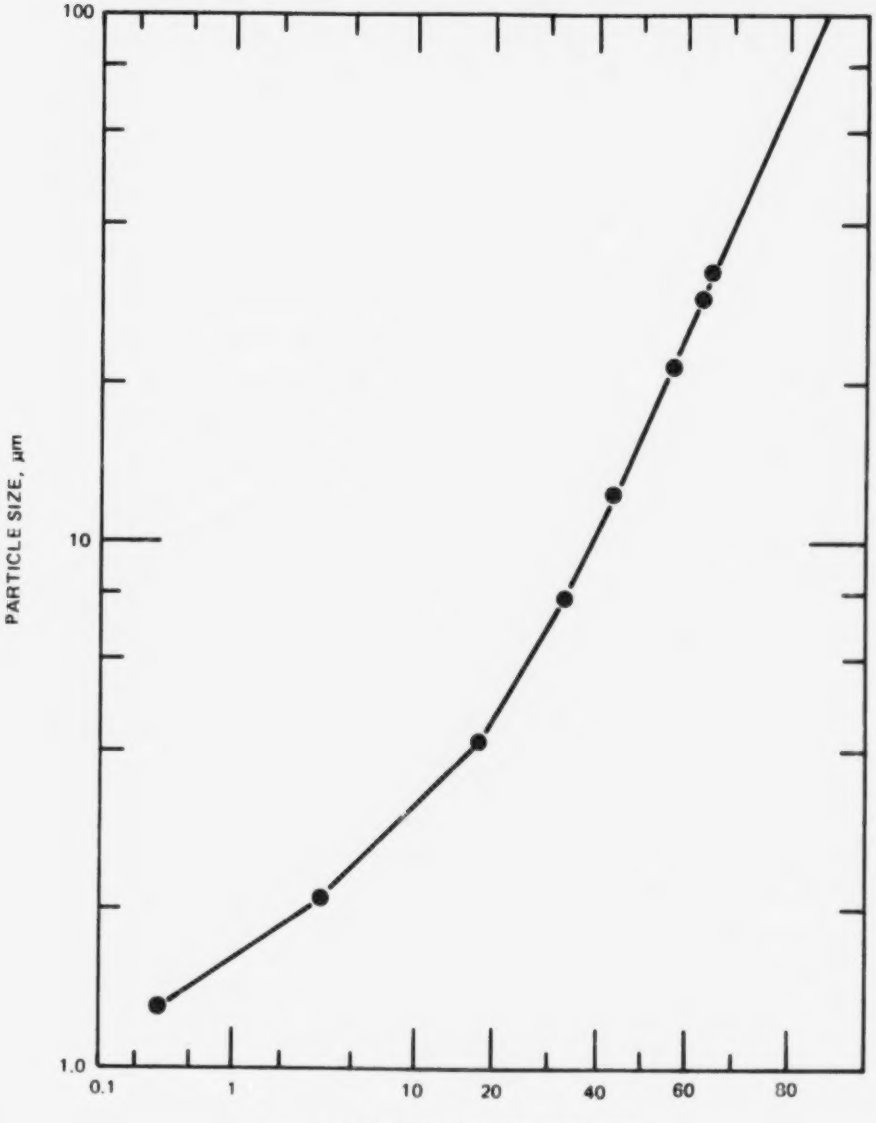

Figure 13. Cumulative particle size distribution of the feed dust, Bahco analysis.

TABLE 3
IN SITU RESISTIVITY DATA

Date	Time	Location	% H_2O	Temp °C	Electric Field at Sparkover	Resistivity at Sparkover	Resistivity from V-I Data
6/23/75	10:45	Inlet	9.3	130	2000 V	0.70×10^{11} Ω-cm	1.02×10^{11} Ω-cm
6/23/75	15:25	Inlet	10.6	150	3300 V	1.02×10^{11} Ω-cm	1.38×10^{11} Ω-cm
6/24/75	12:38	Inlet		124	2200 V	6.16×10^{10} Ω-cm	1.48×10^{11} Ω-cm
6/24/75	15:52	Inlet	10.6	126	1700 V	1.42×10^{11} Ω-cm	3.17×10^{11} Ω-cm
6/25/75	15:25	Inlet		104	1000 V	2.64×10^{10} Ω-cm	5.41×10^{10} Ω-cm
6/25/75	16:20	Inlet	12.3	104			5.09×10^{10} Ω-cm
6/26/75	13:35	Inlet		121	700 V	1.47×10^{10} Ω-cm	5.00×10^{10} Ω-cm
6/26/75	15:15	Inlet	13.0	116	1300 V	3.15×10^{10} Ω-cm	7.50×10^{10} Ω-cm
6/26/75	16:30	Inlet		121			9.00×10^{10} Ω-cm
			Avg.	122°C	Avg.	6.40×10^{10} Ω-cm	

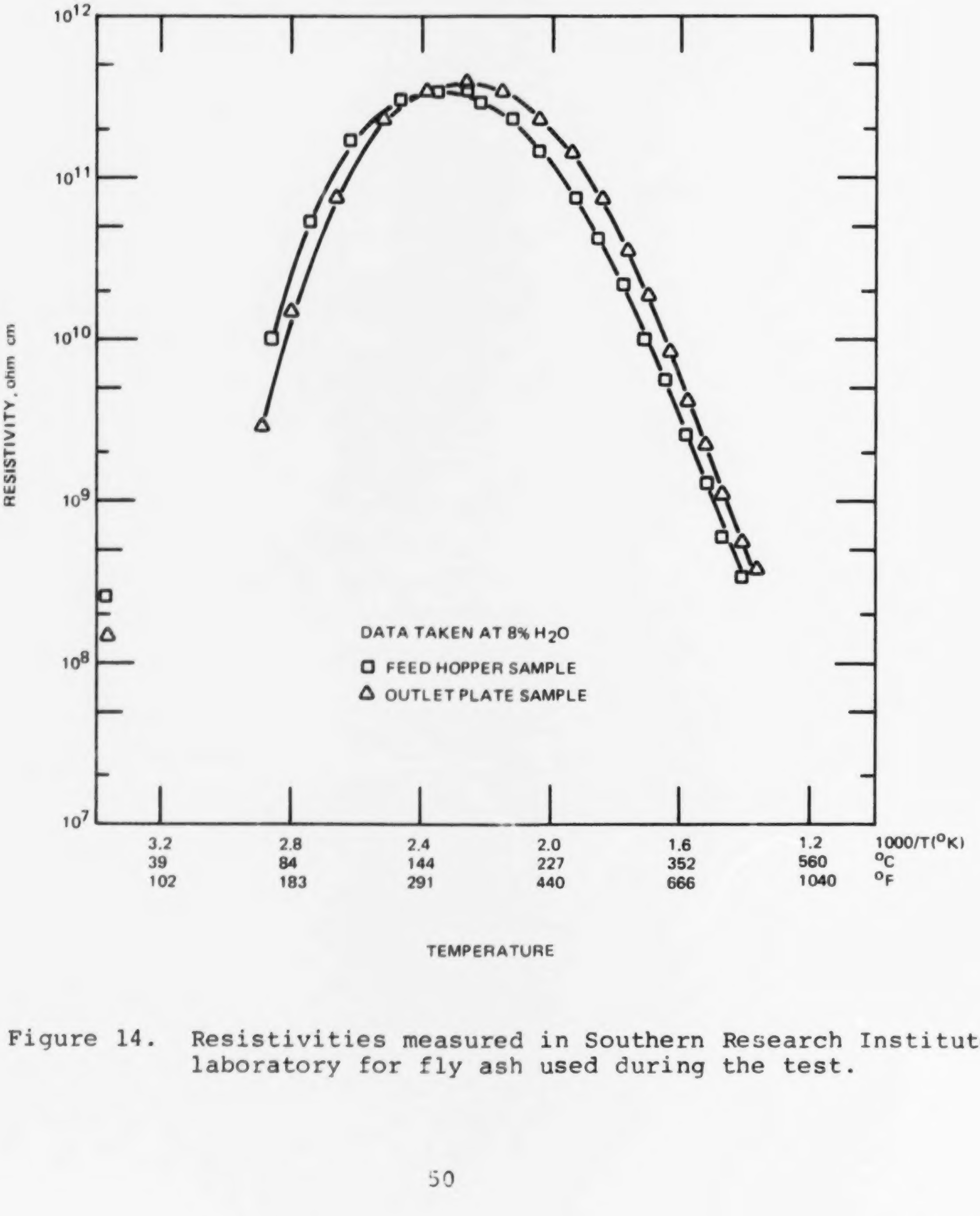

Figure 14. Resistivities measured in Southern Research Institute laboratory for fly ash used during the test.

obtained in a Power Test Code 28 resistivity cell was 56.3% for a sample from the feed hopper and 49.4% for a sample from an outlet plate of the pilot precipitator. These values are used for estimating dust layer thicknesses from the load cell measurements.

Instrumentation for determining the dust cohesion characteristics during the test was not available.

A chemical analysis of the fly ash used in this series of experiments is given in Table 4. The composition of the fly ash appeared to be typical.

GAS COMPOSITION

The compositions of the flue gas samples are shown in Table 5. These measurements, along with the finding that there was no SO_3 and only 16 ppm SO_2 present, indicated that the gas was mostly air with a small contribution of CO_2 from the oil-fired burner that was used to heat the gas. Previous research had indicated that the injection of SO_3 can increase dust cohesion characteristics and decrease rapping reentrainment emissions.[17] An investigation of this effect was considered for this study. However, to fit the test into the available time, a study of the effect was omitted.

ELECTRICAL CONDITIONS AND GAS TEMPERATURE

Operational current densities and voltages significantly affect the collection efficiency of an electrostatic precipitator. A decrease in current density can result in an increase in emissions due to plate rapping by decreasing the recollection of the reentrained particulate. A decrease in current density can also lower the tensile strength of the collected particulate layer. The maximum value of current density for any specific precipitator is set by the resistivity of ash that

TABLE 4

CHEMICAL ANALYSIS OF BLACK DOG FLY ASH, PERCENT BY WEIGHT

	Sample		
	Inlet Plate	Outlet Plate	Feed Hopper
Li_2O	0.03	0.04	0.03
Na_2O	1.75	1.60	1.74
K_2O	1.23	1.50	1.19
MgO	3.08	3.69	3.08
CaO	12.04	13.33	13.69
Fe_2O_3	8.94	7.58	11.51
Al_2O_3	20.71	19.33	18.64
SiO_2	46.93	44.27	44.27
TiO_2	1.04	1.11	1.04
P_2O_5	0.26	0.26	0.25
SO_3	1.78	2.74	1.98
Loss on ignition	3.40	4.84	3.75

TABLE 5

COMPOSITION OF GAS ENTERING THE FLUIDYNE PILOT PRECIPITATOR

Date	Time	CO_2 % by vol.	O_2 % by vol.	H_2O % by vol.
6/23/75	11:10			9.3
6/23/75	4:35			10.6
6/24/75	4:12	3	20	10.6
6/25/75	4:00	3	20.5	12.3
6/26/75	3:50	4	21	13.0
6/27/75	8:40	3	20	10.7

is collected. In turn, the resistivity of any given ash is basically controlled by gas temperature and partly controlled by the flue gas moisture content. A continuous log of the current and voltage to the precipitator and the corresponding average inlet temperature and water feed rates was maintained during the test. (This log is tabulated in Appendix I).

In an attempt to avoid the effects of changes in gas temperature and moisture content, the precipitator was operated at a current density and voltage for which sparking rates were low. However, during the first day of continuous testing, the gas temperature increased during the day and the current density decreased. (See Appendix I, June 23, 1975). During the subsequent test the water feed rate was increased to lower the gas temperature and to increase the moisture content, thus lowering the ash resistivity. These changes are reflected in the data tabulated in Tables 3 and 5. Following these changes, the electrical conditions remained reasonably stable during the test, as shown by the data tabulated in Table 6. Typical V-I characteristics of clean plates and ash covered plates are shown in Figure 15. During the test the average operating voltage was 40.4 kV and the average current density was 23.3 nA/cm^2. When sparking took place it usually occurred in the lanes having expanded metal plates.

The average temperature of the flue gas during each test is tabulated in Table 6.

GAS VELOCITY DISTRIBUTIONS AND VOLUME FLOW RATE

Rapping reentrainment was shown to be a function of gas velocity by Sanayev and Reshidov.[15] The test plans called for measuring the rapping emissions with gas velocities of

Table 6. AVERAGE ELECTRICAL CONDITIONS

	Average voltages, kV	Average Current Resistivity, nA/cm^2	Average Temperature, °C
Test 1	38.25	21.0	141
Test 2	32.60	14.5	141
Test 3	40.25	23.9	125
Test 4	43.50	23.6	128
Test 5	41.00	23.9	127
Test 6	42.25	22.7	130
Test 7	41.00	24.9	128
Test 8	44.00	24.2	130

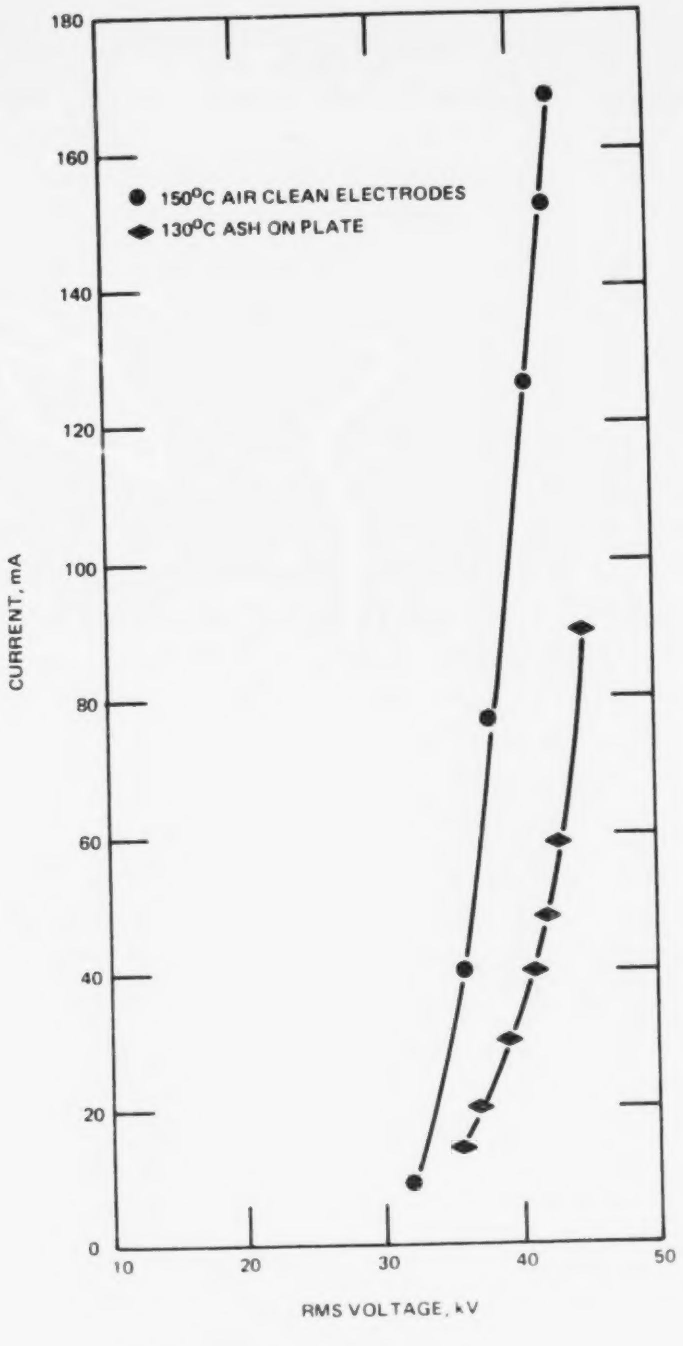

Figure 15. Precipitator electrical characteristics.

0.9 m/sec and 1.8 m/sec between the precipitator plates. These two velocities cover the range found inside most modern precipitators.

During the second week of testing, the average velocity between the precipitator plates was estimated to be 0.86 m/sec (2.8 ft/sec). The estimate was based on measurements 76 cm (30 in.) downstream of the exit baffles. The vertical velocity distribution at this location is shown in Figure 16. The average velocity and standard deviation of the measurements for each test day are tabulated in Table 7. Considering the design of the precipitator, the vertical distribution of the gas flow between the precipitator plates was probably similar to that 76 cm downstream of the exit baffles. The distribution indicates that the velocity was slightly higher in the lower half of the precipitator than in the upper half and that the velocities in the baffled regions were reasonably low. The velocity distributions at the entrance and at the exit of the precipitator are shown in Figures 17 and 18, respectively.

The vertical velocity distribution at the inlet was reasonably good except for a perturbation caused by a structural I-beam. The velocity distribution across the precipitator indicated a lower velocity in the middle than on the two sides of the precipitator.

The total volume flow rates of gas passing through the precipitator were determined from a velocity traverse of the 1.1 m inlet duct. The volume flow rates for each test are tabulated in Table 8. The average flow was 5.04 m^3/sec (dry standard T=21°C, P=760 Torr) with a standard deviation of 0.21 m^3/sec.

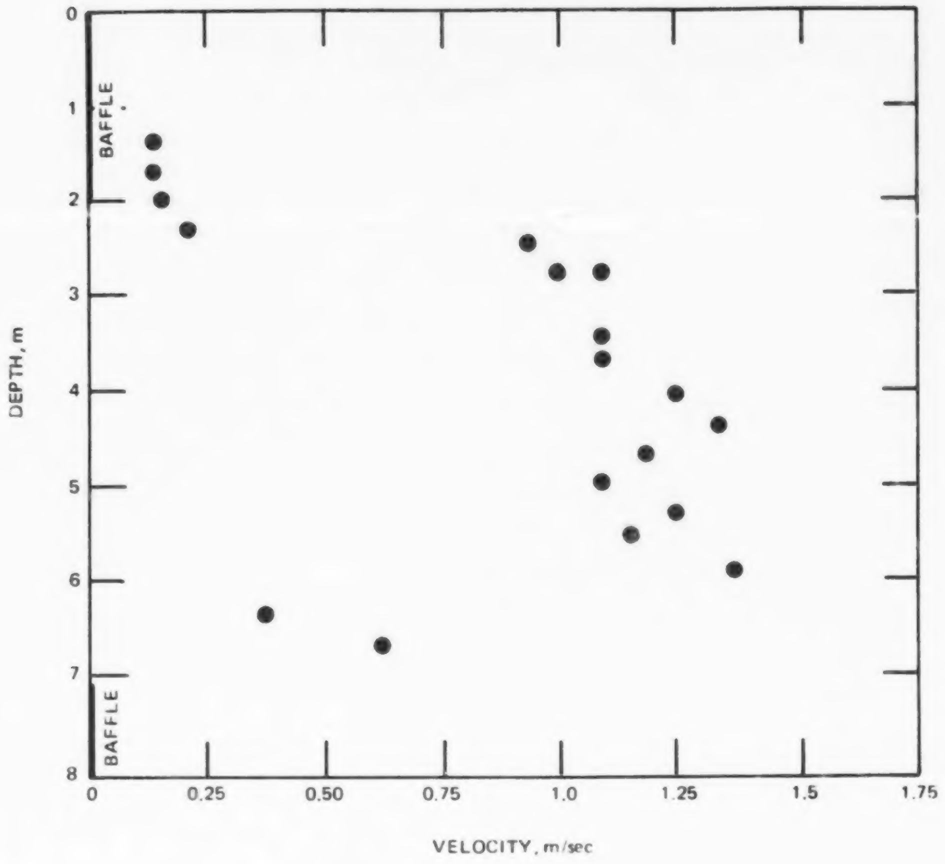

Figure 16. Precipitator outlet velocity profile.

Table 7. Average Velocities 76 cm
Downstream of the Exit Baffles

Date	Test	Average Velocity m/sec	Average Velocity (ft/sec)	Standard Deviation m/sec	Standard Deviation (ft/sec)	Percent Standard Deviation
June 18		1.00	(3.27)	0.30	(0.99)	30
June 19		0.86	(2.82)	0.46	(1.51)	54
June 20		0.69	(2.27)	0.38	(1.24)	54
June 23	1 and 2	0.79	(2.60)	0.43	(1.40)	54
June 24	3 and 4	0.95	(3.13)	0.46	(1.51)	48
June 25	5 and 6	0.88	(2.90)	0.46	(1.52)	53
June 26	7 and 8	0.85	(2.79)	0.50	(1.63)	58

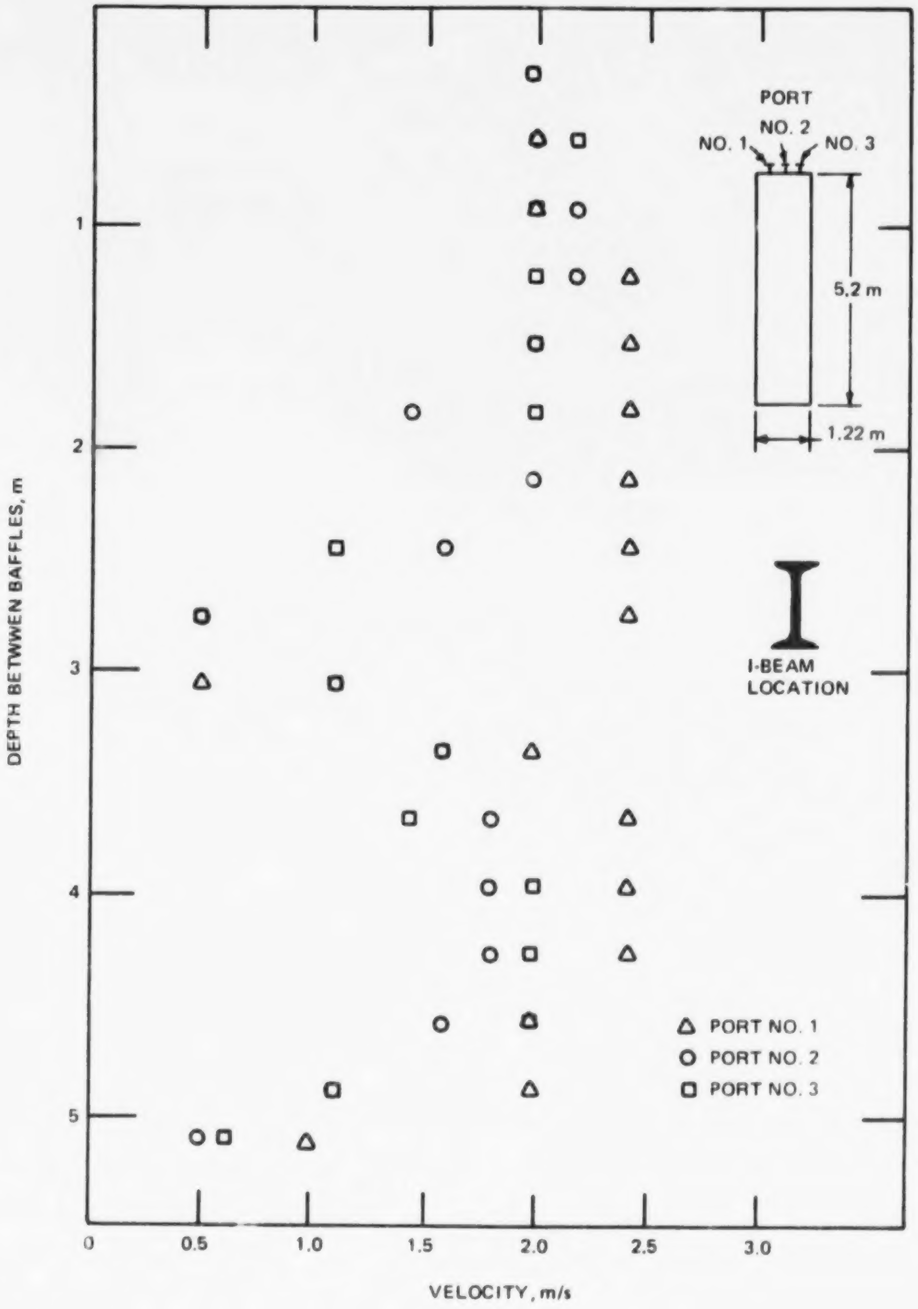

Figure 17. Precipitator inlet velocity profile.

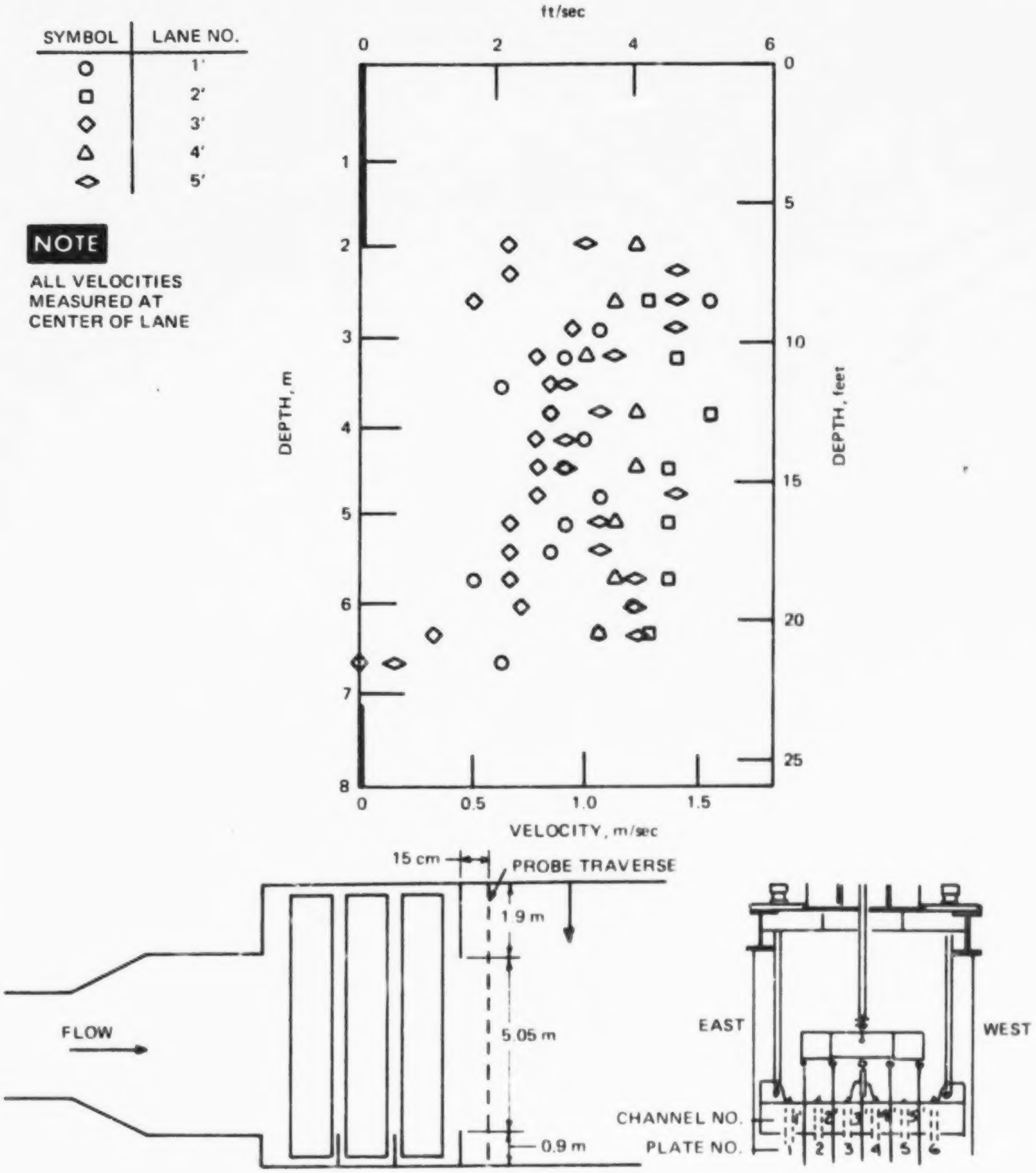

Figure 18. Precipitator outlet velocity profile.

Table 8. VOLUME FLOW RATES DURING THE TEST

Date	Test	Flow rate m^3/sec	(dry standard)* (ft^3/sec)
June 23	1	5.17	(1.53×10^2)
June 23	2	5.08	(1.79×10^2)
June 24	3	5.27	(1.86×10^2)
June 24	4	5.27	(1.86×10^2)
June 25	5	5.04	(1.78×10^2)
June 25	6	5.04	(1.78×10^2)
June 26	7	4.73	(1.67×10^2)
June 26	8	4.73	(1.67×10^2)

Average flow rate 5.04 ±0.21 m^3/sec ($1.78 \pm 0.61 \times 10^2$ ft^3/sec)

---

*Dry standard P = 760 Torr, T = 21°C.

Tests with a gas velocity of 1.8 m/sec scheduled for the last day of test were cancelled due to an electrical short in the precipitator.

Inlet Grain Loading

An average grain loading of 7.62 g/Nm^3 (3.09 gr/dscf) was obtained in the inlet ducting for the eight tests for which rapping data are compared. The measurements for each test are tabulated in Table 9. A comparison with Brink impactor measurements made within one meter of the inlet of the precipitator indicated that the particulate loading had decreased to 6.44 g/Nm^3 (2.61 gr/dscf) at the inlet to the precipitator.

The correlation of the inlet feed rates determined from mass train measurements and the hopper feed rates is shown in Figure 19. These data indicate that 33% of dust leaving the feed hoppers did not reach the precipitator. This was not surprising considering the amount of ducting the gas passed through before reaching the precipitator (See Figure 7).

PLATE ACCELERATIONS

To remove a precipitated dust layer from a surface by rapping, enough acceleration has to be given to the surface to create a force between the dust layer and the surface sufficient to cause the two to separate. If the acceleration is too small, the dust layer is not removed and may even be compacted. If the acceleration is too large, energy can be imparted to the dust layer, reentraining it in the gas stream.

The peak X, Y, and Z axis plate accelerations measured during the test with 1 to 2 mm thick dust layers collected on the plates were averaged for each accelerometer location. These accelerations are tabulated in Tables 10 and 11 for pressure

Table 9. INLET PARTICULATE LOAD AND PARTICULATE FEED RATES

Date	Test	Grain Load g/Nm^3 [c]	Grain Load (gr/dscf)	Feed rate kg/hr	Feed rate (lb/hr)	Hopper Feed rate kg/hr	Hopper Feed rate (lb/hr)
June 19	0-1	9.57	(3.880)	142	(313)		
June 20	0-2	6.78	(2.751)	106	(234)		
June 23	1	5.66	(2.296)[a]	98	(215)	158	(348)
June 23	2	8.06	(3.268)	137	(302)	180	(397)
June 24	3	4.73	(1.920)[a]	—	—	151	(333)
June 24	4	7.79	(3.160)	137	(303)	163	(360)
June 25	5	7.13	(2.892)	120	(265)	156	(344)
June 25	6	6.29	(2.549)	106	(233)	163	(360)
June 26	7	8.37	(3.394)	132	(291)	160	(353)
June 26	8	8.10	(3.286)	127	(280)	176	(389)
Avg. Test 1-8[b]		7.62 ±0.76	(3.092 ±0.316)	127 ±12	(279 ±26)	163	(360)

Avg. collection rate on precipitator plates, (load cells) 110 kg/hr (243 lb/hr)

Feed rate at entrance to precipitator as determined by Brink impactor - 108 kg/hr (239 lb/hr)

---

[a] Hole in filter

[b] Omitted tests 1 and 3 from average

[c] Nm^3 - Normal cubic meter T = 21°C, P = 760 Torr

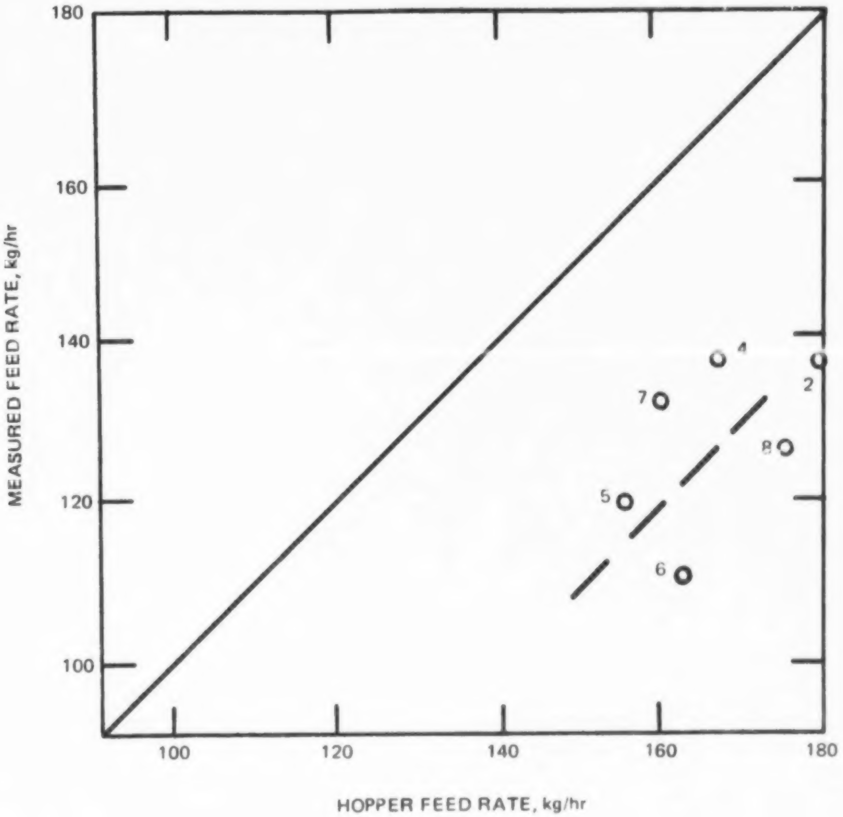

Figure 19. Correlation of measured feed rate and hopper feed rate.

Table 10. Composite Average of Plate Acclerations During Rapping for $\Delta P = 6.2 \times 10^5$ Pa, Dust Covered Plate

Vertical location[a]	Axis	Acceleration, G Plate #1	Plate #2	Plate #3
0.91 m	X	22	—	26
	Y	19 ±1.5	24 ±6	19 ±3
	Z	—	20 ±4	12
3.05 m	X	13	15 ±2	11
	Y	—	20 ±9	18 ±4
	Z	11	11	11
5.18 m	X	—	12	—
	Y	11	14	—
	Z	—	9	—

— No available data

[a] From the top of the plate

Table 11. Composite Average of Plate Accelerations During Rapping for $\Delta P = 4.8 \times 10^5$ Pa, Dust Covered Plate

Vertical location[a]	Axis	Acceleration, G		
		Plate #1	Plate #2	Plate #3
0.91 m	X	—	—	—
	Y	—	19	14
	Z	—	18	13
3.05 m	X	11	14.3	11
	Y	—	11	15
	Z	9	11	11
5.18 m	X	—	—	—
	Y	—	—	—
	Z	—	—	—

— No available data

[a] From the top of the plate

drops across the rapper cylinders of 4.8×10^5 Pa and 6.2×10^5 Pa (70 psi and 90 psi). A problem with the charge amplifiers occurred during the test, thus some acceleration data is missing. The X axis was parallel to the direction of gas flow. The Y axis was in the vertical plane of the plates, and the Z axis was perpendicular to the plates. The method of rapping the plates and the accelerometer descriptions and locations were discussed in an earlier section.

The measurements of the accelerations of plate 5-2 from both the upstream and downstream rappers were averaged. The variations in rapping intensity as a function of the differential pressure across the rappers with no dust load on the plates are shown in Figures 20 and 21 for the Y and Z axis of the accelerometers on plate 4-1. The accelerations obtained at all nine locations without a collected dust layer (P = 6.2×10^5 Pa) are given in Table 12. These accelerations are significantly higher than the accelerations obtained with the dust layers on the plates.

The range of accelerations that were available with dust layers on the plates of the precipitator was small. The change in rapping intensity from 80% to 100% of maximum produced only a small change in plate accelerations (see Tables 10 and 11). A modification of the air reserve for the pneumatic rappers after completion of the test appears to have significantly increased the rapping accelerations (see Table 13). The effects of changing plate accelerations could be studied during any subsequent test with the FluiDyne pilot precipitator.

Typical time traces of plate accelerations with a dust layer on the plates are shown in Figure 22. Time traces of plate

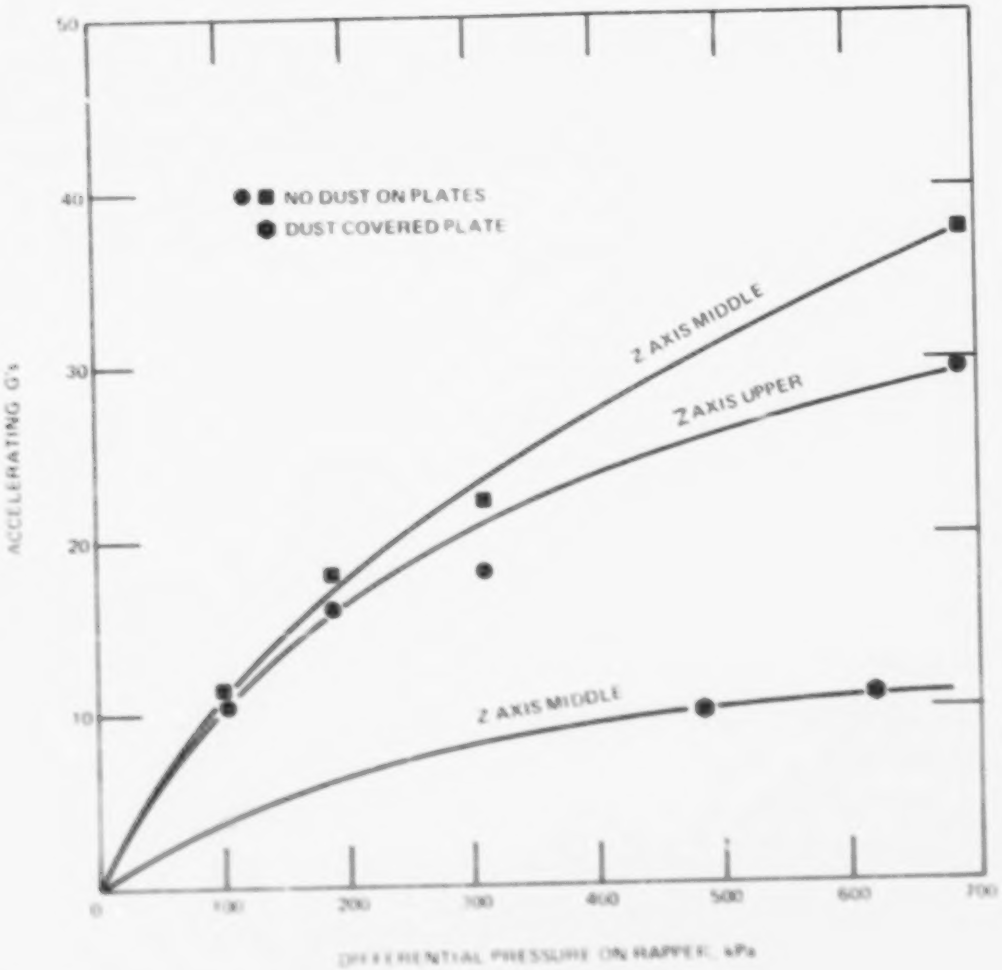

Figure 20. Plate 5-1 accelerations as a functional differential pressure on rapper, upstream rapper.

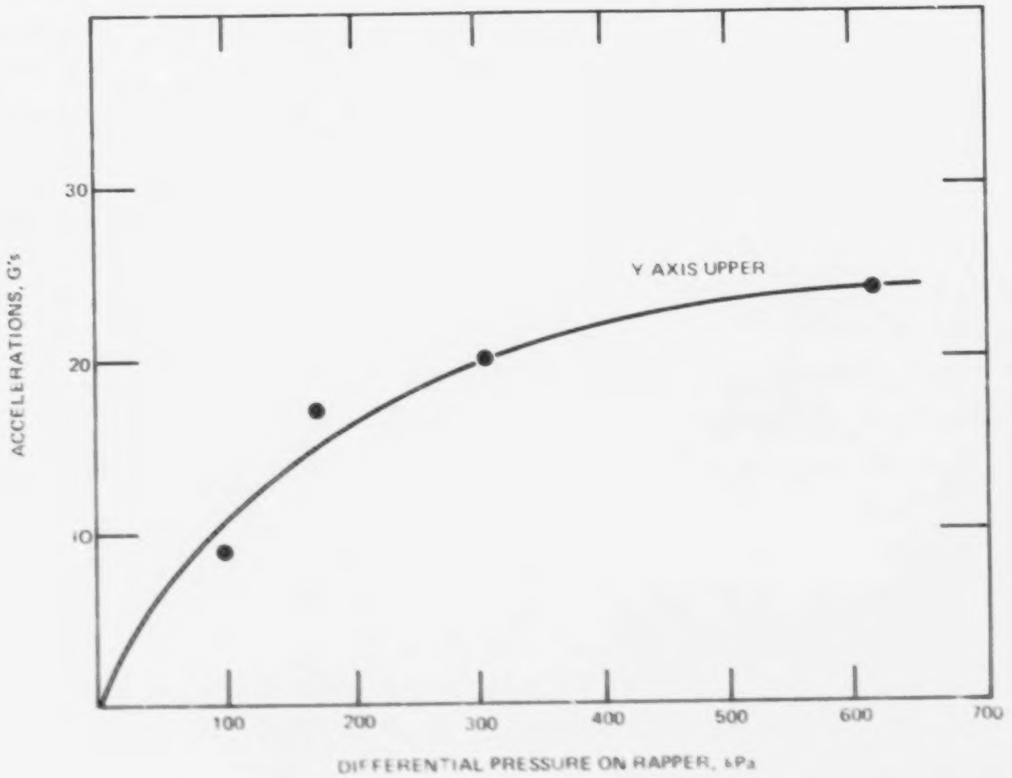

Figure 21. Plate 5-1 accelerations as a functional differential pressure on rapper, upstream rapper, no dust on plates.

Table 12. Composite Average of Plate Accelerations During Rapping for $\Delta P = 6.2 \times 10^5$ Pa, Clean Plates

Vertical location[a]	Axis	Acceleration, G		
		Plate #1	Plate #2	Plate #3
0.91 m	X	49	—	45
	Y	24	38	53
	Z	29.5	34	27
3.05 m	X	34.5	36.5	29.5
	Y	26	24.5	23.0
	Z	37.5	26.0	33
5.18 m	X	28	42.5	32
	Y	20.5	64.5	31
	Z	13.5	17.0	13

— No available data

[a] From the top of the plate

Table 13. Composite Average of Plate Accelerations During Rapping with Modified Rappers for $\Delta P = 6.2 \times 10^5$ Pa, Light Dust Layer

Vertical location[a]	Axis	Acceleration, G		
		Plate #1	Plate #2	Plate #3
0.91 m	X	73	11/-	151
	Y	—	70/107	99
	Z	51	41/47	35
3.05 m	X	41	40/68	105
	Y	80	33/52	33
	Z	—	-/-	—
5.18 m	X	75	69/87	37
	Y	50	51/113	34
	Z	33	35/64	34

— No available data

[a] From the top of the plate

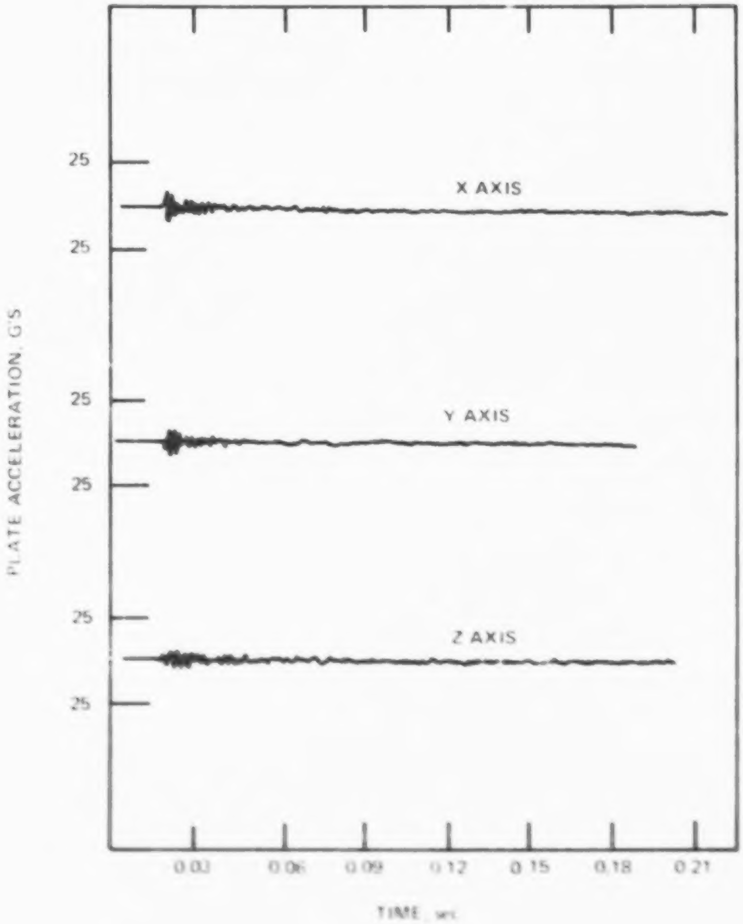

Figure 22. Typical traces of plate accelerations for a dust covered plate [plate 5-2, 3m from top of plate, $\Delta P = 6.2 \times 10^5$ Pa (90 psi)].

accelerations without dust layers are given in Figure 23. The plate accelerations of plate 5-1 were small when the downstream rappers were activated and the acceleration of plate 5-3 were small when the upstream rappers were activated.

The accelerations of plate 4-3 suspended from load cells were compared with the accelerations of plate 5-3. The results of the comparison of peak accelerations for the lower accelerometers is as follows:

	Plate 4-3	Plate 5-3
Y axis	20G	25G
X axis	19G	31G
Z axis	13G	12G

This data indicates that the load cells dampened the accelerations, but that in the important Z axis the accelerations were nearly the same.

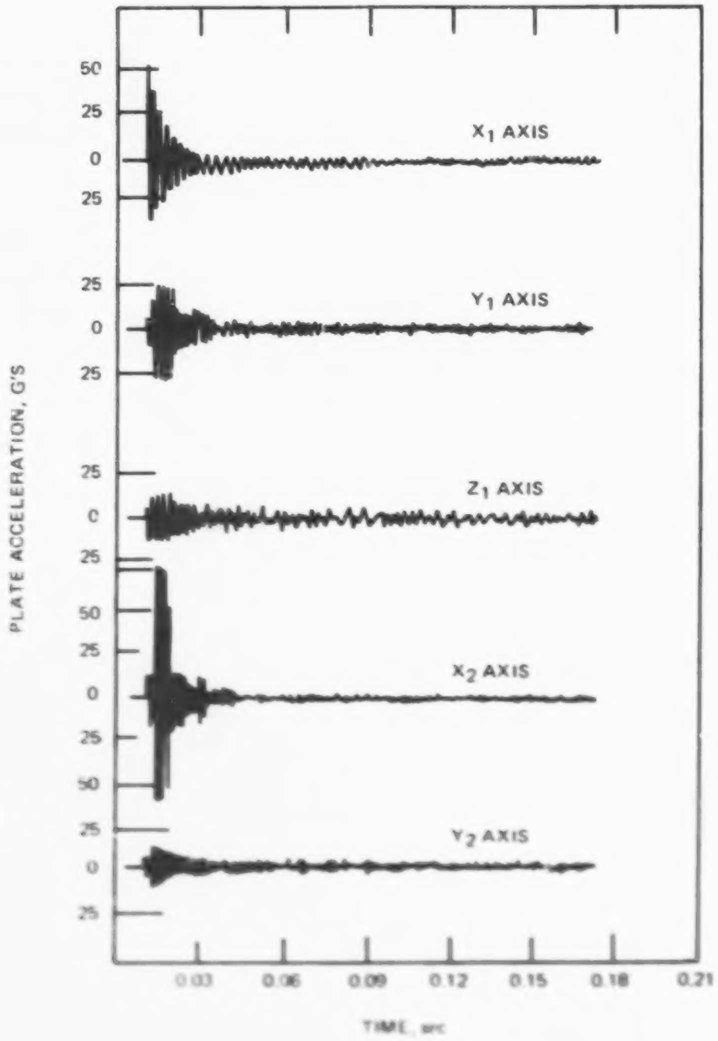

Figure 23. Typical traces of plate accelerations for a clean plate [plate 5-2; X_1, Y_1, Z_1, 0.9 m from top of plate; X_2, Y_2 3m from top of plate; $\Delta P = 6.2 \times 10^5$ Pa (90 psi)].

SECTION V

RESULTS AND DISCUSSION

The measurements discussed in this section were aimed at quantification of rapping reentrainment in terms of the percentage and the particle size distribution of the reentrained particulate and at determining the conditions for removal of dry dust by rapping. The results of the measurements indicate that efficiency of dust removal increases as a function of mass per unit area collected on the plates between raps while the percent of material reentrained decreases as a function of mass per unit area. These results are in agreement with those previously obtained by Plato[11] and by Sanayev and Reshidov.[15] Measurements of particle size distribution showed that the mass median diameters of the particles emitted during the raps increased with increased time between raps or equivalently with mass per unit area collected on the plates between raps.

MASS EMISSIONS

The results of the mass emission measurements provide data for determining the effect of changes in rapping variables, for determining the vertical stratification of the dust at the outlet, and for determining the percentage of total emissions due to reentrainment for various test conditions. Independent measurements of the mass emissions of the dust that passed through the electrified region without being collected and the mass emissions due to rapping reentrainment were made using the apparatus and procedures described in an earlier section. Separate measurements were made of emissions from the upper 68% and the lower 32% of the precipitator.

Separate sets of mass train data were obtained for the following rapping conditions:

	Rapping Intensity	Rapping Interval
Test 1	100% of max	150 minutes
Test 2	100% of max	120 minutes
Test 3	80% of max	12 minutes
Test 4	80% of max	32 minutes
Test 5	100% of max	12 minutes
Test 6	100% of max	32 minutes
Test 7	80% of max	52 minutes
Test 8	100% of max	52 minutes

Since the difference observed in plate acceleration (for the two different rapping intensities) was small (see previous section), data from tests having the same rapping intervals were combined to generate an average set of data. Data for the two tests with rapping intervals of 120 and 150 minutes were also combined and averaged. The resulting set of mass train data showed that hourly emission rates for the emission due to rapping reentrainment decreased as the time interval between raps increased. Emissions due to rapping were reduced by collecting thicker dust layers on the plates before they were rapped.

Precipitator efficiency eventually decreases if the collected dust layer becomes too thick. However, the between rap data showed that the emission rates and particulate loadings between raps remained constant during these tests as the time interval between raps was increased, for time intervals less than 155 minutes. The above effects are illustrated in Figures 24 through 29. The effective particulate loading for the rap contribution given in Figures 27 and 29 were calculated by dividing the rate of emission due to rapping by the

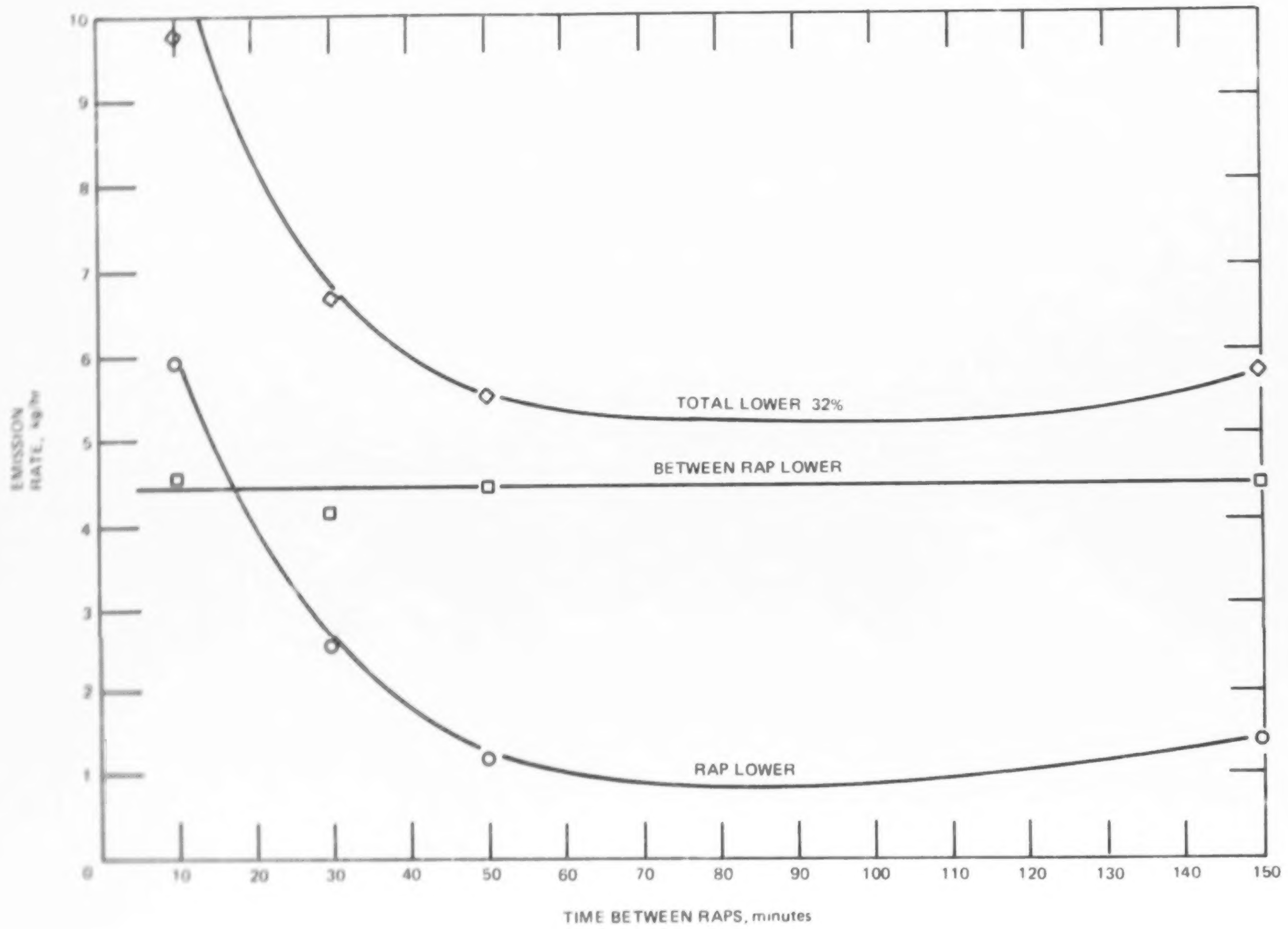

Figure 24. Mass emission rates for lower 32% of the precipitator cross sectional area as a function of the time interval between raps.

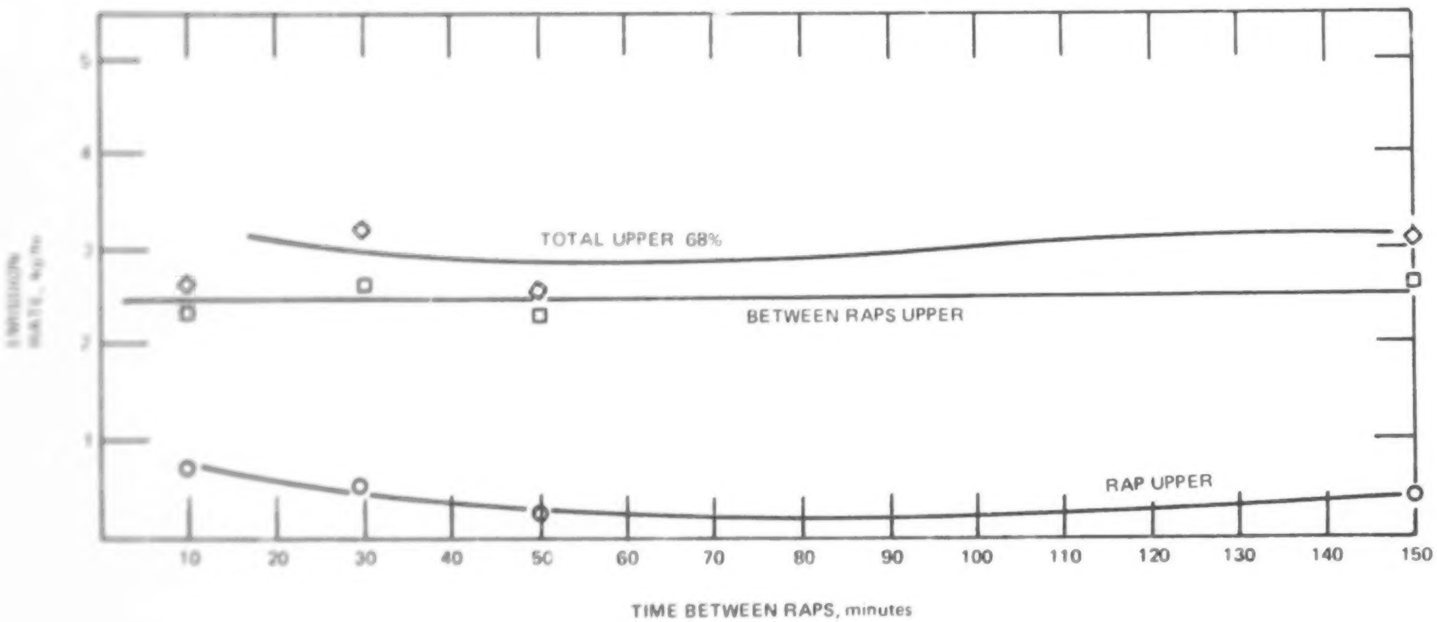

Figure 25. Mass emission rates for upper 68% of the precipitator cross sectional area as a function of the time interval between raps.

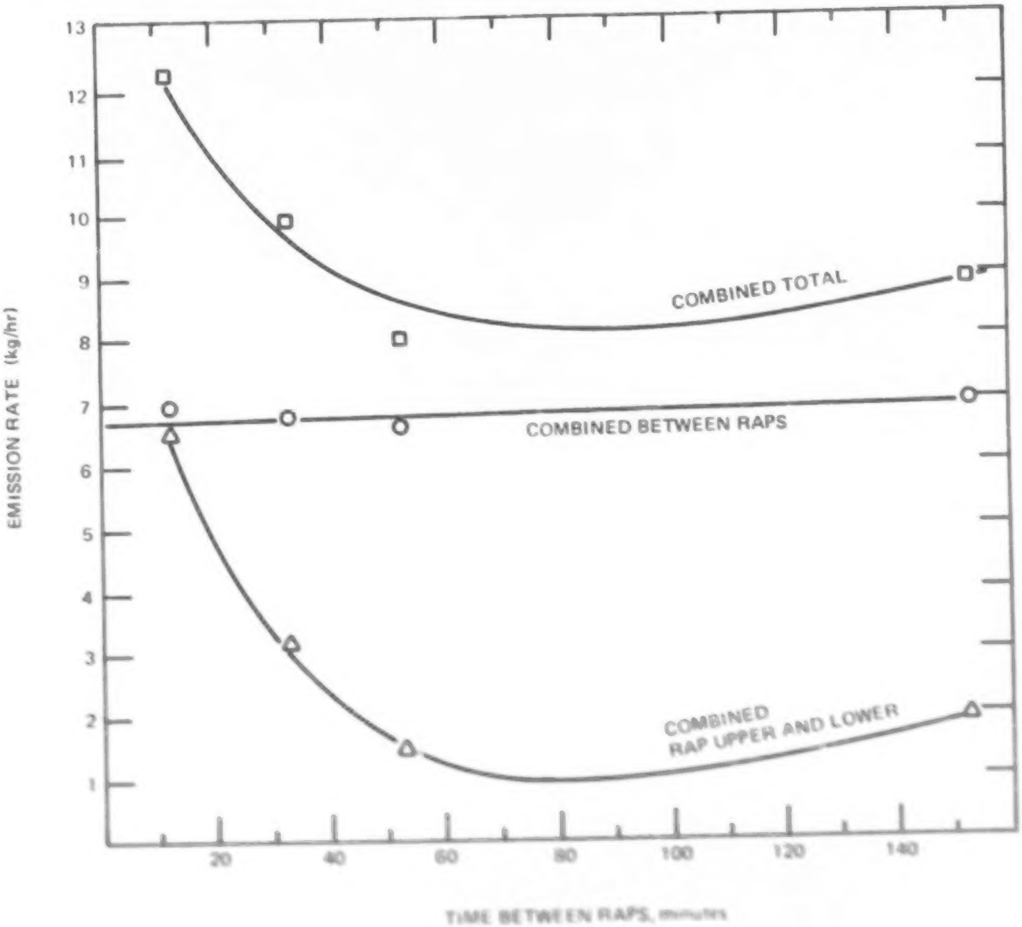

Figure 26. Combined upper and lower mass emission rates as a function of the time interval between raps.

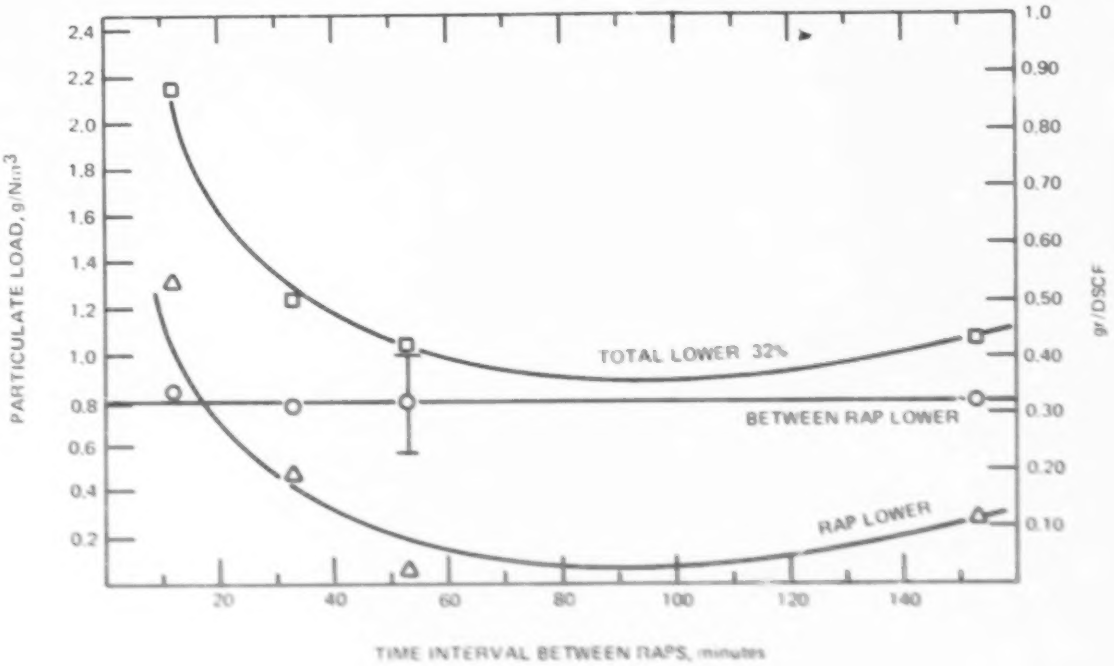

Figure 27. Particulate loading - lower 32% of the precipitator as a function of time interval between raps.

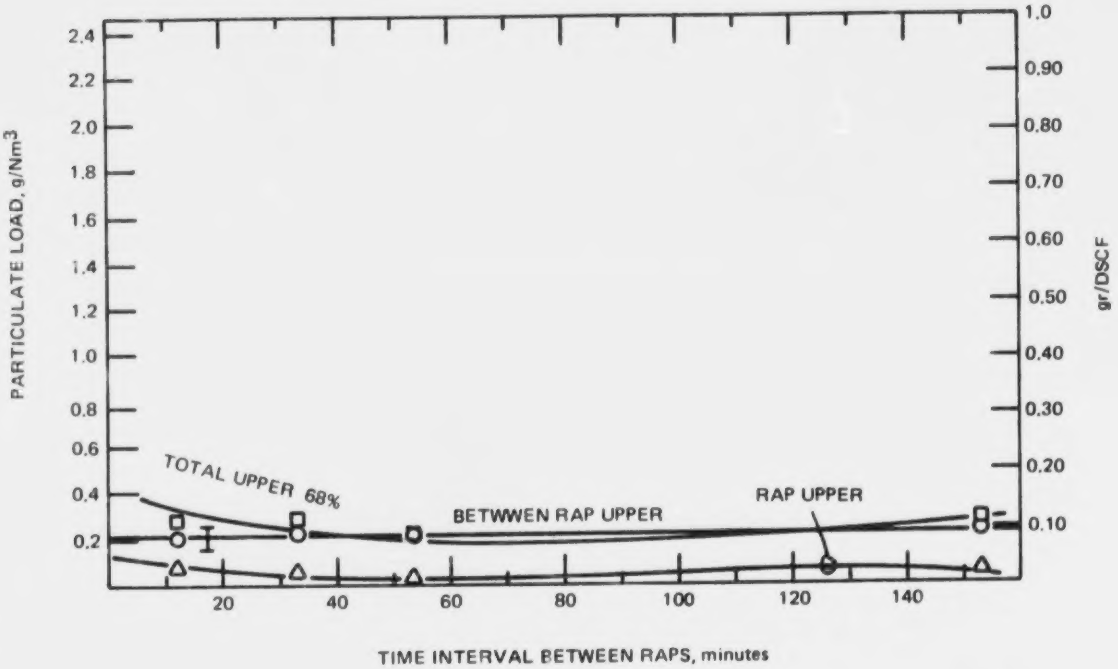

Figure 28. Particulate loading - upper 68% of the precipitator as a function of time interval between raps.

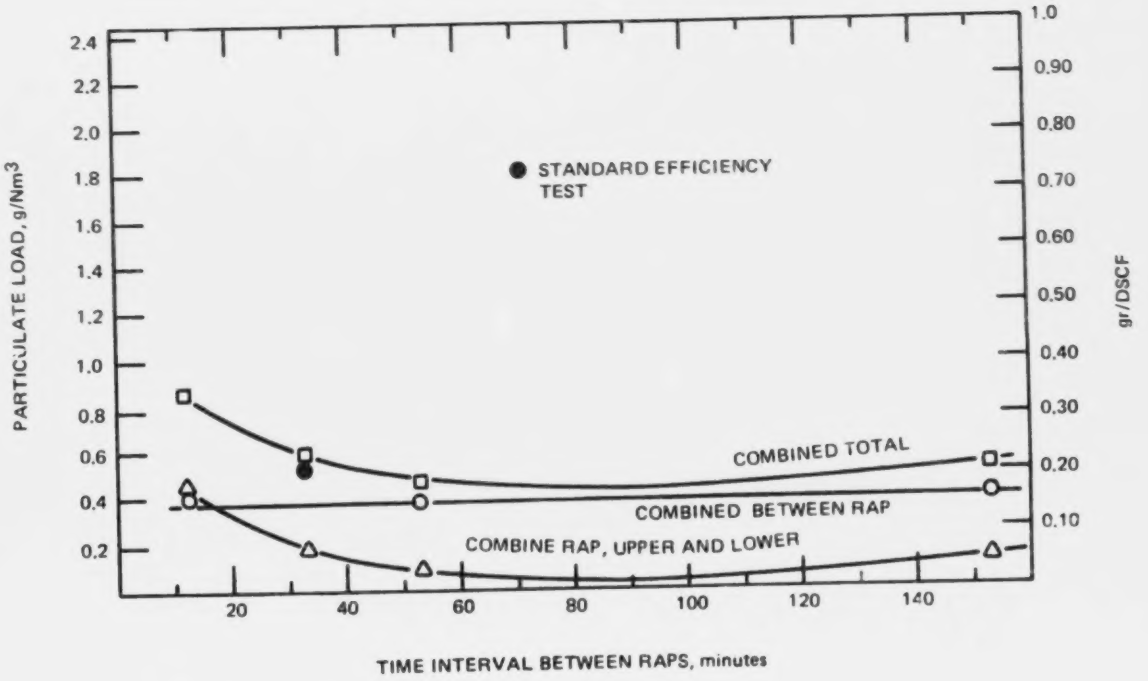

Figure 29. Combined particulate load as a function of time interval between raps.

appropriate volume flow rates. The total emission rates of the combined rap and between rap periods, for the upper and lower portions of the precipitator, were obtained by adding the rap and between rap emission rates. The total upper and lower emission rates were added to give total emission rates. The total effective particulate loading was calculated from the total emission rates.

Good agreement was obtained between the total effective outlet grain loading determined by the above procedure and an outlet grain loading measured when the precipitator was operated in a normal manner. During the normal test, the precipitator was operated with a continuous dust feed. The upstream rapper was activated every 30 minutes and the downstream rapper every 60 minutes. During this test, mass emissions were determined using standard in-stack filter techniques. The procedures used during the intensive test program gave an effective total grain loading of 0.58 g/Nm^3 (0.235 gr/dscf) for the 32 minute interval test and 0.49 g/Nm^3 (0.19 gr/dscf) for the 52 minute interval test. The more nearly normal procedure gave a grain loading of 0.53 g/Nm^3 (0.215 gr/dscf) for the 30-60 minute rap interval test.

Based on the data given in Figure 29 and the average inlet grain loading, the overall precipitator efficiencies were dedetermined to be:

12 minute interval tests	88.6%
32 minute interval tests	92.4%
52 minute interval tests	93.9%
120-150 minute interval tests	93.1%

For the normal test (30-60 minute rap interval) the measured efficiency was 93.0%. The average efficiency of collection without including the rapping loss was 94.8%. These values show that significant changes in emission were obtained by changing rapping intervals. However, it should be noted that the pilot scale precipitator is basically only one section of a full scale unit. The effect of rapping reentrainment for larger, more efficient units is discussed later in this section.

The data given in Figures 24 through 29 show that the emissions between raps and during the raps in the lower 32% of the precipitator were significantly higher than the emissions in the upper 68% of the precipitator. For the tests with 32-minutes rapping intervals, the emission due to rapping in the lower 32% of the precipitator accounted for 82% of the total emissions due to rapping and the emissions between raps in the lower 32% of the precipitator accounted for 60% of the between rap emissions. The between-rap vertical gradient is probably due to gravitational settling, sneakage through the hoppers, and reentrainment in the hoppers. The vertical stratification of the rapping puffs was visually observed and was photographically recorded. The major sources of vertical stratification during the rapping puff appeared to be gravitational settling and hopper "boil-up". The dust removed from the plates appeared to drop into the hoppers and then to boil up over the hopper baffles and be carried out of the precipitator. The vertical stratification in particulate concentration was clearly evident with the real time system and is discussed in more detail later in the report.

As mentioned in the introduction, an improvement in overall efficiency with increasing time between raps had been previously observed during a Southern Research Institute study of rapping reentrainment at the Bull Run Steam Plant in the TVA system,[17] by Plato,[11] and by Sanayev and Reshidov.[15] In Figure 30 the percentage of particulate removed from the plates that escaped the precipitator is shown as a function of mass per unit area of dust collected on the precipitator plates between raps. Data obtained from the Southern Research Institute-FluiDyne experiment and from the laboratory studies of Sanayev and Reshidov are shown. The Southern Research Institute percentages were calculated in two ways. First, the amount of emissions per rap was divided by the average mass collected between raps. The average mass collected was determined for the entire length of the precipitator from load cell measurements which are discussed later in this section. Second, the percentages were calculated in terms of mass collected only in the first 0.9 meters of the precipitator neglecting the smaller quantity of dust collected in the last 1.8 meters. According to this data, during the Southern Research Institute-FluiDyne experiments only 2.7% to 7.2% of the dust collected on the plates was reentrained and emitted from the precipitator. The data of Sanayev and Reshidov show that these percentages depend not only on the dust layer mass per unit area, but also on flow velocity.

The data in Figure 30 indicate that the most efficient removal of the dust from the plates and transfer to the hoppers for the ash used in these experiments was obtained with a dust surface density of 0.5 kg/m^2 or greater. Sanayev and Reshidov[15] explained the dependence of reentrainment on dust surface density as follows. They claimed that thin dust layers are more intensely disaggregated during rapping than thicker layers. The thin layers produce fine aggregates that are easily reentrained, while thicker layers lead to an increase in size and number of large aggregates reaching the hopper.

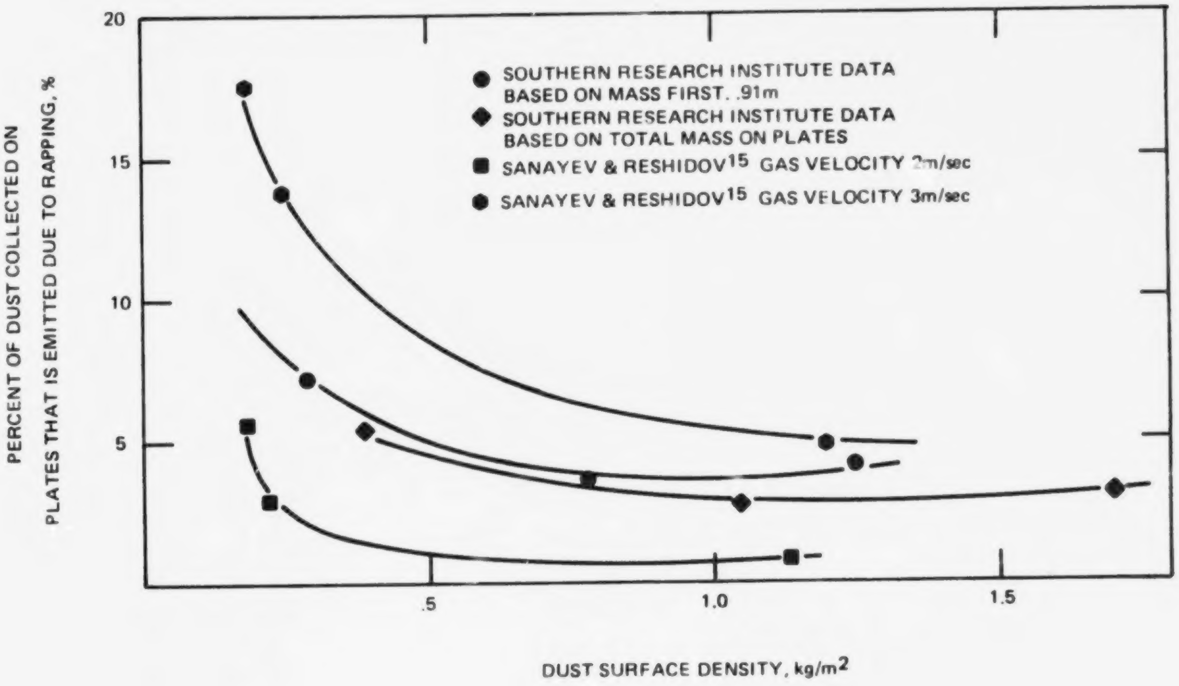

Figure 30. Percent of dust collected on precipitator plates that is emitted due to rapping.

These effects were also observed by Plato.[11] Plato found that with dust surface densities greater than 1 kg/m^2, dust was removed in cakes, and for values less than this it formed clouds. Impactor measurements made during the Southern Research Institute-FluiDyne experiments showed that the thicker layers produced larger aggregates than the thin layers. We expect the percentage of reentrained dust to decrease faster when large agglomerates are produced than when small agglomerates or discrete particles are entrained due to rapping. The large agglomerates will be recollected faster by gravitational settling and by electrostatic precipitation than the small ones.

It should be noted, as mentioned by Sanayev and Reshidov, that the data shown in Figure 30 characterize the optimum conditions for the rapping process and do not consider the precipitation process. At FluiDyne the effect of the collected dust on the precipitation process appeared to be minimal. As is discussed later, this is not the case for higher resistivity dusts.

RESULTS OF IMPACTOR MEASUREMENTS

Precipitator performance, in addition to being a function of many other variables, is a function of the particle size distribution of the dust being collected in the precipitator. Reentrainment when the plates are rapped significantly changes the particle size distribution of the dust in the precipitator. To obtain data on this change, we measured the particle size distribution of the particulate in the gas stream at the inlet, at the outlet between raps and at the outlet during raps. The measurements were made with impactors. The resultant data are used to indicate changes in the particle size distribution of the suspended particulate when the plates are rapped, to calculate fractional collection efficiencies with and without rapping reentrainment and to provide input data for a computer model of electrostatic precipitation of dust including rapping reentrainment.

The particle size distribution of the particulate at the inlet of the precipitator is shown in Figures 31 and 32. A procedure by Davies[22] was used to correct the distribution for an isokinetic error. The impactor samples at the inlet were collected with a sample velocity of 1.5 m/sec while the flue velocity at the sampling point was 1.2 m/sec. The corrected distribution is shown by the dashed curve in Figure 31. The measurements shown in this graph were made within a half meter of the entrance screen of the precipitator.

The average cumulative percent distribution of the inlet particulate distribution is given in Figure 32. This data represents a composite of data obtained from separate locations at the precipitator entrance. This data indicates that the inlet distribution was log normal with a mass median diameter of 13 μm and with a geometric standard deviation of 3.3.

Outlet Between Rap Particle Size Distribution

The average outlet particle size distributions between raps for all of runs is shown in Figure 33. The distributions for both the lower and the upper impactor are shown. In Figure 31, the weighted average of these two distributions is given. The distributions were weighted according to the area of the precipitator sampled by the lower and upper mass trains. The impactors were situated near the middle of each of these areas. The lower impactor showed a higher loading in the 1 to 8 μm range. This was probably due to gravitational settling and sneakage through the hopper area. The finding of the same

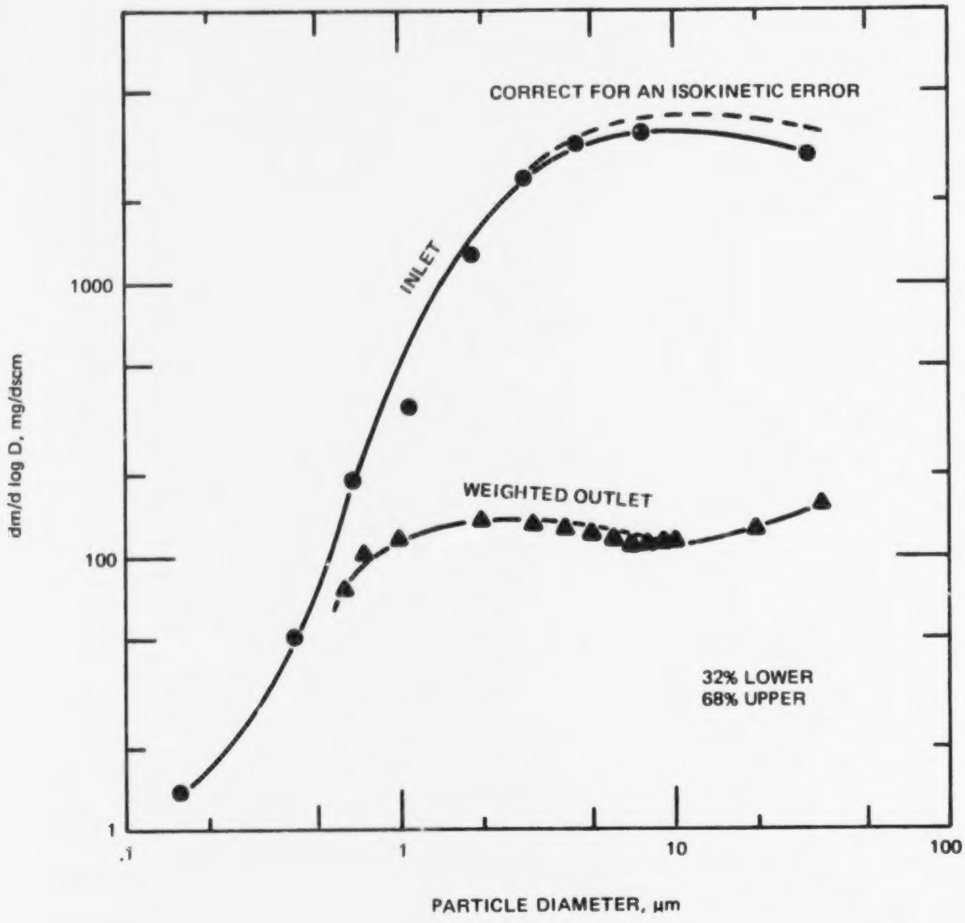

Figure 31. Inlet and weighted outlet particle size distributions, dm/d log D.

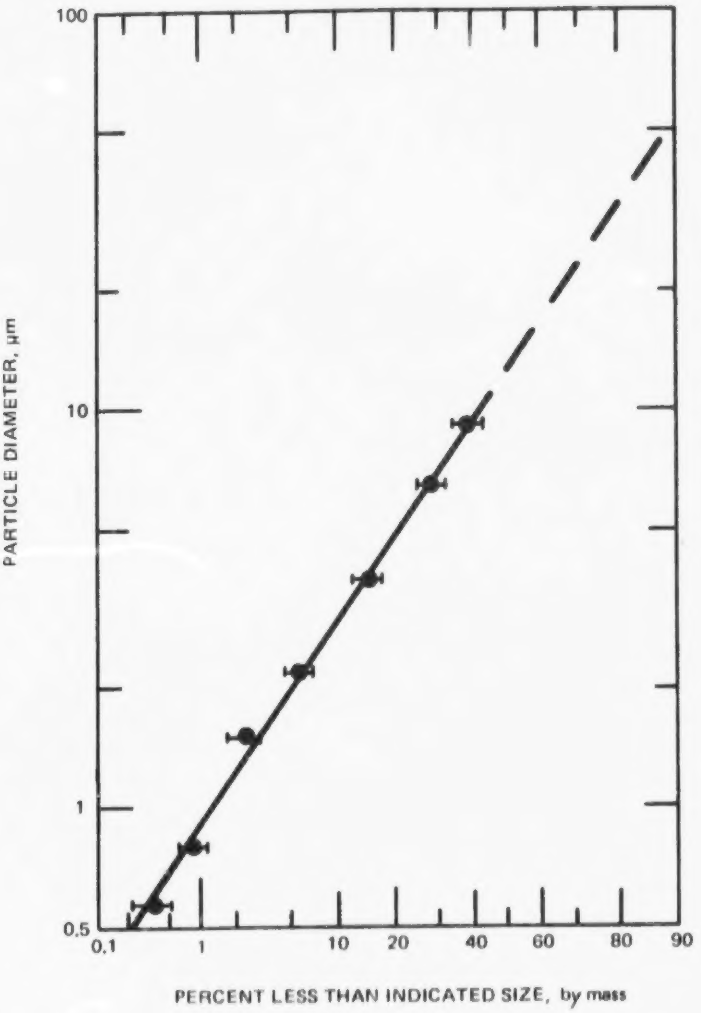

Figure 32. Inlet cumulative percent particle size distribution.

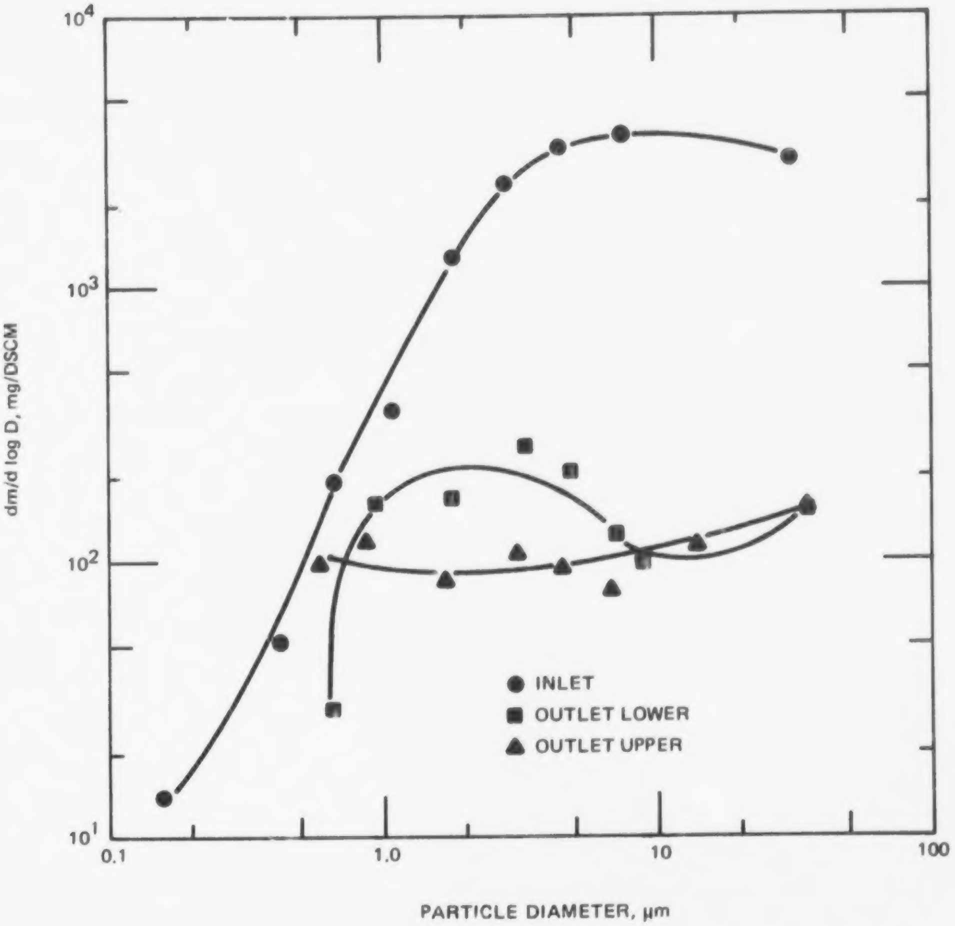

Figure 33. Inlet and outlet (lower 32% and upper 68% of the precipitator) particle size distribution, dm/d log D.

concentrations for particles greater than 10 μm was unexpected and may be an artifact of the measurement methods resulting from the lack of a complete exit plane traverse. The outlet emission rates between raps are given in Figure 34 for various size intervals.

Outlet Particle Size Distribution During Raps

The outlet emissions measurements with the impactors agreed with the results obtained with the mass trains and the real time system. All three systems measured a decrease in emissions as the time interval between raps was increased. The results of the impactor measurements are shown in Figure 35.

The particulate loadings during the rapping puffs determined from the impactor data are shown in Figure 36. These data have considerable scatter. The real time system also showed large variations in rapping puff concentrations. The particulate loading during the rap was as much as 10 to 200 times the particulate loading between raps. The particulate loading during the rapping puffs increased as the dust layer thickness increased. Data given in Figure 35 and 36 also illustrates the vertical stratification of the rapping puffs.

The particle size distribution of the rapping puffs measured with the lower impactor are shown in Figures 37 and 38. The data in Figure 38 indicate that as the time interval between raps was increased the mass median diameter of the particles increased. These data show that a smaller percentage of fine particles and a larger percentage of large particle agglomerates are produced with thick dust layers than thin dust layers. An inspection of the upper impactor stages for impactors sampling rapping puffs indicated that a substantial number of particles smaller than the lower cut off for the stages were present. Particles on these stages appeared to be agglomerates made up of fine particles.

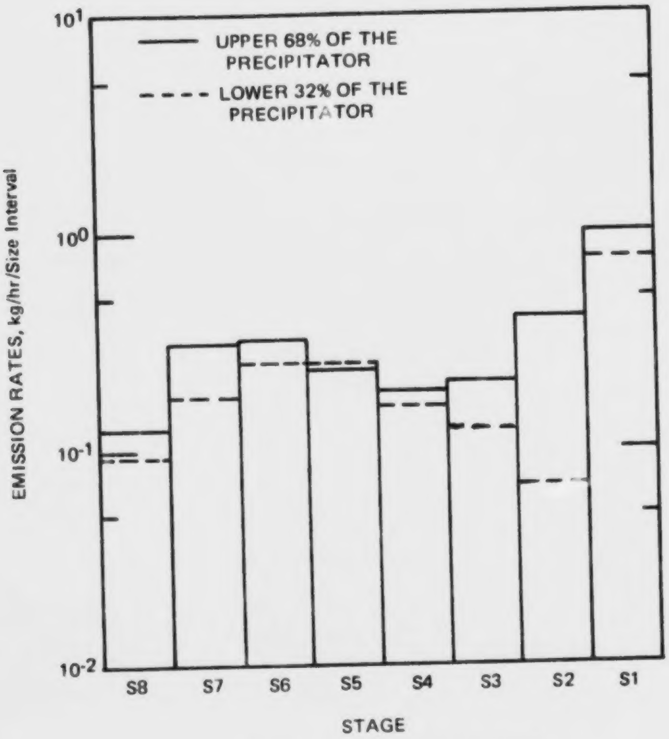

Stage	Size Interval
S1	> – 12.2 µm
S2	8.5 – 12.2 µm
S3	5.3 – 8.5 µm
S4	3.7 – 5.3 µm
S5	2.4 – 3.7 µm
S6	1.1 – 2.4 µm
S7	0.67 – 1.1 µm
S8	0.50 – 0.67 µm

Figure 34. Outlet emission rates between raps for various size intervals.

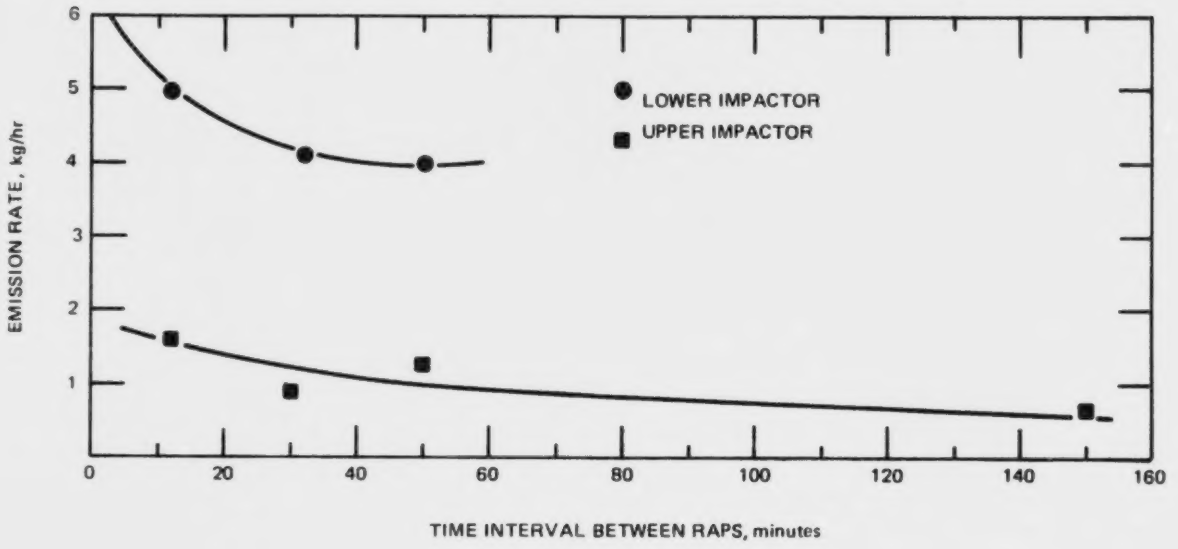

Figure 35. Outlet emission rates measured with the impactors as a function of the time interval between raps.

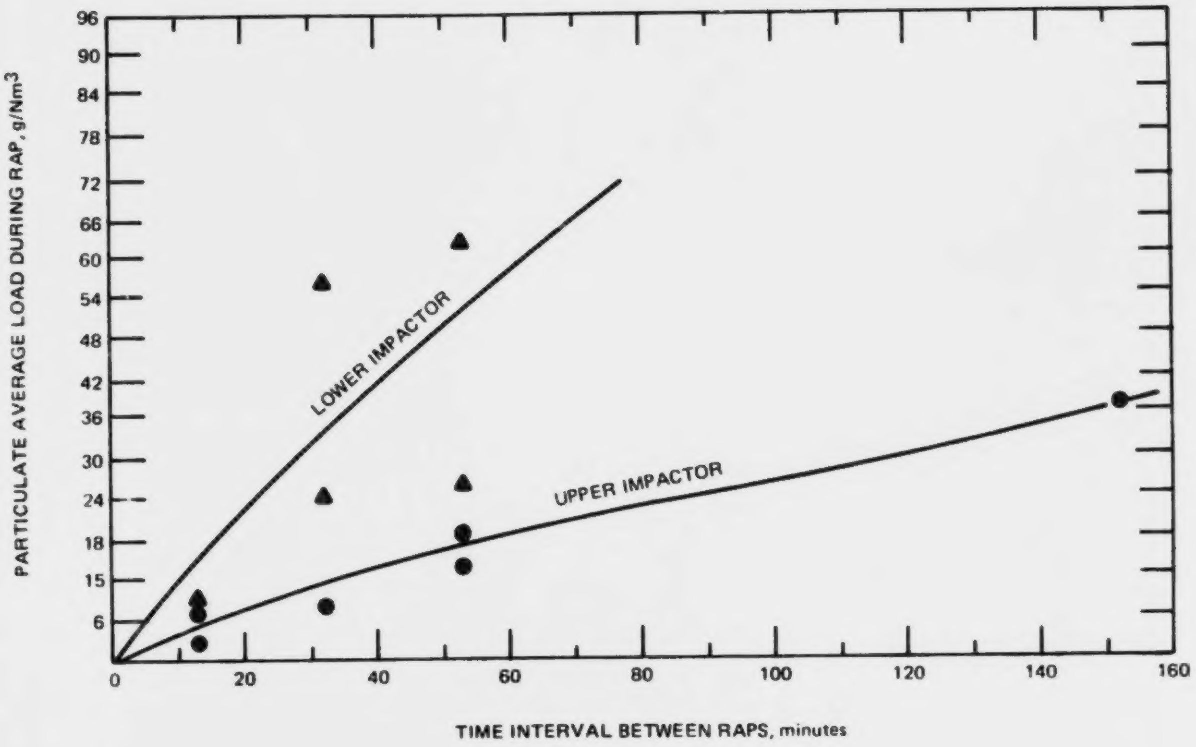

Figure 36. Average particulate load during a rap as a function of the time interval between raps.

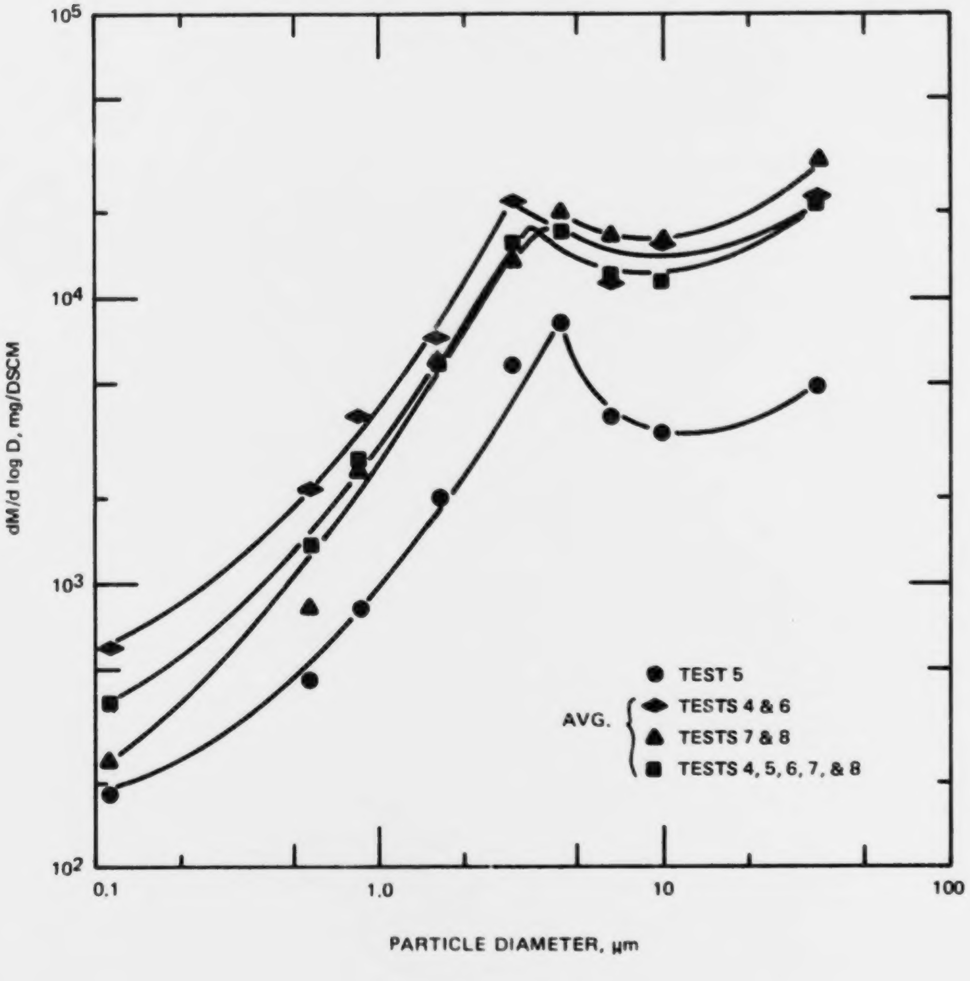

Figure 37. Particle size distribution for rapping puffs, dm/d log D's (average volume of gas sampled during the rapping puffs was determined from the sampling rate and the average persistence time of the rapping puffs) tests 5, 4 & 6, 7 & 8 had 12, 32, and 52 minutes, respectively, between rap intervals.

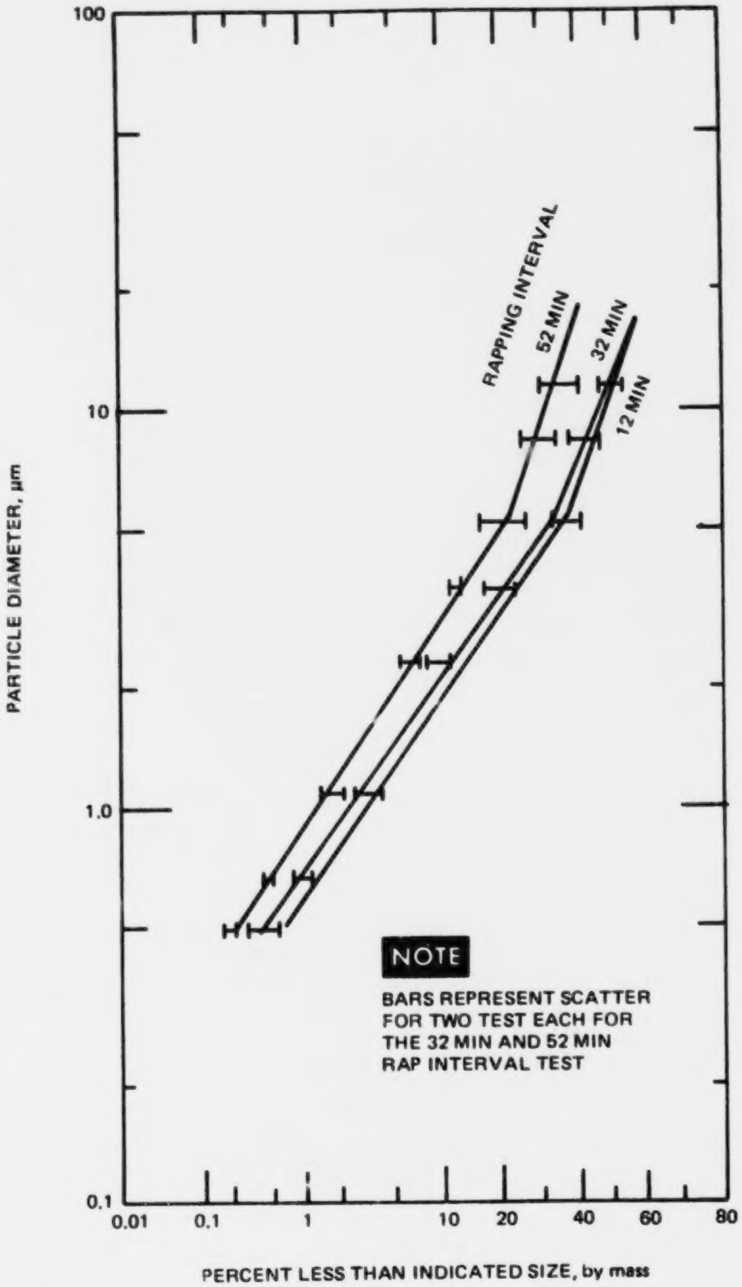

Figure 38. Cumulative percent distribution for rapping puffs, lower 32% of the precipitator cross sectional area, rapping intervals of 12, 32 and 52 minutes.

The emission rates for various particle size intervals (each impactor stage) are shown in Figures 39 and 40 for the upper and the lower impactors. The lower area emission rates were calculated on the basis of a sampled cross sectional area of 5.6 m^2 (60 ft^2) and the upper area emissions were calculated on the basis of a sampled cross sectional area of 8.9 m^2 (96 ft^2). By summing the emission rate measured by the upper and lower impactor in a particle size band, the total emission rate in each size band can be obtained. A comparison of the data shown in Figures 39 and 40 shows that the emissions in the lower portion of the precipitator dominated the rapping emissions. As already mentioned previously, the rapping emissions in the lower portion of the precipitator appeared to be due to gravitational settling and hopper boil-up. The particle size distributions measured in the upper portion of the precipitator have large fluctuations. The fluctuations in the data are possibly due to real variations in the quantity and distribution of the reentrained particulate.

The percent contributions of rapping puffs to total emissions for each particle size are shown in Figure 41. This data shows that rapping puffs contributed up to 60% of the emission of particles with diameters greater than 1 μm. The data also indicate that the percent contribution for the particle sizes less than 3 μm decreases as the time interval between raps is increased. These percentages are equivalent to the percentages defined by equation 5 in the introduction. Their application for computing rapping emissions is discussed later in the report.

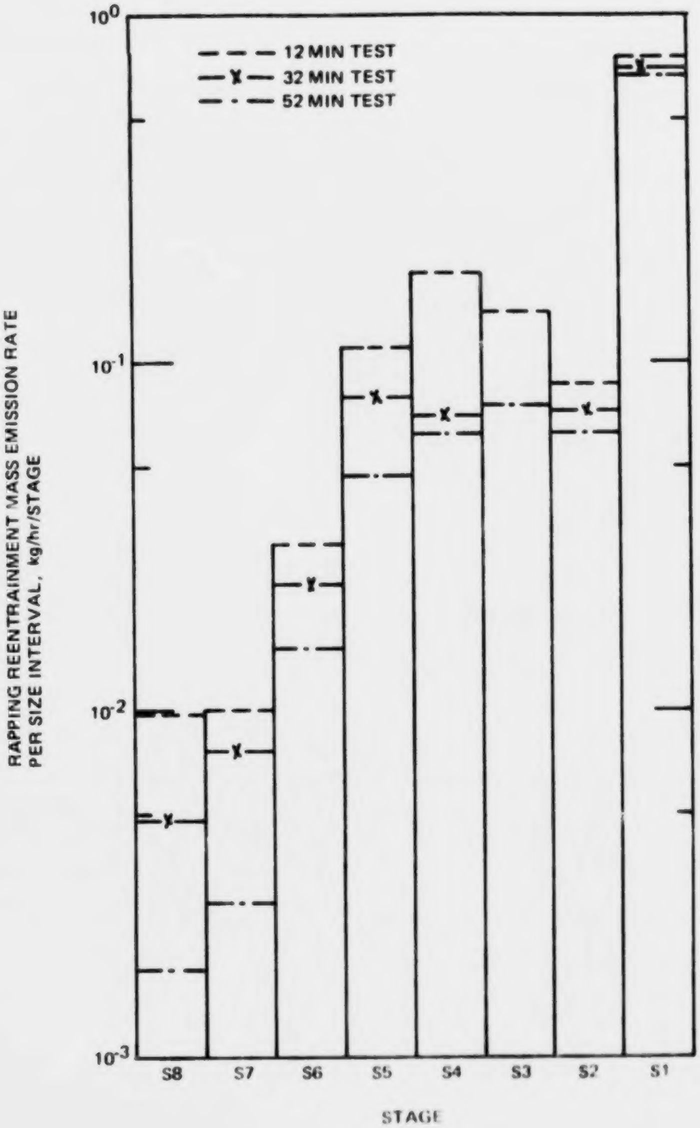

Stage	Size Interval
S1	– 12.2 µm
S2	8.5 – 12.2 µm
S3	5.3 – 8.5 µm
S4	3.7 – 5.3 µm
S5	2.4 – 3.7 µm
S6	1.1 – 2.4 µm
S7	0.67 – 1.1 µm
S8	0.50 – 0.67 µm

Figure 39. Mass emission rates for rapping reentrainment, lower 32% of precipitator exit for various particle size intervals.

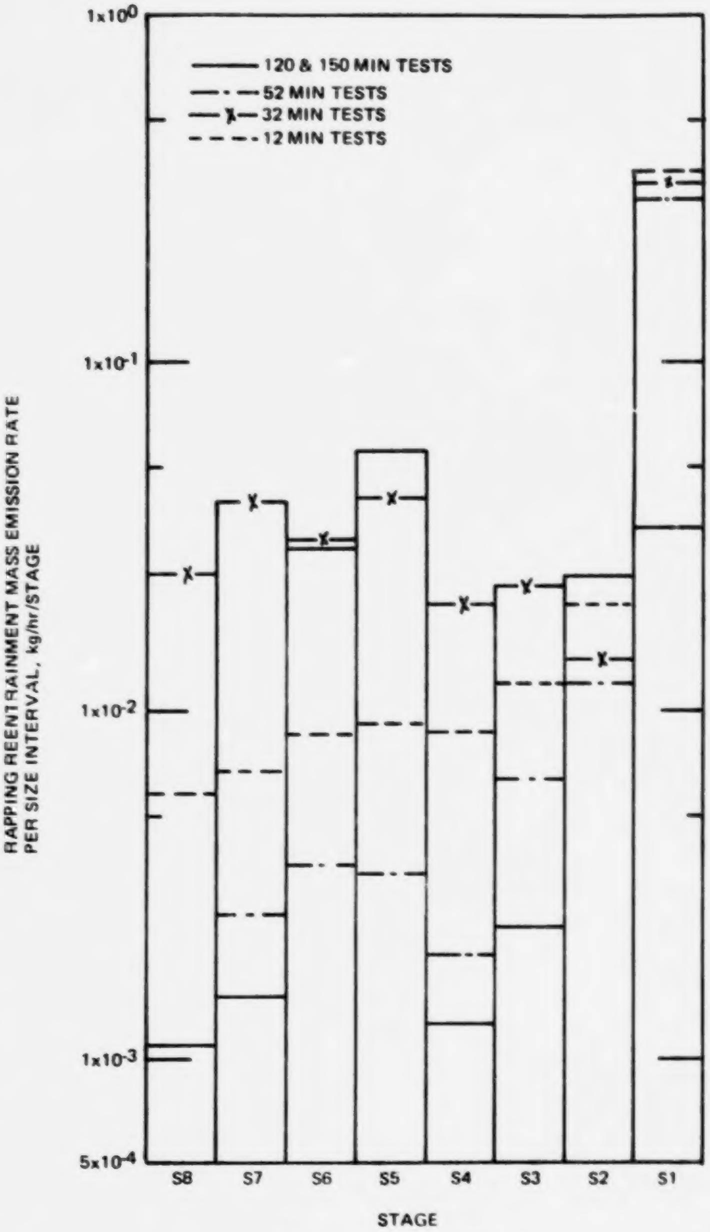

Stage	Size Interval
S1	> – 12.2 μm
S2	8.5 – 12.2 μm
S3	5.3 – 8.5 μm
S4	3.7 – 5.3 μm
S5	2.4 – 3.7 μm
S6	1.1 – 2.4 μm
S7	0.63 – 1.1 μm
S8	0.50 – 0.67 μm

Figure 40. Mass emission rates for rapping reentrainment, upper 68% of precipitator exit for various particle size intervals.

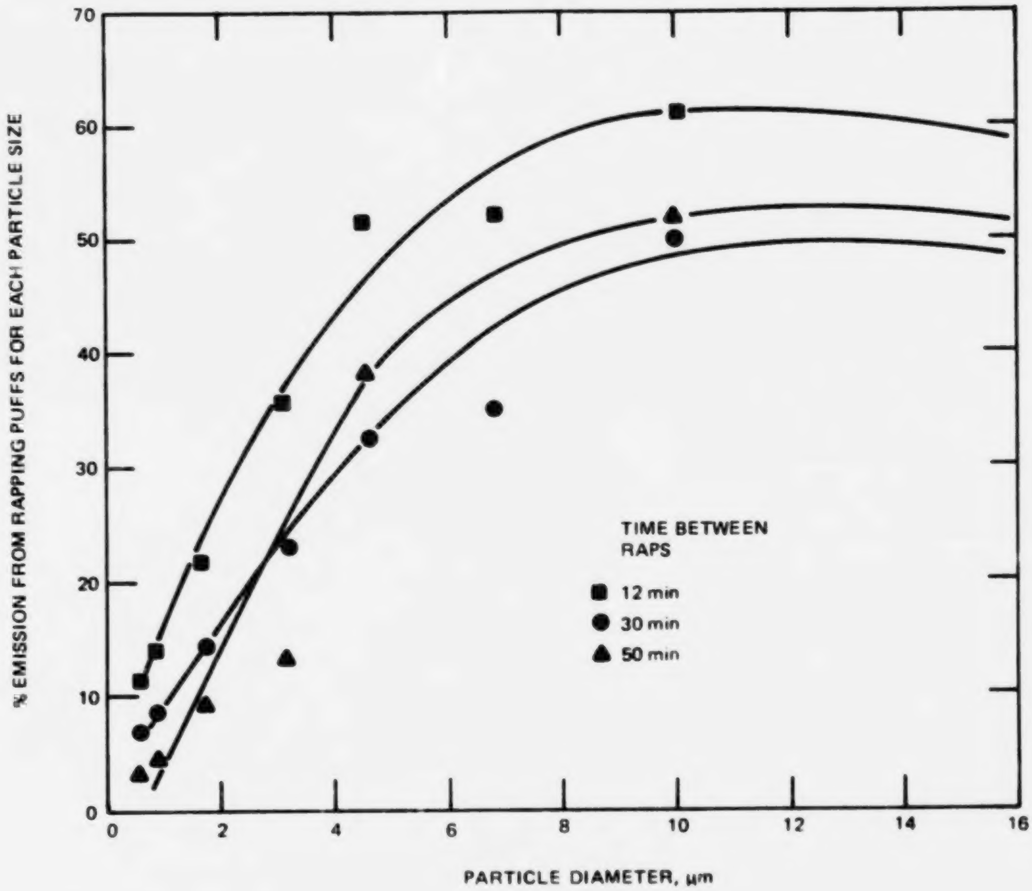

Figure 41. Percent emissions due to rapping reentrainment as a function of particle size.

RESULTS OF REAL TIME MEASUREMENTS OF RELATIVE CONCENTRATIONS IN FIVE SEPARATE PARTICLE SIZE INTERVALS

Dust removal from the precipitator plates by rapping produces temporal and spatial variations in the concentration and particle size distribution of the dust leaving the precipitator. The rapping puffs can account for a significant portion of the emissions for some particle sizes. Two modified Royco Model 225 particle counters with five-channel analog ratemeters were used to monitor rapping emissions in time and space in the following five diameter intervals: 1.5 to 3 μm, 3 to 6 μm, 6 to 12 μm, 12 to 24 μm, and greater than 24 μm.

Relative emissions between raps for each size interval were determined by multiplying average count rates between raps by the time interval between raps. The relative emissions from rapping puffs for each size interval were calculated by integrating the ratemeter output over the time interval for which the rapping puff persisted. The dust feed was turned off when the plates were rapped; thus rapping puff emissions were observed independently of the emissions not due to rapping.

Although a size-selective dilution system was used, concentrations in the 1.5 to 3 μm and 3 to 6 μm diameter intervals were too high for the Royco system during some raps for accurate analysis, while concentrations in the 12 to 24 μm and greater than 24 μm intervals were so low that a statistical analysis based on a Poisson distribution of counts had to be used to determine total relative emissions in the large particle size intervals.

Vertical concentration gradients between raps were explored with the real time system. Significant increases in concentration toward the bottom of the precipitator were observed. Between raps, the vertical distribution of particles in the 1.5 to 3 μm size interval was found to be relatively constant while the vertical distribution in the other particle diameter ranges decreased with increasing elevation. An example of the vertical stratification is shown in Figure 42. These data indicate that there was some change in the particle size distribution of the suspended particulate with increased elevation.

The vertical stratification of the particulate is attributed to several causes. In the lower portion of the precipitator the increased emissions are due to hopper sneakage and to gravitational settling of the particulate, especially for the larger particle sizes. Sneakage through the corona wire and plate support structure appears to explain the increase in emissions observed at the top of the precipitator.

The relative total emissions between raps in the five particle size intervals studied with the real time system were compared for time intervals of 12, 32, and 52 minutes between raps. The data indicated that the between-rap emission rates did not change with the increase from 12 minutes to 32 minutes between raps. However, there were increased emission rates at the sampling point just above the lower baffle for the 52 minute interval test. Emissions at this point are probably dominated by sneakage and may be signficant only for this particular precipitator-hopper geometry. The increase may have resulted from voluntary rapping or "sloughing". Relative emissions with respect to the 12-minute interval between rap tests are tabulated in Table 14. In the absence of changes in collection efficiency with increases in dust layer thicknesses on the plates, the ratios in Table 14 would be expected to be the same as the ratios of the time intervals between raps.

The vertical stratification of the rapping puffs that was observed with the impactors and mass sampling trains is clearly shown by the real time particle size data given in

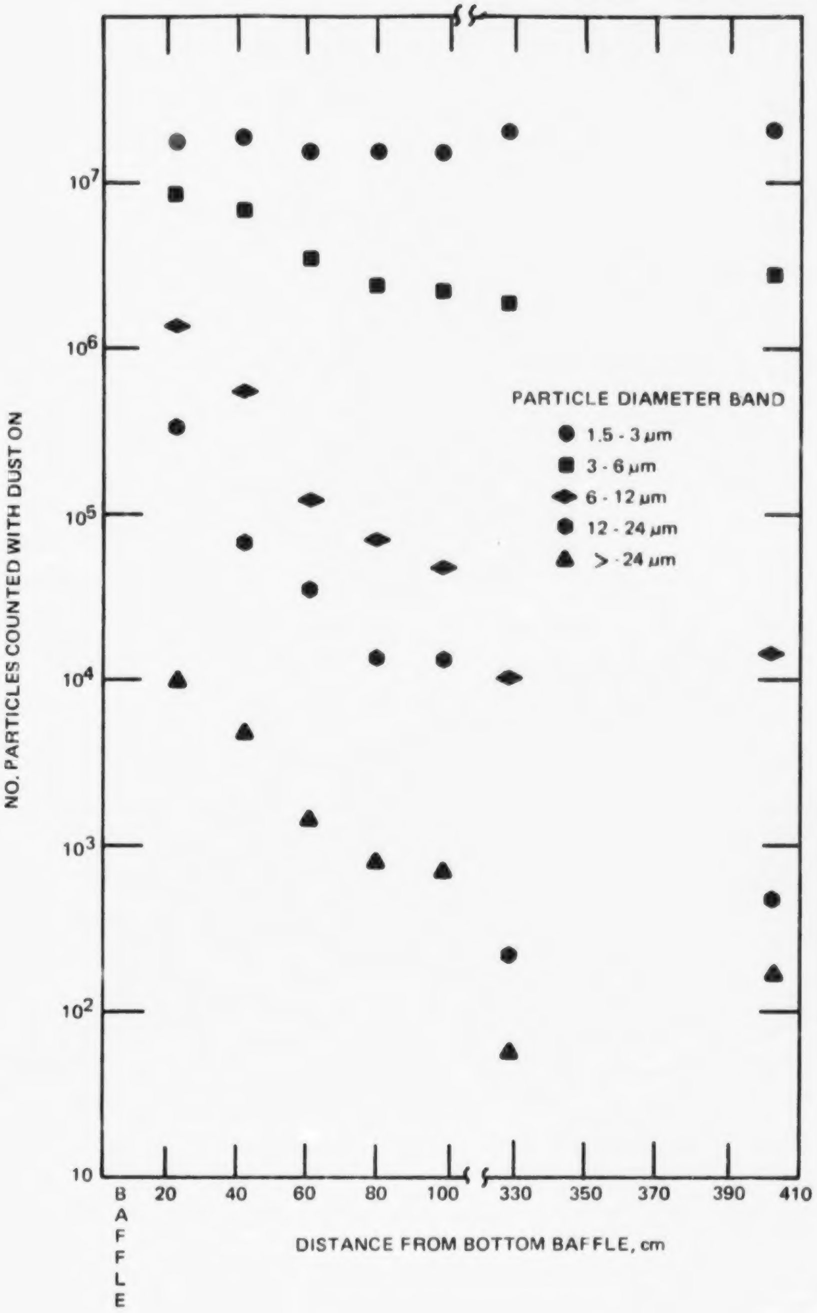

Figure 42. Spatial distribution of between rap emissions for various particle sizes.

Table 14. RATIO OF RELATIVE TOTAL BETWEEN RAP EMISSIONS IN FIVE PARTICLE SIZE INTERVALS FOR RAPPING INTERVALS OF 12, 32, AND 52 MINUTES

Particle Diameter Interval (microns)		1.5-3	3-6	6-12	12-24	>24
Time Between Raps	Time Ratio	Emission Ratio Lower Sampling Points				
12 min	1	1	1	1	1	1
32 min	2.7	2.7	2.9	1.1	2.5	.8
52 min	4.3	6.0 (5.9)	10.0 (12.7)	3.7 (8.0)	6.0 (14.3)	2.9 (5.3)*
		Emission Ratio Upper Sampling Points				
12 min	1	1	1	1	1	1
32 min	2.7	2.7	2.5	2.5	3.1	4.6
52 min	4.3	5.5	7.8	4.4	2.8	2.3

*Includes lowest sampling point

Figures 43 and 44. The data in Figure 44 shows that stratification occurs for both the upstream and the downstream raps. The emissions at 23 cm and 42 cm above the lower baffle were nearly the same. For higher elevations above the baffle the dust concentration in the puffs decreased with increasing height.

The puffs in the lower portion of the precipitator were observed to last approximately 28 seconds and 24 seconds respectively for the upstream and downstream raps. The rapping puffs observed in the upper portion of the precipitator lasted about 9 seconds for the upstream rap and 7 seconds for the downstream rap. Typical traces of upstream and downstream rapping puffs for both the upper and lower sampling locations are shown in Figures 45 through 48. On the basis of the flow velocity ($\sim$ .9 m/sec) through the precipitator, it was estimated that the rapping puffs should last only 2 seconds for both the upstream and downstream rap. This estimate was based on a rap of a 1.8 meter length of the precipitator and the assumption that the reentrained particulate moves with the velocity of the gas through the precipitator. The raps observed with the real time system persisted for 3 to 19 times the 2 second estimate. In the lower half of the precipitator two separate puffs were observed. The first puff appeared to last for approximately 2 seconds, and the second puff approximately 25 seconds for the 1.5-3.0 μm diameter particles. The persistance for large particles was somewhat less. Examples of rapping puffs in the lower portion of the precipitator are displayed in Figure 45 for both upstream and downstream raps. The two separate rapping puffs from both the upstream and downstream raps were recorded on film. This data indicates that some of the dust removed from the plates when they are rapped is reentrained directly into the gas stream and is carried out of the precipitator at the gas velocity. The remainder of the dust drops into the hoppers. Of the dust that drops into the

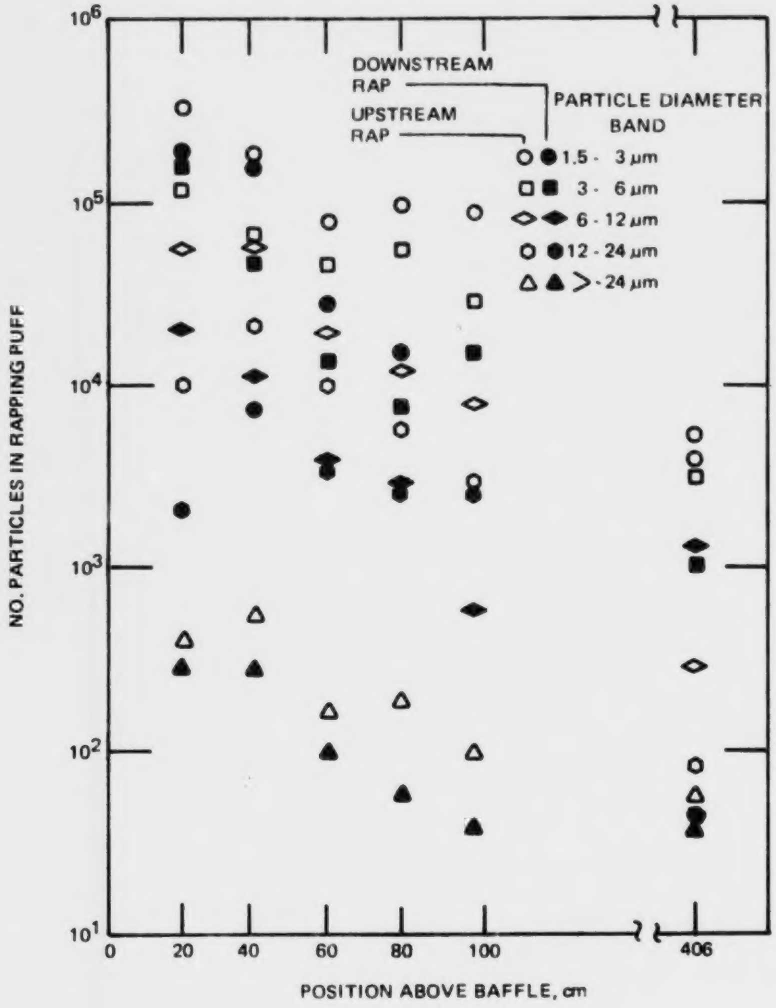

Figure 43. Spatial distribution of particles in upstream and downstream rapping puffs for 12 minute rap interval test

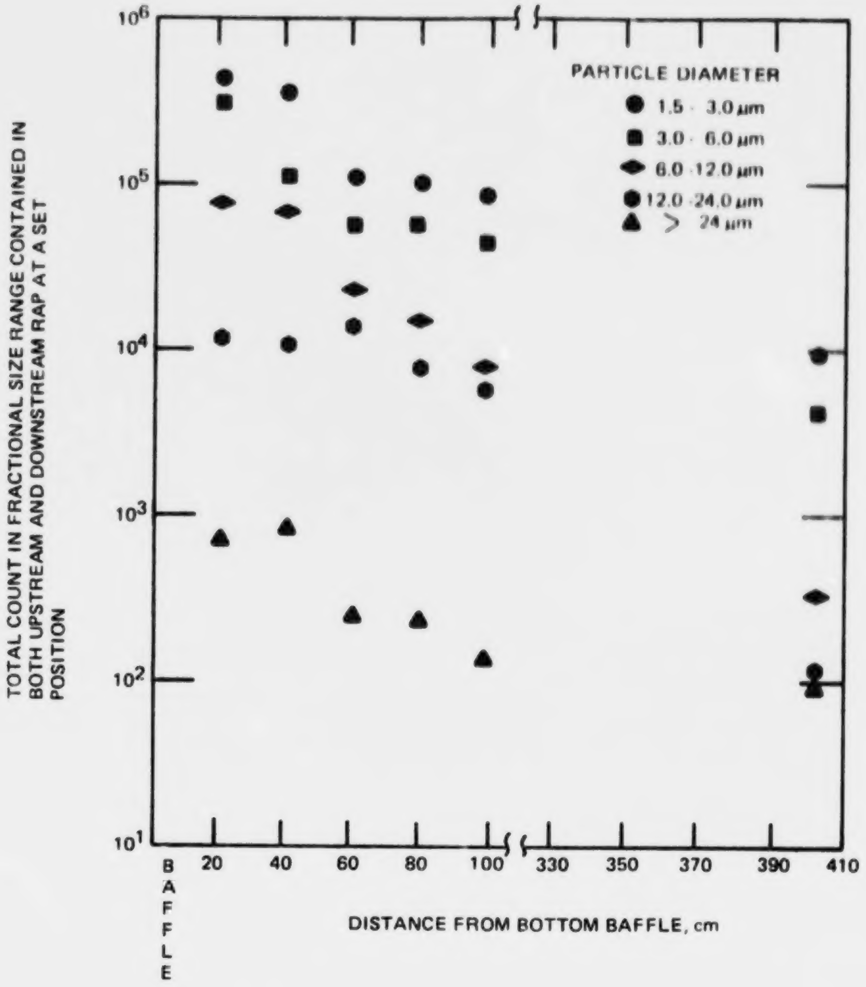

Figure 44. Spatial distribution of particles in combined upstream and downstream rapping puff.

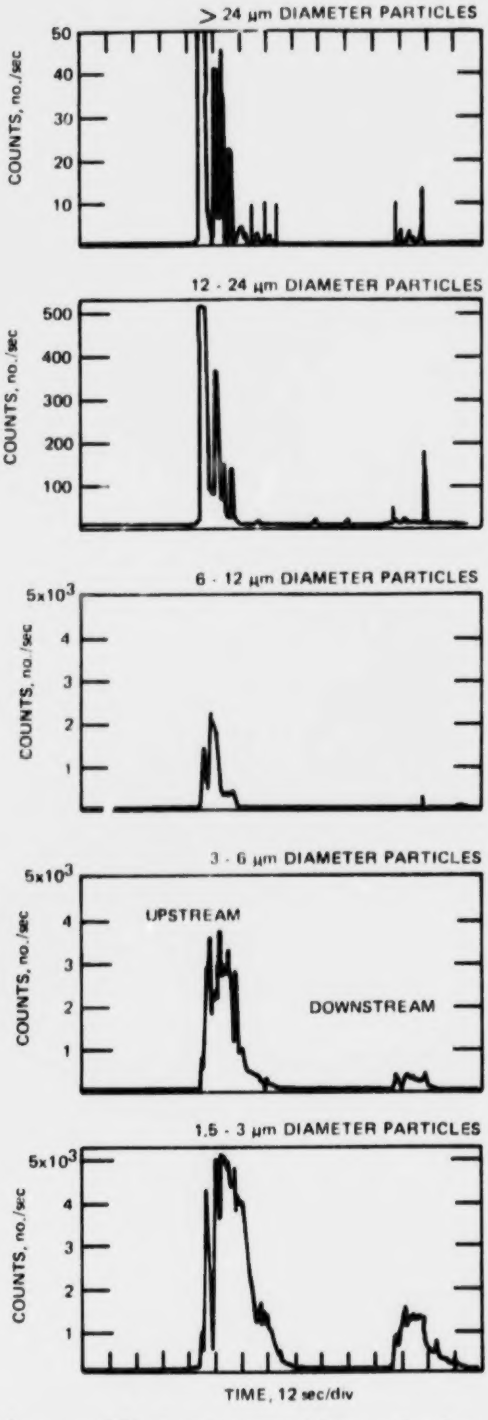

Figure 45. Rapping puffs lower portion of the precipitator, 32 minutes between raps. First set of puffs, upstream rap. Second set of puffs, downstream rap.

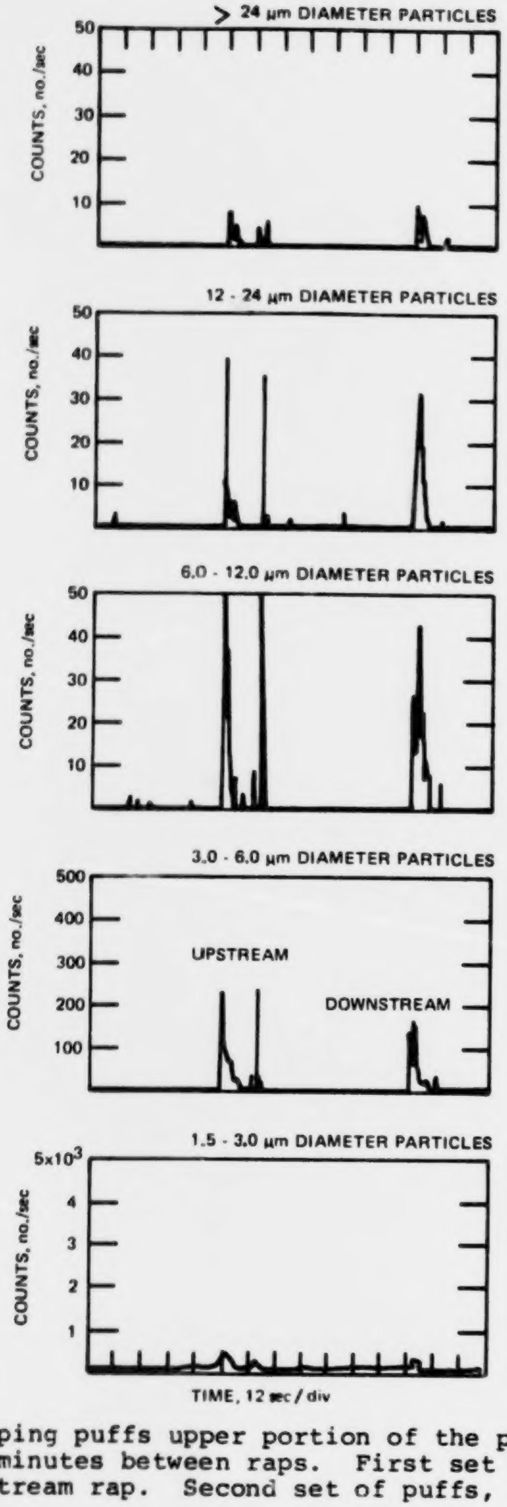

Figure 46. Rapping puffs upper portion of the precipitator, 32 minutes between raps. First set of puffs, upstream rap. Second set of puffs, downstream rap.

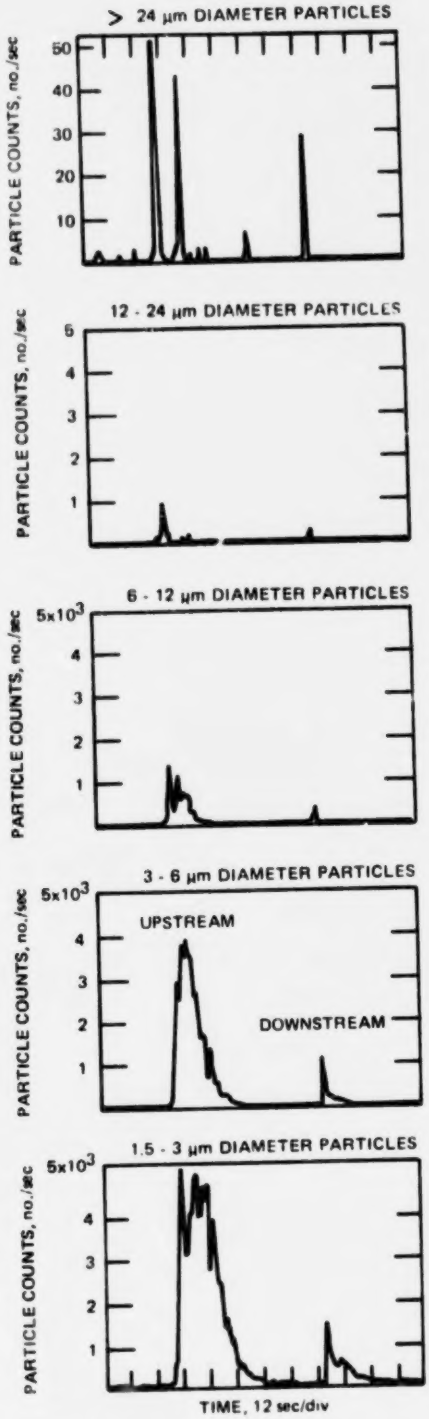

Figure 47. Rapping puffs, lower portion of the precipitator. 12 minutes between raps. First set of puffs, upstream rap. Second set of puffs, downstream rap.

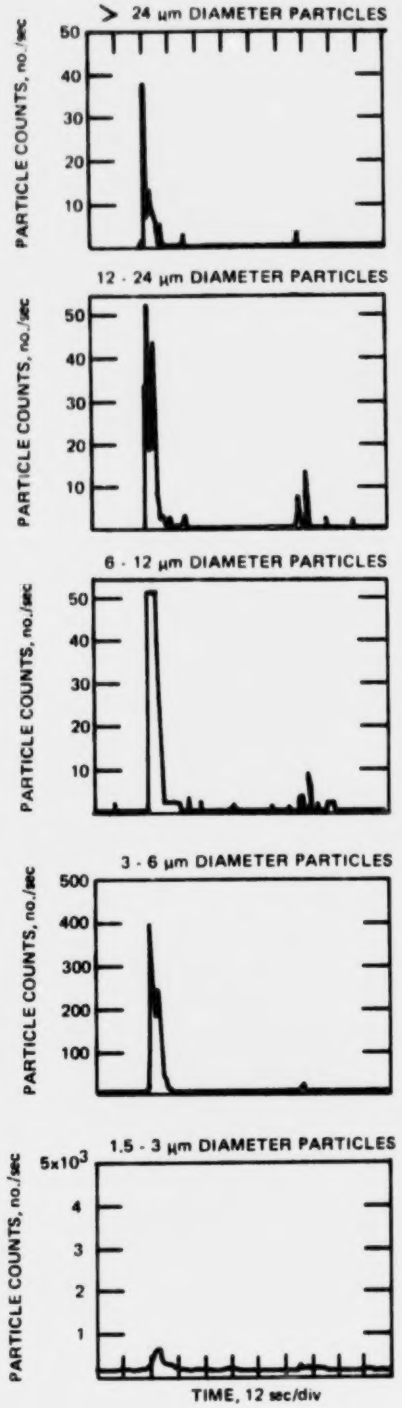

Figure 48. Rapping puffs, upper portion of the precipitator. 12 minutes between raps. First set of puffs, upstream rap. Second set of puffs, downstream rap.

hoppers a portion rebounds, breaks up, and is carried out of the precipitator. At FluiDyne the time separation of the maxima in concentration for the two puffs were approximately 7 seconds for the upstream rap and 10 seconds for the downstream rap. It was also noted that the puff from the upstream rap for the lower portion of the precipitator was first observed approximately 3 seconds after the rapper was activated and the downstream puff was observed approximately 1 second after the downstream rapper was activated. The puffs in the upper portion of the precipitator lasted for approximately 4 seconds. Multiple puffs were also observed in the upper sampling area with each puff persisting approximately 2 seconds. There are several possible mechanisms for the secondary puffs in the upper region of the precipitator. The most likely mechanism is a secondary breakaway of the dust initially dislodged by the rap but not immediately removed from the plate. Some of the upper secondary puffs were observed to occur as much as 17 seconds after the primary puff. These delayed puffs may have been due to hopper boil-up and turbulent transport of the hopper boil-up. Examples of rapping puffs in the upper portion of the precipitator are shown in Figures 46 and 48.

The data displayed in Figure 43 and the rapping puffs shown in Figures 45 and 47 show that in the lower portion of the precipitator the upstream rap always produced the largest contribution to the rapping emissions in the lower half of the precipitator. This phenomenon occurs because precipitators collect dust in an exponential fashion. The first plate of the FluiDyne precipitator collected the thicker dust layer. Since the dust surface density was higher than in other parts of the precipitator and the particle size larger, the dust was more easily removed from the first plate. Thus, on rapping, a larger quantity of dust is removed from the first two plates and dropped into the hoppers than from the third plate. Some of this dust rebounds and passes through the hoppers without being recollected. On the downstream plate, the dust surface density was much smaller thus did not contribute as much to rapping emissions. In the upper portion of the precipitator, the relative size of the rapping puffs from the upstream and downstream rap did not depend on the amount of hopper boil-up. When the dust surface density in the downstream section was too small for dust removal, the upstream rap contributed the larger portion of the emissions in the upper portion of the precipitator, as indicated by the rapping puffs shown in Figure 48, which were obtained with a 12 minute interval between raps. However, when the dust surface density on the downstream plates was high enough that dust was removed, the downstream rap produced the largest quantity of dust in the upper portion, as shown by the rapping puffs displayed in Figure 46 which were recorded with a 32 minute interval between raps. Although a larger quantity of material was initially reentrained in the inlet of the precipitator, some of this particulate was reprecipitated. Reprecipitation also occurs for material reentrained in the outlet section, but at a much lower efficiency. It is for this reason that outlet field raps in full scale precipitators play a major part in rapping reentrainment, while reentrainment from the inlet section is usually not a severe factor in performance unless hopper boilup can sneak through the hoppers. The data from FluiDyne indicates that the effect of inlet raps on outlet emissions will depend on what happens to the hopper boilup. Hopper boilup in the outlet section of a full scale precipitator can play a major part in rapping reentrainment according to these experiments.

The total percent contribution of the raps to total emission in each size band determined with the Royco system for different time intervals between raps are given in Figure 49. The percentages obtained with the real-time system are

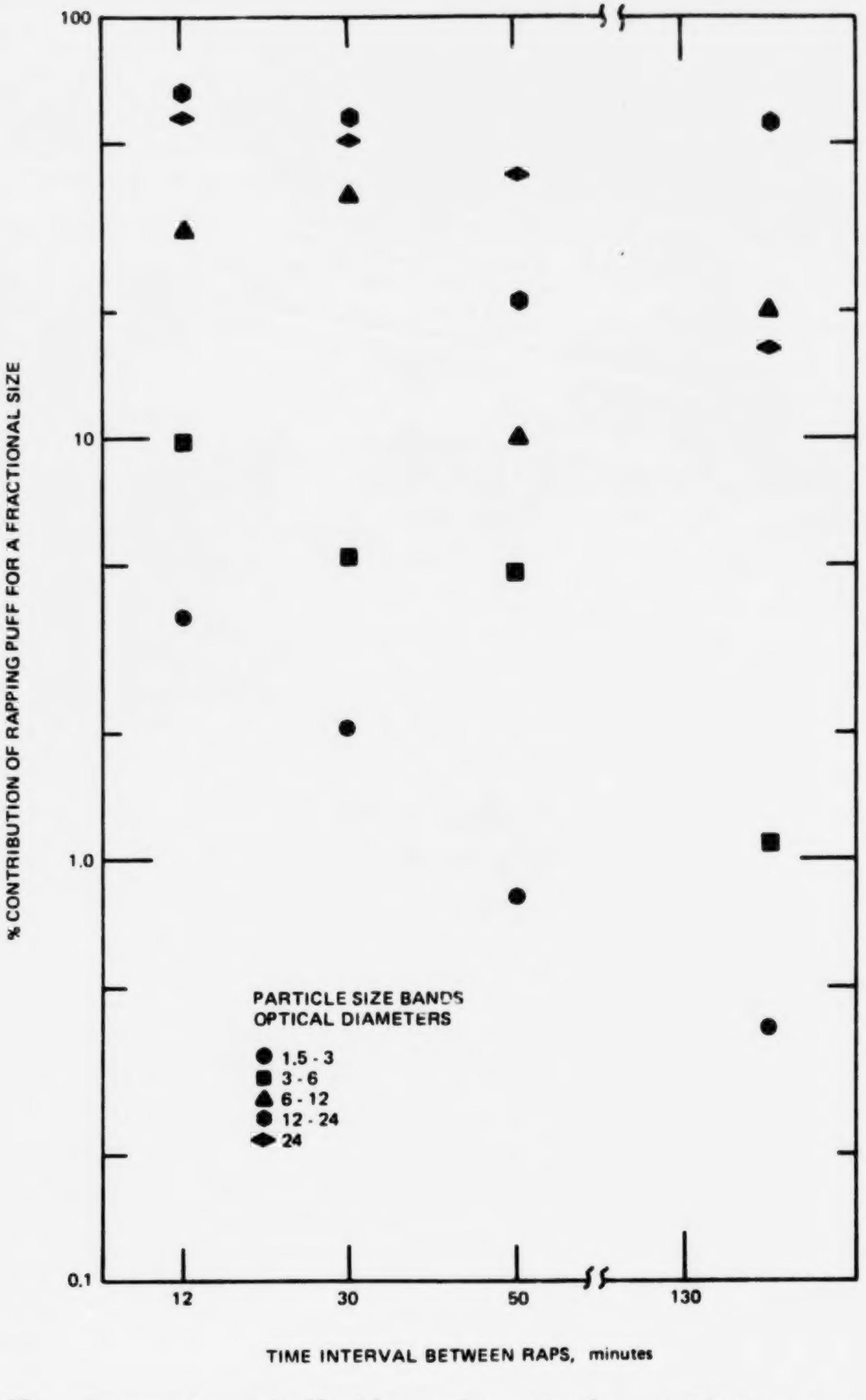

Figure 49. Percent contribution of a rapping puff to total emissions for several particle size bands as a function of the time interval between raps.

comparable to the percentages calculated from the impactor data. The real-time system data show a decrease in the net total emission rates as the time interval between raps is increased, in agreement with the impactor and mass train data. The decrease was most significant for particles with optical diameters less than 6 μm. As mentioned previously, this is most likely due to agglomeration of the particles with the thicker dust layers. The data given in Figures 41 and 49 shows that the percent increase in the concentration of the large particles during rapping is significantly larger than the percentage increase for the small particles. This occurs because the rapping puffs emissions have a larger percentage of large particles than the between rap emissions. For a high efficiency precipitator which removes nearly 100% of the large particles entering the precipitator, rapping can contribute up to 100% of the particle emissions for particles with large diameters. Total percent emissions were not determined from the real time system, since comparison could only be made for data from the same size interval without correcting the data for size dependent probe losses, size selective dilution and anisokinetic sampling. Correction factors for probe losses, size selective dilution, and anisokinetic sampling were not considered accurate enough to justify the effort, especially since the percent of total emissions due to rapping were available from mass train and impactor data. However, one comparison between the real time data and the impactor data for a between rap case was attempted.

Expected counting rates for various particle sizes were generated from the impactor data. The expected counting rates included the correction factors for probe losses, size selective dilution, and anisokinetic sampling in the real time system. The results of the comparison are given in Table 15. The sampling flow rate used with the real time system was approximately 3 times greater than that required for isokinetic

Table 15. COMPARISON OF REAL-TIME SYSTEM DATA AND IMPACTION DATA OBTAINED BETWEEN RAPS

Particle Diameter μm	Predicted Count Rate from Impactor Data number/sec	Measured Count Rate number/sec
1.5-3	4240	4500
3-6	590	475
6-12	12	4
12-24	2.3	0.4
24-48	0.83	0.2

sampling. This high flow rate was used to solve a condensation problem in the diluter. The real time test results obtained during the test with 120 minute and 150 minute intervals between raps were confused by condensation forming in the diluter. Increasing the sample flow velocity raised the temperature in the diluter enough that the condensation did not occur during the other tests.

The real time particle size system also proved useful for studying variations in between-rap outlet concentrations as a function of precipitator currents and voltages.

CONTINUOUS MONITORS, KONITEST AND TRANSMISSOMETER

The dust concentrations at the outlet were continuously monitored with a Lear Siegler RM41p transmissometer and with a Konitest meter. These instruments provided fast real time response for determining changes in precipitator operation during the test. The effects of sparking and changes in current density were immediately observed with these instruments.

The amplitude of the Konitest current tended to correlate with the amount of dust removed from the plates, as shown in Figure 50. Unfortunately, neither the transmissometer nor the Konitest were monitored closely enough during the test and the majority of the rapping puffs produced signals that were off-scale on the recording instruments. Thus, these instruments were not used to make quantitative measurements of rapping emissions. An additional reason for not using the transmissometer data is that the transmissometer output is a function of the particle size distribution of the particulate in the view volume and this changed when rapping puffs occurred.

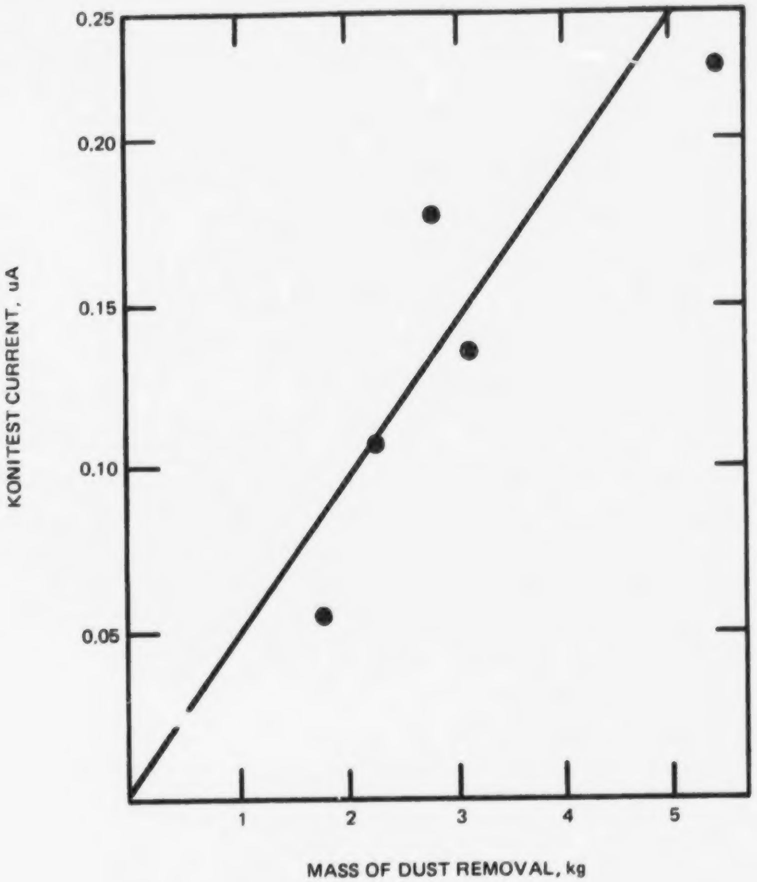

Figure 50. Correlation of mass of dust removed from plate 4-1 and amplitude of Konitest meter current output for the upstream rapping puff for test 5 (12 minute rap interval).

Between-rap data obtained with the Konitest during tests 5 and 6 indicated an increase in the between-rap loading during the tests. However this was not observed during the previous tests 3 and 4 with the Konitest nor during any of these tests with the transmissometer.

DUST COLLECTION RATES ON THE PLATES AND DUST REMOVAL FROM THE PLATES

In this section, the removal of the collected particulate from the plates is discussed. The data provide a background for modelling the process of removal of the collected particulate from the precipitator plates by rapping and for determining optimum rapping conditions.

In the FluiDyne test facility the suspended particulate is collected on large plates by electrostatic precipitation and removed from the plates by rapping them with a pneumatic rapper. The design of the rapping system was described in an earlier section. In place of the pneumatic system, mechanical drop hammers, magnetic drop hammers, or vibrators might have been used with similar results.

For proper rapping, these systems must supply sufficient force to remove dust from the plates and at the same time not directly reentrain the dust into the gas stream. Ideally, the collected layer should be freed just enough to slide down the precipitator plates and into the hoppers. Even under this ideal condition dust can still be reentrained when it falls into the hoppers.

The rapping system at FluiDyne was successful in removing dust from the plates of the first meter (3 ft) of the precipitator but unsuccessful in removing the collected particulate efficiently from the last 1.8m(6 ft) of the precipitator. The mass of particulate collected on plates 4-1, 4-2, and 4-3 as a function time for tests with rap intervals of 12 and 32 minutes are shown in Figures 51 through 54.

From this load cell data and similar load cell data for the various test conditions, we calculated the collection rates, removal rates, and percentage removal rates as functions of the time between raps.

The data given in Figure 51 shows that no dust was removed from plate 4-1 until more than 15 kg of particulate had collected on the plate. The data also show that the residual layer remaining after a rap increased throughout the 12-minute interval rap test. The data in Figures 52 and 54 showed that very little dust was removed from the outlet plate when it was rapped.

It was also observed that during the night about 10 kg of dust fell off plate 4-1. According to the load cell data, dust fell off the plates every time the precipitator was turned off after several hours of testing.

The collection rates determined from load cell data are displayed in Figure 55. The collection rates show the expected theoretical exponential dependence on precipitator length and a collection rate that is independent of the time interval between raps. A decrease in collection rate with increasing time between raps was expected. This was not observed. From data, it was estimated that 76% of the particulate was collected in the first meter of the unit.

Particulate removal from the plates was observed to vary as a function of the time interval between raps and as a function of location in the precipitator. The dependence of particulate

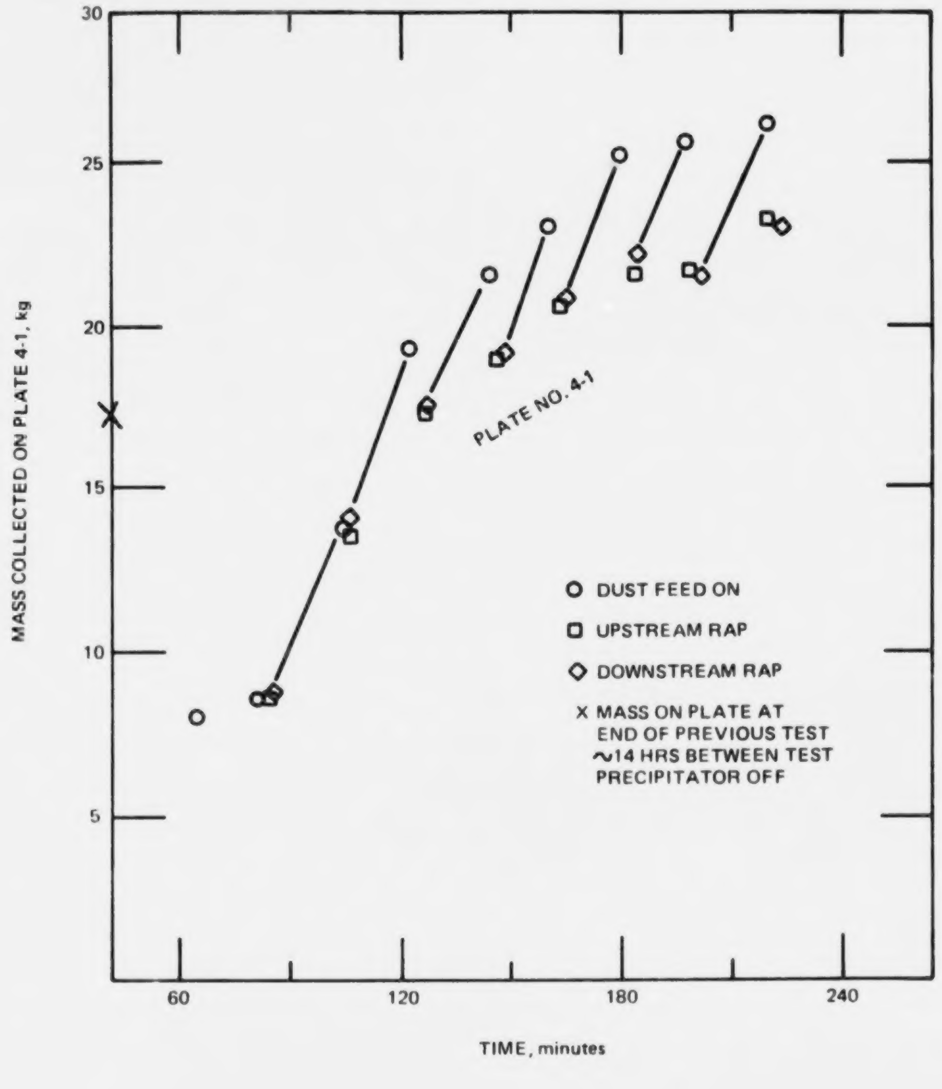

Figure 51. Load cell data, mass collected on plate 4-1, 12 minute interval between raps.

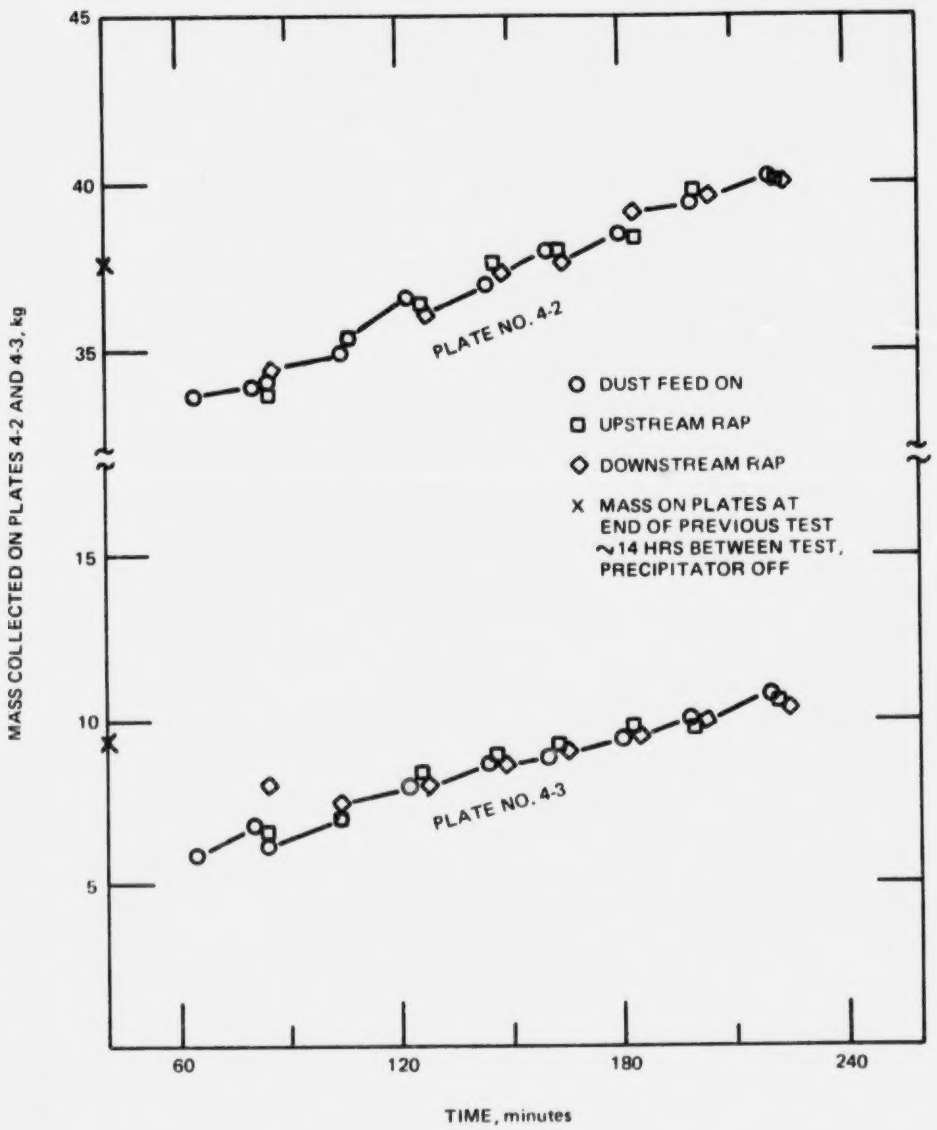

Figure 52. Load cell data mass collected on plates 4-2 and 4-3, 12 minute intervals between raps.

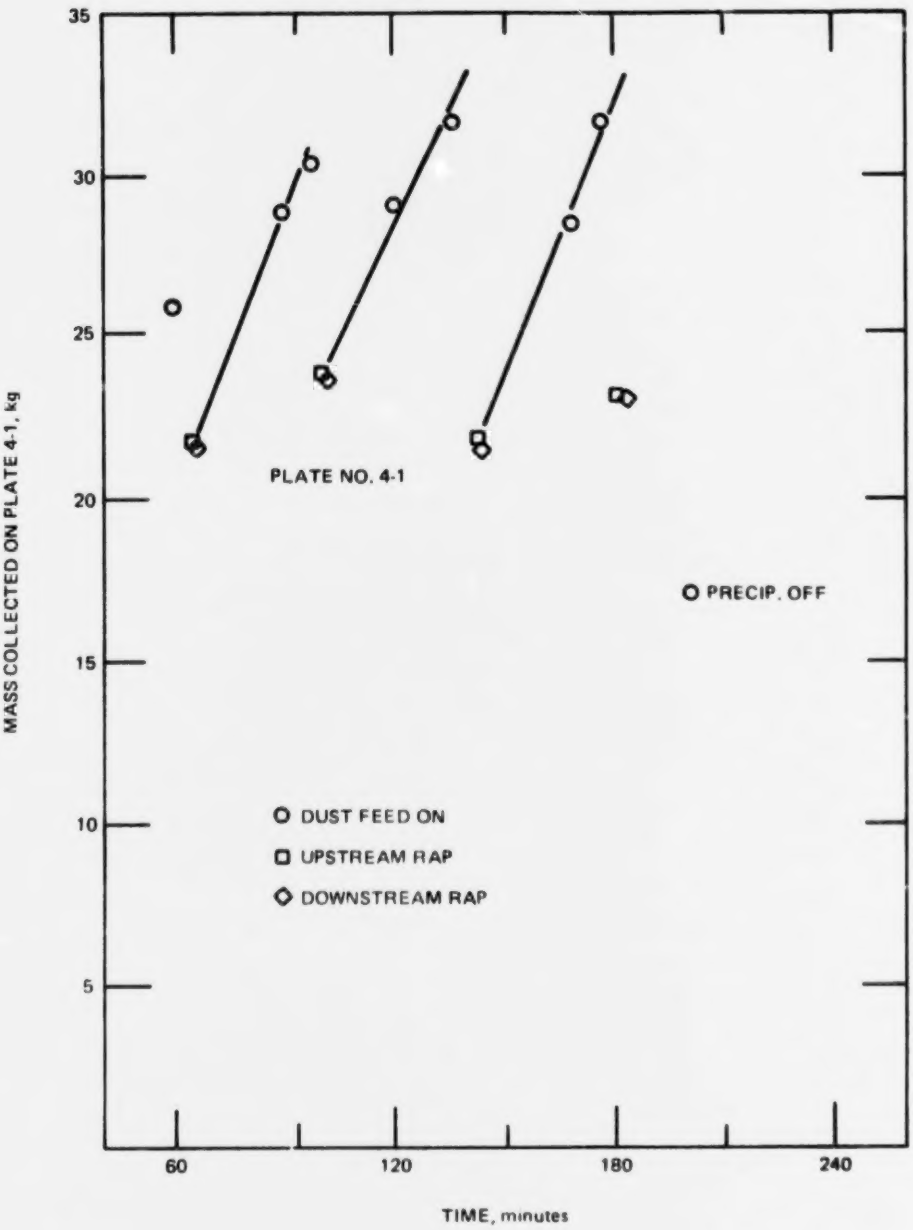

Figure 53. Load cell data, mass collected on plate 4-1, 32 minute intervals between raps.

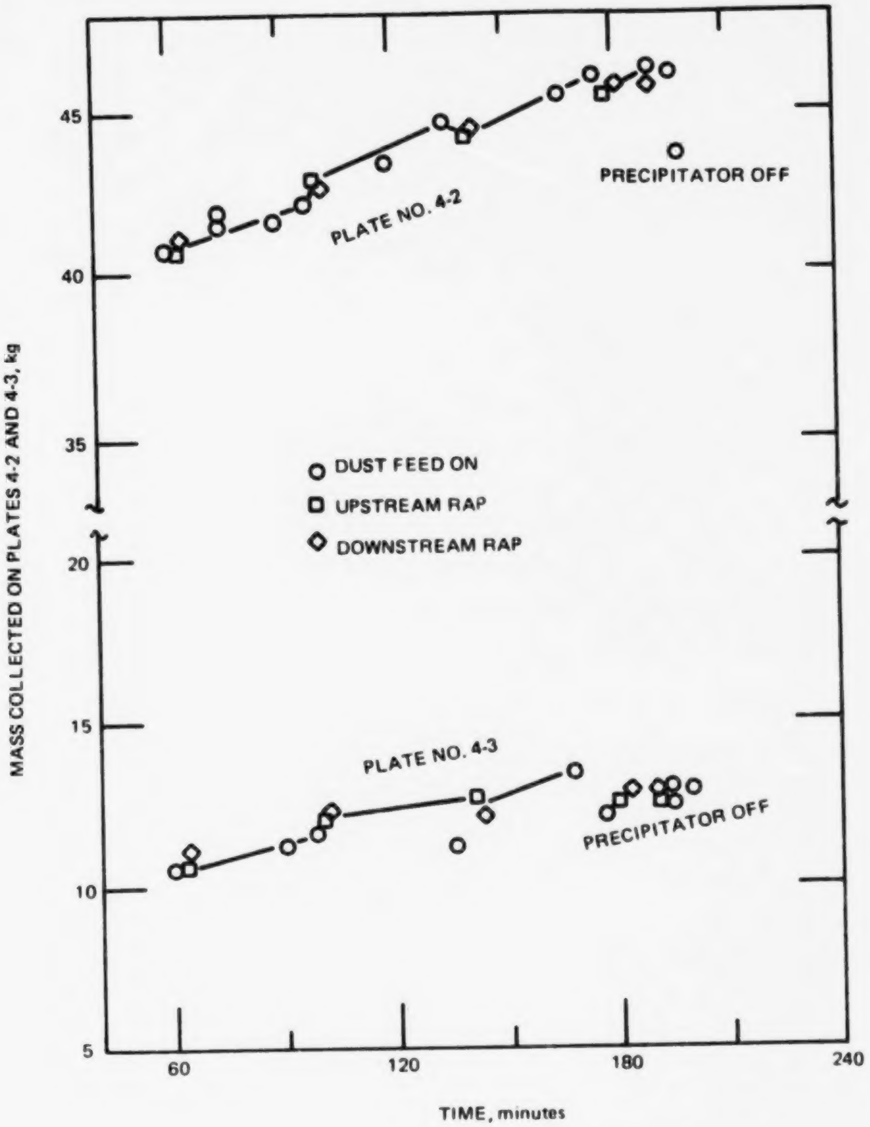

Figure 54. Load cell data, mass collected on plates 4-2 and 4-3, 32 minute intervals between raps.

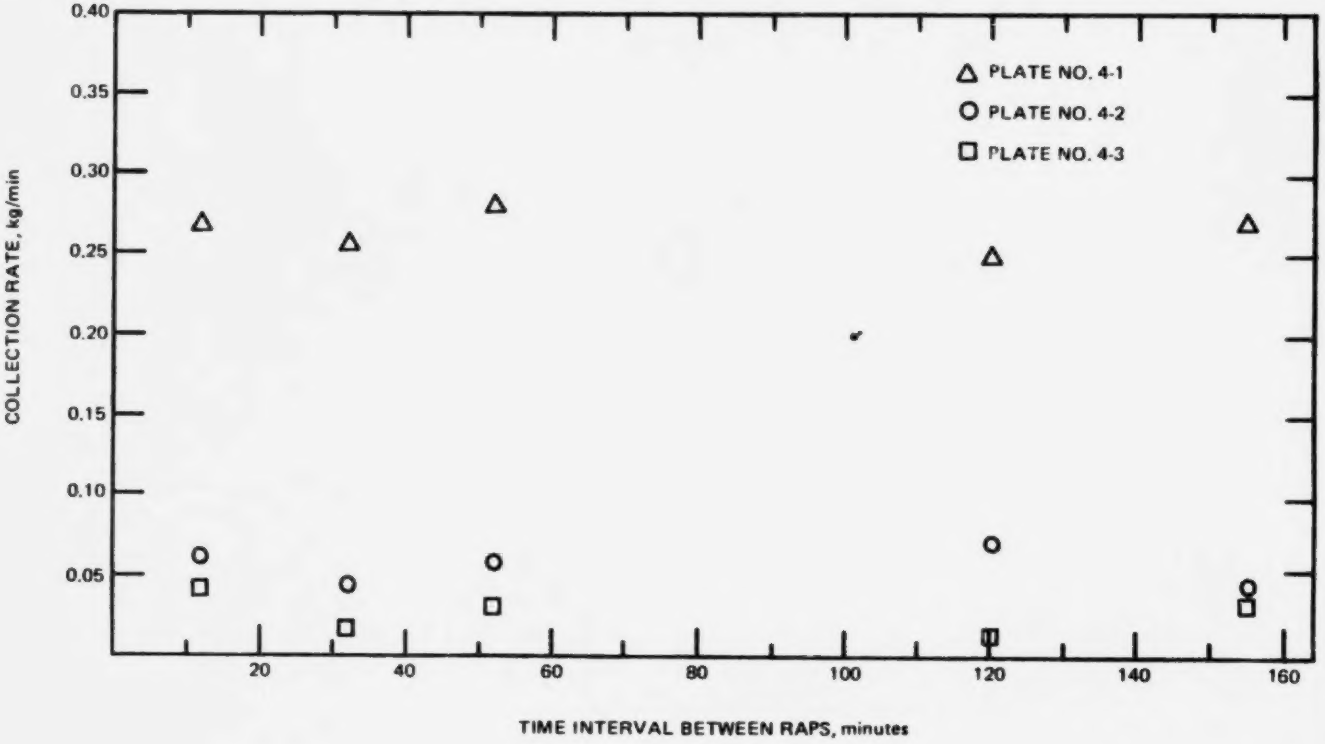

Figure 55. Collection rate of particulate as a function of time interval between raps.

removal on these parameters can be explained by the effect that dust surface density (mass per unit ares) plays in removal of the dust from the plates and the effects of consolidation time on the cohesion characteristics of the collected dust layer. In Table 16, the removal efficiencies, the percent of freshly collected dust that is removed by a rap, and the percent of total mass on the plate that is removed by a rap are given for time intervals of 12, 32, 52, and 120 minutes between raps. The removal efficiencies versus time between raps are displayed in Figure 56. These data were computed from load cell data similar to that in Figures 51 through 54. The data show that efficient removal (>75%) of the dust collected between raps occurred only when the mass per unit area collected between raps exceeded .8 kg/m^2. It should be noted that the percentage dust removed from the plates varied from rap to rap even for the same conditions. There are also indications that no removal occurred unless the mass per unit area on the plates was greater than 2.5 kg/m^2. The dust that is not removed with the first rap after it is collected appears to develop higher tensile and shear strengths than the freshly collected layer. The load cell data for plates 4-1, 4-2 and 4-3 indicated that dust was not removed even when the mass per unit area of the dust collected on these plates finally exceeded the levels for which freshly collected dust was removed from plates. Raps with insufficient intensity to remove the dust layer may have compacted the dust layer making it even harder to remove.

In addition to the consolidation that appears to have occurred during these experiments, it is suspected that the collected layer is harder to remove from the second and third plates due to changes in the physical properties of the layer.

Table 16. MASS PER UNIT AREA ON PLATES WHEN RAPPED, MASS PER UNIT AREA COLLECTED BETWEEN RAPS AND MASS PER UNIT AREA REMOVED BY RAP

Test	Rap Interval minutes	Plate	Mass per Unit Area of Dust on Plate When Rapped kg/m^2	Mass per Unit Area of Dust Collected Between Raps kg/m^2	Mass per Unit Area Removed By Raps kg/m^2	Efficiency of Removal of Particulate Collected Between Raps %
3	12	4-1	2.54	0.40	0.27	68
		4-2	3.30	0.08	0.00	00
		4-3	0.78	0.05	0.00	00
4	32	4-1	2.78	0.82	0.77	94
		4-2	3.98	0.13	0.02	15
		4-3	1.08	0.09	0.03	33
7	52	4-1	3.03	1.35	1.07	79
		4-2	2.60	0.23	0.01	4
		4-3	1.65	0.12	0.00	0
2	120	4-1	4.54	2.91	3.16	109
		4-2	—*	1.07	0.77	72
		4-3	—*	0.25	0.04	16

*Load cell zero shifted.

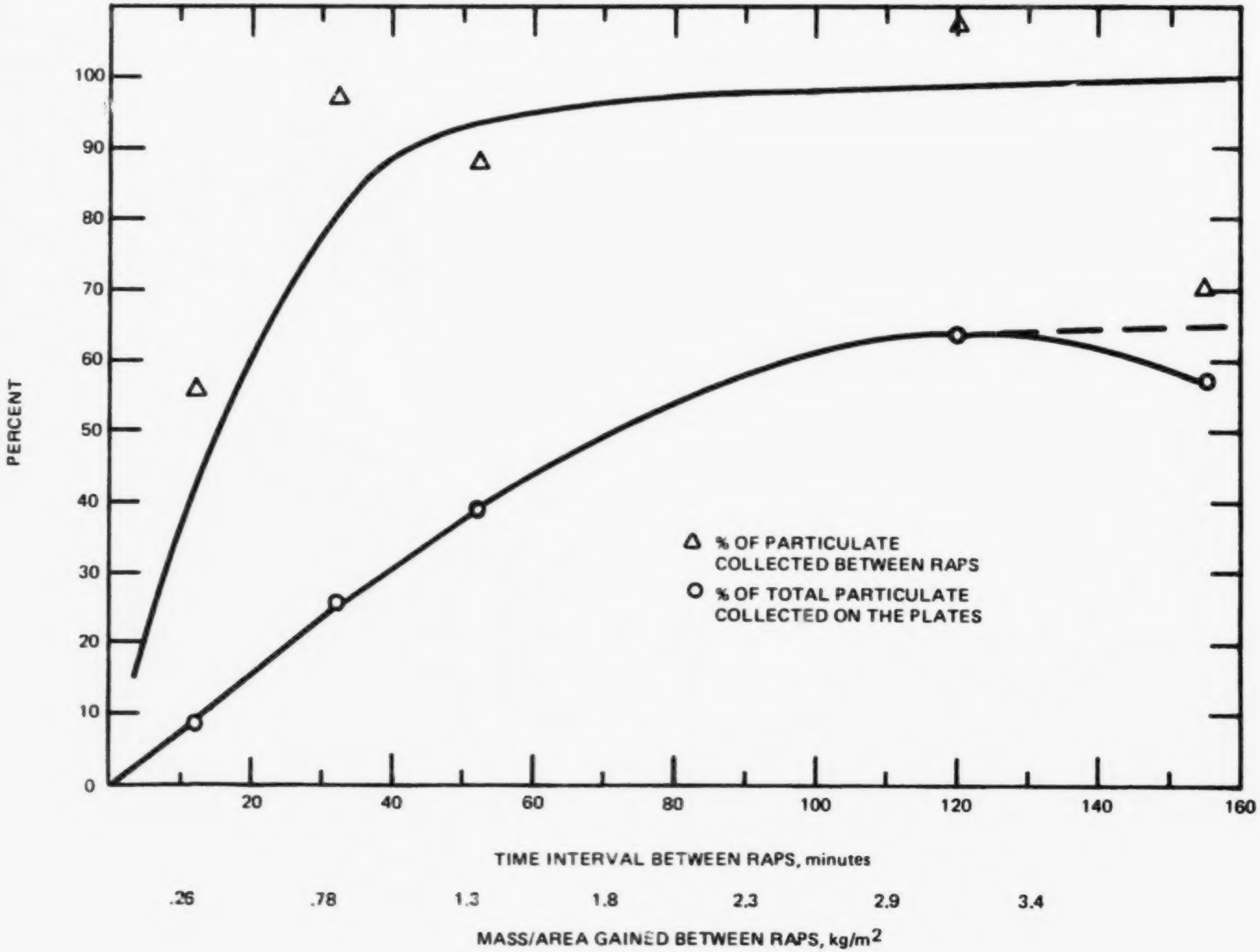

Figure 56. Dust removal efficiency for dust on plate 4-1 versus the time interval between raps.

The cohesive strength of the collected dust layer theoretically increases along the length of the precipitator, since the particulate is fractionated into particle size distributions with decreasing mass median diameters from the inlet to the outlet. The feed dust at FluiDyne had a mass median diameter of 16 μm and the dust collected in the last 20 cm length of the precipitator had a mass median diameter of ∿3 μm.

The simple theory of dust removal discussed in the introduction (see equations 2 and 3) indicates that, for a given acceleration perpendicular to the collection plates, the collected layer will be removed if the mass per unit area exceeds some minimum value. The average acceleration perpendicular to the plates at FluiDyne was approximately 1.1×10^4 cm/sec^2 (11 G). An estimated value for the tensile strength of the collected dust layer is $\sim2\times10^3$ dynes/cm^2 based on the tensile strength tabulated in Table 1.

The application of this tensile strength to other precipitated fly ash layers is highly uncertain, since cohesion and adhesion of dust layers depend on many parameters, including the physical properties of the dust, the electrical conditions at the collection plate, and the chemical composition of the gas from which the dust is precipitated. If we ignore the above objections to the use of this tensile strength, a minimum mass per unit area of 1.8 kg/m^2 was calculated for dust removal (from the ratio of the above tensile strength and plate acceleration). This minimum dust surface density agrees nicely with the data from the FluiDyne experiment, which indicates that 100% removal of the freshly collected layer occurred at a mass per unit area between 1 and 3 kg/m^2.

These load cell data show that if plate accelerations and time intervals between raps are not properly chosen to match the dust layer tensile strength, 100% removal of the dust from the precipitator plates will not occur. The data indicate that larger percentages of dust were removed from the plates as the time interval between the raps was increased. The data also indicate that, if the residual dust layers collected during the test were to be removed, plate accelerations needed to be increased. The amount of increase needed was not determined, but estimates could possibly be obtained by measuring dust removal with increased plate accelerations or by measuring the effects of consolidation time, particle size, and vibrational compaction on the tensile strength of the precipitated dust layer.

The FluiDyne experiments show the buildup of a residual dust layer. Precipitator performance is often observed to degrade after a week or two weeks of operation after starting with clean plates. This degradation is usually ascribed to the buildup of a steady-state layer of collected particulate on the precipitator plates. One solution to the residual dust layer may be the use of a set of auxiliary rappers that would rap the plates with enough force to remove the layers on a daily or weekly basis. An increase in plate acceleration to continually prevent any buildup would in many cases produce undesirable reentrainment characteristics.

The data indicate that for efficient dust removal from the plates, the plates should not be rapped at all until there is sufficient dust buildup to give a reasonable chance for efficient removal with the available plate acceleration.

The upper limit on the time interval between raps is set by the effect the dust layer has on precipitator operation. Obviously, if the dust layers become too thick they interfere with gas flow through the precipitator and inhibit performance. The collected dust layers also affect the electrical operation of the precipitator. For low resistivity dust the electrical effects are small but for high resistivity dust they can be significant. The resistivity of the dust layer affects precipitator operation in two ways: (1) by setting the current density at which the precipitator operates, if the resistivity is high enough that the current density is limited by back corona to a current density below the maximum clean plate current density, and (2) by adding a resistivity element to the circuit. The first effect is relatively independent of the thickness of the dust layer and depends only on the dust resistivity. The second effect depends on the thickness of the dust layer, dust resistivity, and current density. To prevent an excessive voltage drop in the dust layer, the thickness of the layer must be kept to a reasonable value.

Another electrical effect of collecting too thick a layer before rapping is a reduction of collection efficiency during rapping due to corona quenching produced by the space charge that develops with a large particulate load in the gas stream. The impactor data indicate that particulate loads range from 4.9 to 49 g/Nm^3 (2 to 20 gr/dscf) during the rapping puffs. However, the data from these experiments also indicate that the collected mass per unit area would need to exceed ~ 4 kg/m^2 for the particulate load produced by rapping to have a large effect on overall emissions.

This data on dust removal from precipitator plates does not supply all the information desired for modelling dust removal in any full scale precipitator. The effects of variations in dust properties and in plate acceleration were not determined. The

FluiDyne data showed substantial variations in the removal efficiency as a function of location in the precipitator and as a function of the time interval between raps. It is suspected that the variations will be even larger in full scale precipitators. These variations present problems for the modelling of rapping reentrainment. The data show that only under ideal conditions can it be assumed that all the dust collected at a particular location on a plate is subject to reentrainment every time the plates are rapped.

COLLECTION RATES, FRACTIONAL EFFICIENCIES, AND CONTRIBUTION OF RAPPING REENTRAINMENT TO TOTAL EMISSIONS

During this study of rapping reentrainment, the performance of the precipitator excluding rapping reentrainment losses was determined by measuring the fractional efficiency between raps and by measuirng the collection rate of the particulate on the precipitator plates between raps. The collection rate data and the fractional efficiency data obtained between raps were compared with predictions made with the Southern Research Institute computer model of electrostatic precipitation.[1] The comparison of the collection rates measured with the load cells and the collection rates calculated with the computer model is shown in Figure 57. Reasonable agreement between measured and calculated rates was obtained. However, the computer model calculation was low for the last meter of the precipitator length. This discrepancy could be due either to a load cell error or to an unmodelled collection effect.

The measured fractional efficiency between raps and the measured fractional efficiency including rapping losses were compared with theoretical fractional efficiencies (Figure 58). The theoretical fractional efficiencies were calculated using the Southern Research Institute computer model, the design parameters for the FluiDyne pilot

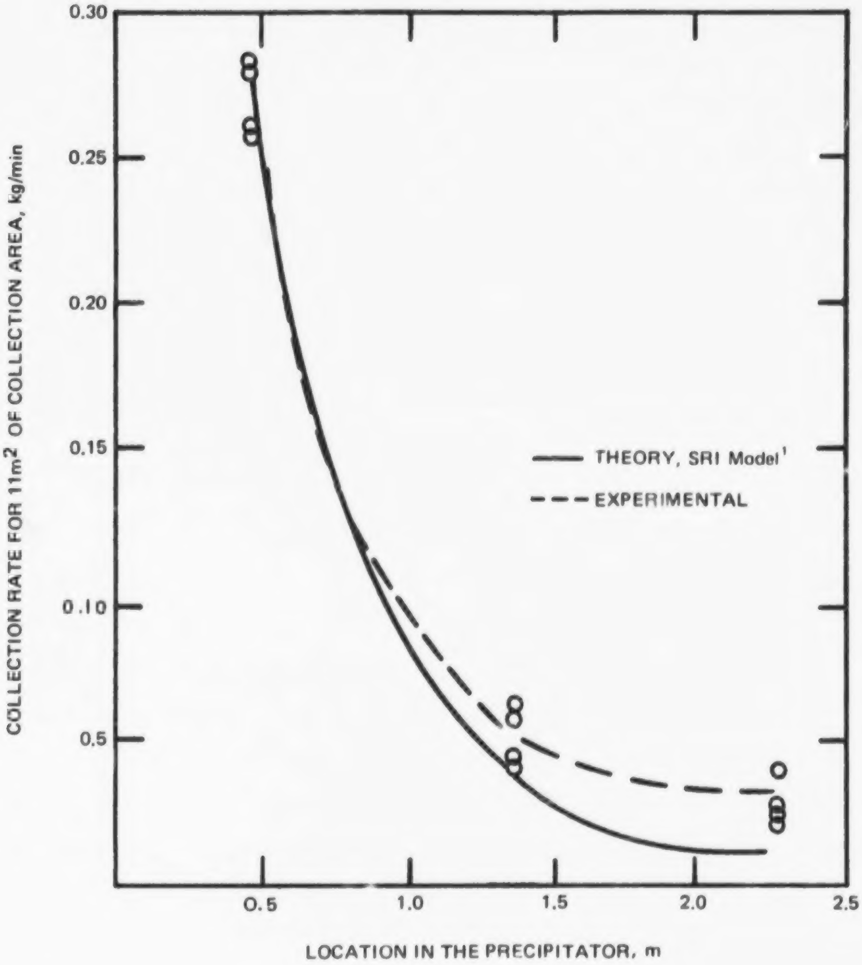

Figure 57. Collection rate versus horizontal location in the precipitator.

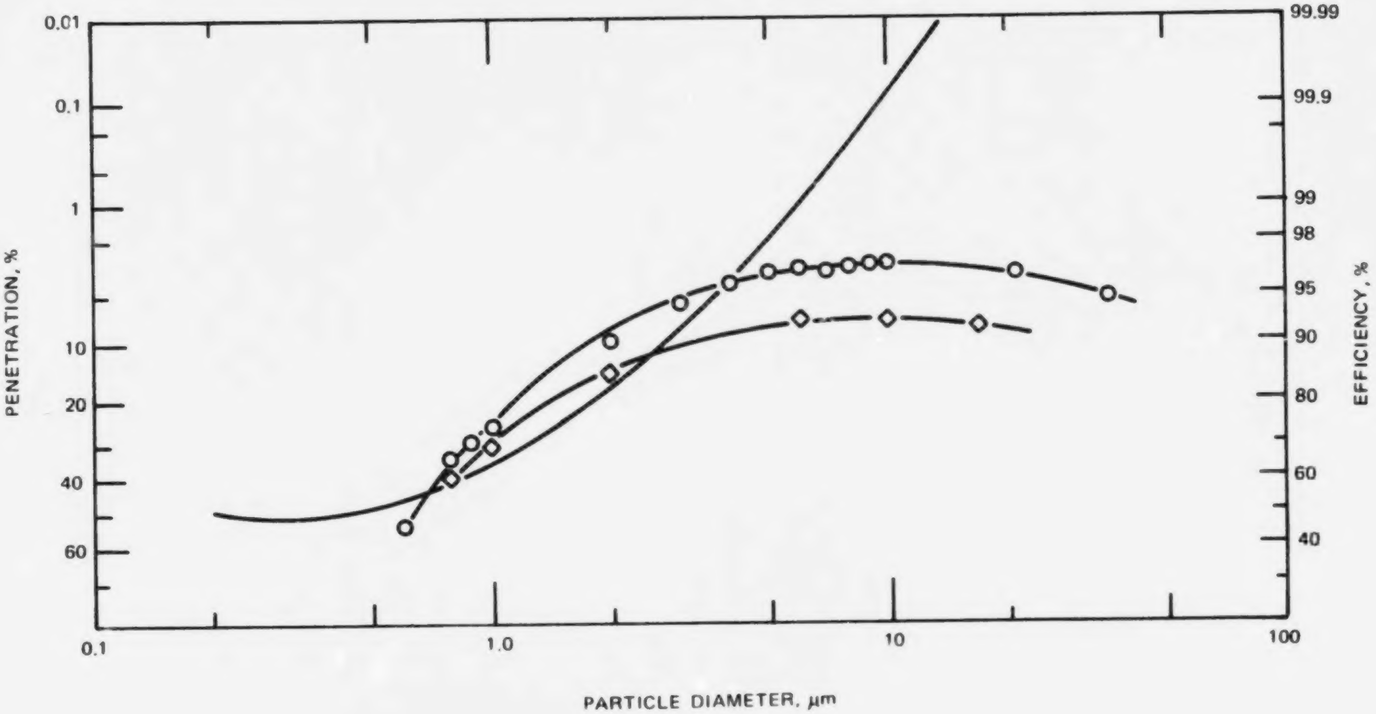

Figure 58. Fractional collection efficiency versus particle diameter, solid line theory, circles experimental between rap, diamonds experimental, include rapping reentrainment.

precipitator, and the measured electrical conditions, volume flow rate, and inlet particle size distribution for the FluiDyne test. The fractional efficiencies are compared for the case in which nonidealities are excluded from the computer calculations. The shapes of the computed and measured fractional efficiency curves did not agree either when rapping losses were included or when they were excluded. For the no rap condition, the computer model underpredicted the fractional collection efficiencies for particle sizes between .7 µm and 4.5 µm and overpredicted the fractional collection efficiencies for particle sizes greater than 4.5 µm. The discrepancy for the large particles has been previously reported.[23] It was speculated that the discrepancy was due to rapping reentrainment. The measured fractional efficiency curve without rapping reentrainment losses indicates that rapping reentrainment is not the only cause for the discrepancy. A comparison of the computed and measured fractional efficiency curves indicates a shift in the particle size distribution of the particulate inside the precipitator that is not accounted for by the different migration velocities calculated for each particle size. A portion of the discrepancy is undoubtedly due to reentrainment between raps. The reentrainment between raps of agglomerates from hoppers, collection plates, chamber walls, corona wires, plate support structures, etc., was not included in the computer calculations. Sneakage of particulate through hoppers, and corona wire and plate support areas which permits large particles to escape collection can also cause the discrepancy. Coagulation of the particulate in the gas stream may be another possibility. Strong electric fields in electrostatic precipitators produce coagulation and increase the efficiency of precipitation.[24] This effect is not included in the present computer model and possibly could produce the effects observed, explaining the load cell measurements and the fractional efficiency curve without rapping losses.

The fractional efficiency curve including rapping given in Figure 58 is for the tests with 12 minute intervals between raps. The largest rapping emissions were observed during these tests. The fractional efficiency curve including rapping was computed from the measured inlet feed rates in each size band and the calculated total outlet emission rates in each size band. The total outlet emissions were obtained by summing outlet emissions for each size band for the raps and for the between rap intervals.

As expected, the inclusion of the rapping losses increased the discrepancy between the computed fractional efficiencies and the measured fractional efficiencies for the large particles.

Contribution of Rapping Reentrainment to Total Emissions

In the FluiDyne tests, rapping losses were observed to account for a significant portion of the total emissions. The percentage of total emissions resulting from rapping reentrainment ranged from 18% to 53%, depending on the amount of dust on the plates when they were rapped.

A plot showing the percentage contribution of the rapping puffs to total emissions for all size bands is given in Figure 59. This data indicates that minimum rapping losses would have been obtained with a time interval between raps somewhere between 52 and 150 minutes.

Since the FluiDyne test was conducted under conditions representative of the inlet sections of many precipitators attached to coal-fired boilers, the data indicate that improvements in efficiency can be obtained by increasing the time interval between raps. Many field units operate with time intervals between raps for inlet sections on the order of 2 to 6 minutes; the FluiDyne data indicate that these times

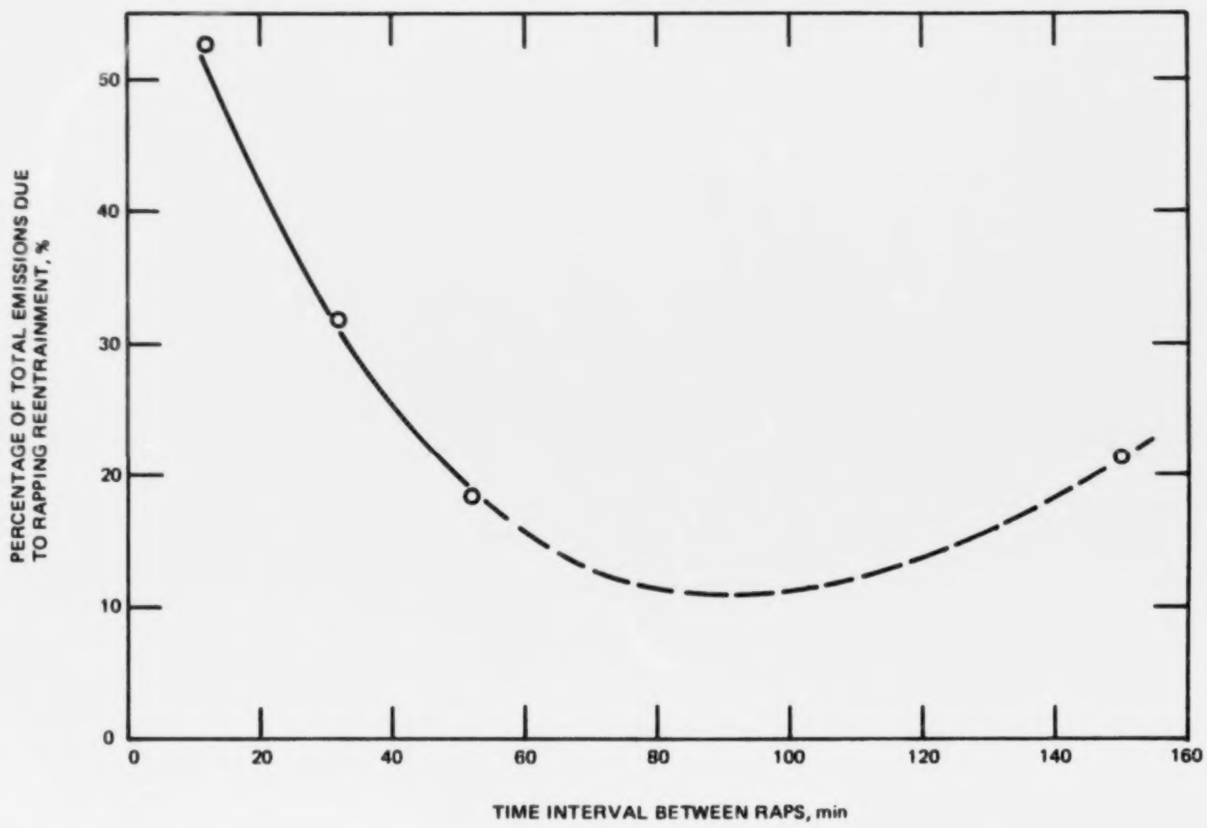

Figure 59. Percentage of total emission due to rapping reentrainment.

should be increased by a factor of 6 to 15. The exact factor depends on many parameters, including the effect on between-rap operation.

EFFECT OF RAPPING REENTRAINMENT ON EFFICIENCY, PENETRATION, AND SIZING OF ELECTROSTATIC PRECIPITATORS

Generally, if rapping reentrainment were entirely prevented the percentage increase in efficiency would be small, but the percentage decrease in penetration would be large. Examples using the percentages obtained during the FluiDyne experiments are given in Tables 17 and 18. These examples also show that the percentage increase in efficiency decreases with increasing efficiency of the precipitator. Due to the exponential dependence of precipitator efficiency on particle migration velocity, plate collection area, and gas volume flow rate, the effect of rapping reentrainment on the size of a precipitator required for a given efficiency is substantial. Estimates of the effect of rapping reentrainment on precipitator size are also tabulated in Tables 17 and 18 for various conditions. Two approaches were used to generate the tabulated values. One approach was to assume that the percentage penetration due to rapping was independent of the size of the unit. This assumption, although not strictly true, may fairly represent real situations. According to the data obtained during the experiments at FluiDyne, the rapping puff concentration has a significant vertical gradient and the particle size distributation of the rapping puff consists of large particles. Thus, in a multi-section precipitator the rapping puffs from upstream sections may be recollected in the lower portion of a succeeding section and later transferred from this lower position into the hoppers without making any significant contibution to outlet emissions. In this case, outlet fields would contribute the largest portion of the rapping emission

Table 17. EFFECT OF RAPPING REENTRAINMENT ON EFFICIENCY FOR RAPPING LOSSES ACCOUNTING FOR 20%, 30%, 40% AND 50% OF EMISSIONS FOR VARIOUS OVERALL EFFICIENCIES

(first approach)

Assumed percent of total penetration due to rapping reentrainment	Penetration			Assumed Overall Efficiency η, %	Efficiency without rapping reentrainment, η_R, %	Increase in η without rapping reentrainment, %	SCA* required				Additional SCA required because of reentrainment		Additional SCA, %
	Due to rapping reentrainment, %	Without rapping reentrainment, %	Total %				For η without rapping reentrainment, $m^2/m^3/sec$	$(ft^2/1000\ ft^3/sec)$	For η_R or for η with rapping reentrainment, $m^2/m^3/sec$	$(ft^2/1000\ ft^3/sec)$	$m^2/m^3/sec$	$(ft^2/1000\ ft^3/sec)$	
50	3.75	3.75	7.50	92.50	96.25	3.90			16.2	(82)			
	2.25	2.25	4.50	95.50	97.75	2.31			21.3	(108)			
	0.75	0.75	1.50	98.50	99.25	0.76	26.2	(133)	35.5	(180)	9.3	(47)	35.3
	0.25	0.25	0.50	99.50	99.75	0.25	41.8	(212)	53.2	(270)	11.4	(58)	27.4
	0.05	0.05	0.10	99.90	99.95	0.05	68.9	(350)	81.7	(415)	12.8	(65)	18.6
40	3.00	4.50	7.50	92.50	95.50	3.24							
	1.80	2.70	4.50	95.50	97.30	1.88			18.7	(95)			
	0.60	0.90	1.50	98.50	99.10	0.61	26.2	(133)	32.9	(167)	6.7	(34)	25.6
	0.20	0.60	0.50	99.50	99.70	0.20	41.8	(212)	50.2	(255)	8.5	(43)	20.3
	0.04	0.06	0.10	99.90	99.94	0.04	68.9	(350)	78.8	(400)	9.8	(50)	14.3
30	2.25	5.25	7.50	92.50	94.75	2.43							
	1.35	3.15	4.50	95.50	96.85	1.41							
	0.45	1.05	1.50	98.50	98.95	0.46	26.2	(133)	30.5	(155)	4.5	(23)	16.5
	0.15	0.35	0.50	99.50	99.65	0.15	41.8	(212)	47.3	(240)	5.5	(28)	13.2
	0.03	0.07	0.10	99.90	99.93	0.03	68.9	(350)	75.8	(385)	6.9	(35)	10.0
20	1.50	6.00	7.50	92.50	94.00	1.62							
	0.90	4.60	4.50	95.50	96.40	0.94							
	0.30	1.20	1.50	98.50	98.80	0.30	26.2	(133)	29.2	(148)	3.0	(15)	11.3
	0.40	0.10	0.50	99.50	99.90	0.10	41.8	(212)	68.9	(350)	3.5	(18)	8.5
	0.08	0.02	0.10	99.90	99.92	0.02	68.9	(350)	73.3	(372)	4.3	(22)	6.3

*Specific Collection Area (SCA) based on data given by Gooch, et al.[5] (Figure 26 computed performance curves at 20 nA/cm^2).

Table 16. EFFECT OF RAPPING REENTRAINMENT ON PERFORMANCE FOR VARIOUS REENTRAINMENT PERCENTAGES AS A FUNCTION OF NUMBER OF SECTIONS AND A CONSTANT COLLECTION EFFICIENCY PER SECTION.

Assumed percent of collected material per section reentrained	Number of Sections	Penetration			Percent of penetration due to rapping reentrainment, %	Efficiency η, %	Assumed efficiency η_R without rapping reentrainment, %	Increase in η with no rapping reentrainment, %	SCA* Needed				Additional SCA		Additional SCA, %
		Due to rapping reentrainment, %	Without rapping reentrainment, %	Total %					Without rapping reentrainment to obtain η		With rapping reentrainment				
									m^2/m^3/sec	(ft^2/1000 ft^3/sec)	m^2/m^3/sec	(ft^2/1000 ft^3/sec)	m^2/m^3/sec	(ft^2/1000 ft^3/sec)	
5.9	1	6.2	5.2	11.4	52	88.6	94.8	6.54							
	2	1.02	0.27	1.29	79	98.7	99.73	1.03	28.0	(142)	51.6	(262)	23.6	(120)	84
	3	0.136	0.014	0.150	91	99.85	99.986	0.14	62.1	(315)	105.4	(535)	43.3	(220)	69
	4	0.0193	0.0007	0.020	97	99.98	99.9993	0.02	98.5	(500)	108.3	(550)			
2.3	1	2.23	5.20	7.43	30	92.57	94.80	2.35							
	2	0.28	0.27	0.55	51	99.45	99.73	0.28	40.4	(205)	51.6	(262)	11.2	(57)	28
	3	0.027	0.014	0.041	66	99.959	99.986	0.03	83.7	(425)	105.4	(535)	21.7	(110)	25
	4	0.0023	0.0007	0.0030	77	99.997	99.9993	0.002	108.5	(550)	108.3	(550)			
0.97	1	0.90	5.20	6.1	15	93.9	94.8	0.95							
	2	0.10	0.27	0.37	27	99.63	99.73	0.10	46.3	(235)	51.6	(262)	5.3	(27)	11
	3	0.009	0.014	0.023	39	99.97	99.986	0.016	91.0	(462)	105.4	(535)	14.4	(73)	16
	4	0.0007	0.0007	0.0014	50	99.9986	99.9993	0.001	108.3	(550)	108.3	(550)			

*Specific Collection Area (SCA) based on data given by Gooch, et al.[5]
(Figure 26 computed performance curves at 20 nA/cm^2).

and the percent emission due to rapping should be independent of the size of the unit. Estimates based on this approach are tabulated in table 17.

The second procedure was based on the development by Francis,[18] which was discussed in the introduction. This approach assumes that the fraction of collected dust per section reentrained and emitted is the same for every section, that the between-rap sectional efficiency is constant from one section to another, and that the recollection efficiency for the rapping puffs is the same as the between rap sectional efficiency. According to Francis' procedure, the penetration of any downstream section is equal to the penetration of the first section (P_1) raised to the power of the number of preceding sections plus one. Thus, the penetration of the N section (P_N) is given by:

$$P_N = (P_1)^N \tag{8}$$

Using this equation, the efficiencies of a precipitator having 1, 2, 3, or 4 sections with a between-rap sectional efficiency of 94.8% were calculated for percent penetrations of the first section due to rapping reentrainments of 52%, 30%, and 15%. These percentages correspond to 5.9%, 2.3%, and 0.97% of the collected material per section being reentrained and emitted from a section. These values were chosen to correspond with those obtained during the FluiDyne experiments. The results of the calculations based on this procedure are tabulated in Table 18. According to this second procedure for the conditions corresponding to the worst rapping reentrainment case at FluiDyne, the contribution of rapping reentrainment to total emissions would be greater than 90% for a three or four section precipitator with 94.8% sectional efficiency. For a case in which reentrainment accounts for only 15% of the emissions for the first section, a situation slightly better than the best obtained during the FluiDyne experiments, rapping reentrainment according to the Francis procedure would account for 39% of emissions for a 3-section precipitator and 50% of emissions for 4-section precipitator, if the precipitator had a sectional efficiency of 94.8%. These calculations indicate that, as the size of the precipitator increases, the percentage contribution of rapping reentrainment to total emissions increases. As previously discussed, this may not happen. Further investigations with a multi-section precipitator are needed.

To obtain an indication of the effect of rapping reentrainment on the sizing of a precipitator, estimates of the theoretical specific collection area needed to obtain a given collection efficiency for a particular set of conditions were obtained from the model developed by Gooch, et al.[1] For the example case, a typical particle size distribution for an ash from a coal-fired boiler plant was selected and a precipitator operating current density of 20 nA/cm^2 was assumed (see the report of Gooch, et al,[1] for further details).

The theoretical specific collection area (SCA) required to obtain a desired collection efficiency with rapping reentrainment was compared with a theoretical SCA that would give the same efficiency if there were no rapping emissions. This gave an estimate of the increase in SCA needed to counterbalance the rapping reentrainment emissions. The theoretical SCA needed to obtain the desired efficiency with rapping reentrainment was determined by first computing the efficiency that would be obtained if there were no rapping reentrainment, by assuming that either the percentage of emissions due to rapping reentrainment or the fraction of collected dust reentrained and emitted from a section due to rapping were known. Once this efficiency was calculated and assuming that there were no other nonidealities beside rapping reentrainment, the required theoretical SCA was obtained from data given by Gooch, et al. Then, again using the data given by Gooch, et al, the SCA was determined that would give the desired efficiency if there were no nonidealities such as rapping reentrainment. For the particular cases considered, the increase in required SCA due to the rapping reentrainment ranged from 6% to 84% (see Tables 17 and 18). Thus, although the percentage decrease in efficiency due to rapping reentrainment is relatively small, the effect on the size required for a given efficiency can be significant. The data obtained from the FluiDyne experiments indicates that even moderate changes in rapping parameters can significantly affect the size of a precipitator for a given efficiency.

EFFECT OF AGGLOMERATION AND FRACTIONAL REENTRAINMENT PERCENTAGES OF COLLECTED PARTICULATE FOR VARIOUS PARTICLE SIZES

Modern electrostatic precipitator technology is concerned not only with the overall collection efficiency but also with the fractional collection efficiency,that is, the collection efficiency for various particle size ranges. The fraction of collected material that is emitted due to rapping reentrainment for various particle sizes is in the over simplified case independent of particle size.

For a homogeneous mixture of discrete particles of various sizes if one quarters out from the mixture a sample, theoretically the percentage of particles removed from the mixture would be the same for all sizes. Rapping reentrainment does not produce this simplified case. The particle size distribution of the discrete particles reentrained is not the same as the particle size distribution of the individual particles collected on the plates. Many of the discrete particles that are reentrained are agglomerates of the individual particles that were collected on the precipitator plates. The size distribution of the particles in the rapping puff that escape from a section are also affected by the recollection efficiency which is a function of particle size. In addition, the particle size distribution of the reentrained material probably varies along the length of the precipitator and from one precipitator to another due to variations in the particle size distribution of the collected dust. These factors complicate detailed modelling of rapping reentrainment.

An estimate of the fraction of collected material emitted due to rapping for various particle sizes was obtained by using data generated from the FluiDyne experiments and a rearrangement of equation 5. The measured between-rap fractional efficiencies given in Figure 58 and the fractional emissions due to rapping reentrainment given in Figure 41 (32 minute test only) were used for input data. Equation 5 was rearranged to obtain:

$$R_i = \frac{(1 - n_i)\ f_i}{N_i\ (1-f_i)} \qquad (9)$$

where R_i = fraction of collected material for a given particle size i that is emitted due to rapping reentrainment from a section

n_i = fractional collection efficiency per section

f_i = fraction of emissions for a given particle size that were due to rapping reentrainment.

The results of calculations using this equation are tabulated in Table 19. R_i is nearly constant. However, it increases slightly with particle size reflecting the effect of agglomeration of the reentrained material.

Table 19. FRACTION OF COLLECTED MATERIAL FOR A GIVEN PARTICLE DIAMETER i THAT WAS EMITTED DUE TO RAPPING REENTRAINMENT

Particle Diameter μm	f_i	n_i	R_i
1	.09	.75	.033
3	.165	.945	.012
5	.345	.953	.026
7	.425	.958	.032
9	.47	.96	.037
11	.48	.96	.038
13	.49	.96	.040
15	.49	.96	.040
17	.49	.958	.042

Based on data from the 32 minute Rapping Interval Tests at FluiDyne.

The general applicability of these numbers is somewhat limited since the theory on which they were calculated has an implicit assumption that there is no transfer of particles from one size band to another when the particles are reentrained. Unfortunately for modelling purposes, emissions due to rapping reentrainment in a particular particle size can be either reduced or increased by agglomeration. An example of a problem with equation 9 is that an infinite value for R_i is obtained if emissions in a particular size are due one hundred percent to rapping reentrainment. In practice this can occur due to agglomeration if there are no corresponding particles in the inlet size distribution or if all the corresponding particles are collected before the outlet section. An extension of Francis' modelling efforts is needed that will include the effect of agglomeration if accurate fractional efficiency curves including rapping reentrainment are to be determined for full-scale precipitators.

REFERENCES

1. Gooch, J.P., J.R. McDonald, and S. Oglesby, Jr. A Mathematical Model of Electrostatic Precipitation. Environmental Protection Agency, Washington, D.C. Publication No. EPA-650/2-75-016. April 1975.

2. Sproull, W.T. Minimizing Rapping Loss in Precipitators at a 2000 Megawatt Coal-Fired Power Station. Paper No. 71-125, APCA Meeting, Atlantic City, N.J., 1971.

3. Tassicker, O.J. Some Aspects of Electrostatic Precipitator Research in Australia. J. Air Pollut. Control Assoc. 25: 122-128, February 1975.

4. Tassicker, O.J. Aspects of Forces on Charged Particles in Electrostatic Precipitators. Dissertation, Wollongong University College, University of New South Wales, Australia, 1972.

5. Sproull, W.T. Fundamentals of Electrode Rapping in Industrial Electrical Precipitators. J. Air Pollut. Control Assoc. 15:50-55, February 1965.

6. Ruckelshausen, K. Über die Beseitigung von Staubansätzen auf technisch glatten Oberflächen durch Klopfen ober Vibrieren. [The Removal of Dust Deposits from Flat Plates by Rapping or Vibrating]. Dissertation, Technische Hochschule, Stuttgart, 1957.

7. Brandt, W. The Stage of Development of Electrostatic Dust Precipitators with Special Consideration of Cleaning Problems. Staub 21:392-397, 1961.

8. Watson, K.S. and K.J. Blecher. Further Investigation of Electrostatic Precipitators for Large Pulverized Fuel-Fired Boilers. Air Water Pollut. Int. J. (Oxford, England) 10:573-582, September 1966.

9. Koschany, E.M. Basic Investigation Concerning the Cleaning of Collection Electrodes in Electrostatic Precipitators. Staub-Reinhalt. Luft (in English) 28:5-9, July 1968.

10. Tassicker, op. cit., p. 88.

11. Plato, H. Rapping of Collecting Plates in Electrostatic Precipitators. Staub-Reinhalt. Luft (in English). 29:22-30, August 1969.

12. Tassicker, op. cit., p. 118.

13. Penney, G.W. and E.H. Klingler. Contact Potentials and the Adhesion of Dust. Trans. Amer. Inst. Elec. Eng. Part I, 81:200-204, 1962.

14. Dalmon, J. and D. Tidy. The Cohesive Properties of Fly Ash in Electrostatic Precipitation. Atmos. Environ. (Oxford, England) 6:81-92, February 1972.

15. Sanayev, Yu. I. and I.K. Reshidov. Study of Dust Reentrainment Phenomena and Their Influence on Efficiency of Industrial Electrostatic Precipitators. Promyshlennaya Sanitarnaya Ochistka Gazov [Industrial and Sanitary Gas Cleaning] (Moscow, USSR). 1974(1):1-5.

16. Schwartz, L.B. and M. Lieberstein. Effect of Rapping Frequency on the Efficiency of an Electrostatic Precipitator at Municipal Incinerator. Proceedings of the Fourth Annual Environmental Engineering and Science Conference, March 4-5, 1975, University of Louisville, Louisville, Kentucky.

17. Nichols, G.B., H.W. Spencer, and J.D. McCain. Rapping Reentrainment Study. Report to Tennessee Valley Authority, TVA Agreement TV36921A, November 1975.

18. Gooch, J.P. and N.L. Francis. A Theoretically Based Mathematical Model for Calculation of Electrostatic Precipitator Performance. J. Air Pollut. Control Assoc. 25:108-113, February 1975.

19. Beutner, H.P. J. Air Pollut. Control Assoc. 24:865, September 1974.

20. Sem, G.J., et al. State of the Art: 1971 Instrumentation for Measurement of Particulate Emissions from Combustion Sources - Vol. II - Particulate Mass - Detail Report. Report APTD-0734, Thermo-Systems, Inc. April 1971.

21. Nichols, G.B. and H.W. Spencer, III. Test Methods and Apparatus for Conducting Resistivity Measurements. Report to Environmental Protection Agency, EPA Contract No. 68-02-1083, March 1975 (Draft).

22. Davies, C.N. The Entry of Aerosols into Sampling Tubes and Heads. J. Phys. D. 1:921, 1968.

23. Nichols, G.B. Particulate Emission Control from Pulp Mill Recovery Boilers with Electrostatic Precipitators. IEEE Conf. Rec. 1975 Ann. Pulp Paper Ind. Tech. Conf., 75 CH0972-01A, pp. 1-17. June 1975.

24. Fuchs, N.A. The Mechanics of Aerosols. Daisley, R.E. and M. Fuchs (transl.), Davies, C.N. (ed.). New York, Macmillan, 1964, p. 3.3.

Appendix I
Log of Precipitator Data, June 23, 1975

Test 1

			Power Supply	
Time	Water, gal/min	Avg. duct Temp. @ inlet, °F	Secondary voltage kV	Secondary current mA
1040	4.5	283	36	43
1050	4.5	283	38	43
1100	4.5	278	39	43
1110	4.5	278	39	43
1120	4.6	278	39	42
1130	4.6	278	39	42
1140	4.6	278	39	42
1150	4.6	283	39	42
1200	4.6	283	39	42
1210	4.6	283	40	42
1220	4.6	283	38	24
1230	4.6	283	38	24
1240	4.6	288	39	32
1250	4.6	288	39	32
1300	4.6	293	39	32
1310	Dust off and on			

Appendix I
Log of Precipitator Data, June 23, 1975

Test 2

			Power Supply	
Time	Water, gal/min	Avg. duct Temp. @ inlet, °F	Secondary voltage kV	Secondary current mA
1320	4.6	293	38	23
1330	4.6	293	37	24
1440	4.6	303	37	24
1450	4.6	308	37	24
1500	4.6	308	37	24
1510	4.6	308	37	24
1520	4.1	308	37	24
1530	5.0	293	40	34
1540	5.5	278	40	34
1600	5.5	273	40	34
1610	5.5	273	40	34
1620	5.5	273	38	16
1630	5.5	273	38	16
1640	5.5	263	39	17
1650	5.5	263	39	17
1700	5.5	263	42	32
1710	5.5	263	42	32

Appendix I
Log of Precipitator Data, June 24, 1975
Test 3

			Power Supply	
Time	Water, gal/min	Avg. duct Temp. @ inlet, °F	Secondary voltage kV	Secondary current mA
1110	6.0	250	38	40
1120	6.0	250	40	40
1130	6.0	250	41	40
1140	6.0	258	41	40
1150	6.0	258	41	40
1200	5.8	258	41	40
1210	Dust off			
1220	Dust on			
1230	5.8	263	42	40
1240	Dust off and on			
1250	5.8	263	42	40
1300	Dust off and on			
1310	5.8	263	42	40
1320	Dust off and on			
1330	5.8	266	42	40

Appendix I
Log of Precipitator Data, June 24, 1975
Test 4

Time	Water, gal/min	Avg. duct Temp. ° inlet, °F	Power Supply Secondary voltage kV	Secondary current mA
1500	5.8	258	42	31
1510	5.8	263	44	41
1520	5.8	263	43	40
1530	5.8	263	43	41
1540	Dust off and on			
1550	5.8	263	43	40
1600	5.8	266	43	40
1610	5.8	266	43	39
1620	Dust off and on			
1630	5.8	266	43	40
1640	5.8	266	43	40
1650	6.0	260	44	40
1700	Dust off			

Appendix I
Log of Precipitator Data, June 25, 1975
Test 5

Time	Water, gal/min	Avg. duct Temp. @ inlet, °F	Power Supply Secondary voltage kV	Power Supply Secondary current mA
0950	5.7	256	40	40
1000	5.8	256	40	40
1010	5.8	263	40	40
1020	5.8	263	40	40
1030	5.8	263	40	40
1040	5.5	268	40	40
1050	5.5	268	41	40
1100	5.7	268	41	40
1110	5.7	258	42	40
1120	5.7	258	42	40
1130	5.7	258	42	40
1140	5.7	258	40	40
1150	5.7	262	42	40

Appendix I

Log of Precipitator Data, June 25, 1975

Test 6

Time	Water, gal/min	Avg. duct Temp. @ inlet, °F	Power Supply Secondary voltage kV	 Secondary current mA
1200	5.7	262	42	40
1210	5.7	262	40	40
1220	5.7	262	40	40
1350	5.7	274	43	40
1400	5.8	264	43	40
1410	5.9	264	43	40
1420	5.9	264	43	40
1430	6.0	264	44	40
1440	6.0	264	44	40
1450	6.0	264	42	36
1500	6.0	264	42	39
1510	6.0	264	43	37
1520	6.0	264	44	40
1530	5.9	265	44	38
1540	5.9	266	44	40
1550	5.9	266	44	40
1600	5.9	266	44	40
1610	5.9	266	44	40
1620	5.9	267	44	38
1630	5.9	268	44	38
1640	5.9	268	44	38
1650	5.9	269	44	38
1700	5.9	269	44	38

Appendix I
Log of Precipitator Data, June 26, 1975
Test 7

			Power Supply	
Time	Water, gal/min	Avg. duct Temp. @ inlet, °F	Secondary voltage kV	Secondary current mA
0950	5.9	257		
1000	5.9	257		
1010	5.9	257	39	40
1020	5.9	258	40	44
1030	5.9	258	40	44
1040	5.9	258	40	41
1050	5.9	264	41	41
1100	5.9	264	41	41
1110	5.9	267	41	41
1120	6.0	267	41	41
1130	6.0	267	42	40
1140	6.0	261	42	40
1150	6.0	269	42	40
1200	6.0	269	43	41
1210	6.0	269	41	41

Appendix I
Log of Precipitator Data, June 26, 1975
Test 8

Time	Water, gal/min	Avg. duct Temp. @ inlet, °F	Power Supply Secondary voltage kV	Secondary current mA
1220	6.0	269	43	40
1230	6.0	269	43	40
1240	6.0	269	43	41
1250	6.0	269	43	40
1300	6.0	269	43	40
1310	6.0	269	43	40
1420	6.0	264	43	40
1430	6.0	265	43	40
1440	6.0	265	43	40
1450	6.0	265	43	40
1500	6.0	265	43	40
1510	6.1	267	43	40
1520	6.1	267	44	40
1530	6.1	267	44	40
1540	6.1	264	44	40
1550	6.1	264	44	40
1600	6.1	264	44	40
1610	6.1	264	44	40
1620	6.1	264	45	40
1630	6.1	264	45	40
1640	6.1	264	45	40
1650	6.1	264	43	40
1700	6.1	264	44	40
1710	6.1	264	45	40
1720	6.1	264	45	40
1730	Test stopped			

Precipitator Ash Loading Data

Tests 1 and 2

	Time	(lbs)	Actual Feed Rate (lbs/hr)	Comments
Test 1	1050	930	348	
	1108	850		
	1126	760		
	1139	700		
	1151	900		
	1155	875		
	1210	800		
	1230	675		
	1247	560		
	1300	500		
	1310	440		Dust off (13:04-15:25) - reload hopper
Test 2	1333	440		
	1440	1300		
	1500	1300		
	1525	1300		
	1547	1200	407	
	1608	1075		
	1625	950		
	1645	825		
	1700	725		
	1715	640		Dust off

Precipitator Ash Loading Data

Tests 3 and 4

	Time	(lbs)	Actual Feed Rate (lbs/hr)	Comments
Test 3	1116	1300	332	
	1133	1300		Dust on
	1144	1280		
	1155	1225		
	1203	1160		Dust off (12:05-12:10)
	1216	1140		
	1232	1075		Dust off (12:25-12:30)
	1250	1000	338	Dust off (12:42-12:48)
	1308	925	335	Dust off (13:01-13:07)
	1327	875	369	Dust off (13:18-13:25)
Test 4	1500	1175	342	Dust off (13:37-14:56)
	1514	1090		
	1527	1010		
	1546	950	380	Dust off (15:37-15:44)
	1600	875		
	1615	760		
	1627	740	358	Dust off (16:17-16:24)
	1649	600		
	1658			Dust off

Precipitator Ash Loading Data

Test 5

	Time	(lbs)	Actual Feed Rate (lbs/hr)	Comments
Test 5	0951	1225	358	
	1005	1130		
	1014	1080		
	1025	1035		
	1039	970	352	Dust off (10:25-10:31)
	1043	925		Dust off (10:43-10:51)
	1051	925	340	Dust off (11:04-11:13)
	1104	860		Dust off (11:26-11:34)
	1113	860	326	Dust off (11:48-11:55)
	1122	775		Fill hopper
	1126	750		
	1134	750	327	
	1143	700		
	1148	680		
	1155	680	400	
	1207	620		Dust off

Precipitator Ash Loading Data

Test 6

	Time	(lbs)	Actual Feed Rate (lbs/hr)	Comments
Test 6	1356	1200	362	Fill hopper Dust off (12:07-13:56)
	1407	1150		
	1414	1100		
	1423	1050		
	1432	990		
	1442	930		
	1446	920		Dust off (14:46-14:55)
	1455	920	357	
	1504	870		
	1527	720		Dust off (15:27-15:33)
	1533	720	358	
	1542	670		
	1549	630		
	1559	560		
	1607	520		Dust off (16:07-16:20)
	1620	520	360	
	1626	480		
	1634	430		
	1642	380		
	1648	350		
	1655	310		
	1700	270		Dust off

Precipitator Ash Loading Data

Test 7

	Time	(lbs)	Actual Feed Rate (lbs/hr)	Comments
Test 7	1009	1100	341	
	1027	980		
	1048	870		
	1057	810		
	1127	660	350	Dust off (11:11-11:15)
	1151	520		
	1200	470		
	1208	420		Dust off (12:08-12:15)
	1224	360	356	
	1238	280		
	1246	230		
	1257	170		
	1308	100		

Precipitator Ash Loading Data

Test 8

	Time	(lbs)	Actual Feed Rate (lbs/hr)	Comments
Test 8	1426	1250	382	Fill hopper Dust off (13:08-14:26)
	1447	1120		
	1457	1060		
	1506	1000		
	1515	950		
	1523	900		
	1535	820		
	1544	760		
	1552	700		
	1613	590	420	Dust off (15:52-16:00
	1617	560		
	1624	520		
	1634	450		
	1643	400		
	1651	340		
	1707	280	350	Dust off (16:51-16:59)
	1716	220		
	1724	160		
	1730			Dust off

TABLE OF CONVERSION FACTORS

MASS

1 grain = 0.0648 grams
1 gram = 15.4324 grains

AREA

1 ft^2 = 0.0929 m^2
1 m^2 = 10.76 ft^2

VOLUME

1 ft^3 = 0.0283 m^3
1 m^3 = 35.31 ft^3

PRESSURE

1 kPa = 0.1451 Psi
1 Pa = 1 N/m^2
1 Psi = 6.894 kPa (kilopascal)

ACCELERATION

1 G = 9.8 m/sec^2

VELOCITY

1 m/sec = 0.3048 ft/sec
1 ft/sec = 3.28 m/sec